AN ANALYTICAL METHOD FOR THE ACCURATE AND EFFECTIVE THERMAL MODELLING OF ALGAN/GAN HEMTS

A THESIS SUBMITTED TO
THE GRADUATE SCHOOL OF NATURAL AND APPLIED SCIENCES
OF
MIDDLE EAST TECHNICAL UNIVERSITY

BY

MOHAMMAD AZARIFAR

IN PARTIAL FULFILLMENT OF THE REQUIREMENTS
FOR
THE DEGREE OF MASTER OF SCIENCE
IN
MECHANICAL ENGINEERING

JANUARY 2017

Approval of thesis:

AN ANALYTICAL METHOD FOR THE ACCURATE AND EFFECTIVE THERMAL MODELLING OF ALGAN/GAN HEMTS

submitted by **MOHAMMAD AZARIFAR** in partial fulfilment of requirements for degree of **Master of Science in Mechanical Engineering Department, Middle East Technical University** by,

Prof. Dr. Gülbin Dural Ünver
Dean, Graduate School of **Natural and Applied Sciences** _____

Prof. Dr. R. Tuna Balkan
Head of Department, **Mechanical Engineering** _____

Asst. Prof. Dr. F. Nazlı Dönmezer Akgün
Supervisor, **Mechanical Engineering Dept., METU** _____

Examining Commitee Members:

Assoc. Prof. Dr. Almıla Güvenç Yazıcıoğlu
Mechanical Engineering Dept., METU _____

Asst. Prof. Dr. F. Nazlı Dönmezer Akgün
Mechanical Engineering Dept., METU _____

Assoc. Prof. Dr. Hakan Ertürk
Mechanical Engineering Dept., Boğazici University _____

Asst. Prof. Dr. Özgür Bayer
Mechanical Engineering Dept., METU _____

Asst. Prof. Dr. Kıvanç Azgın
Mechanical Engineering Dept., METU _____

Date: **20.01.2017**

I hereby declare that all information in this document has been obtained and presented in accordance with academic rules and ethical conduct. I also declare that, as required with these rules and conduct, I have fully cited and referenced all materials and results that are not original to this work.

Name, Last name: Mohammad Azarifar

Signature:

ABSTRACT

AN ANALYTICAL METHOD FOR THE ACCURATE AND EFFECTIVE THERMAL MODELLING OF ALGaN/GaN HEMTS

Azarifar Mohammad

M.Sc., Department of Mechanical Engineering

Supervisor: Asst. Prof. Dr. F. Nazlı Dönmezer Akgün

January 2017, 89 pages

AlGaN/GaN high electron mobility transistors (HEMTs) are popular solid-state electronic devices used for high power and frequency applications. Concerns exist about their reliability and performance due to harsh self-heating effects, which makes it necessary to correctly characterize their thermal performance. In the past many researchers used thermal modelling approaches for thermal characterization since variety of limiting factors still exist in the experimental measurements. In this study diversities and important parameters in various thermal models are investigated to provide a roadmap for the future thermal models. In addition, an analytical solution technique with high efficiency and accuracy is introduced for the correction of 2D models and for fast parametric thermal studies of HEMT devices. Using this analytical technique comprehensive thermal performance comparison of GaN-on-SiC and GaN-on-diamond for various device geometries and operating conditions is also performed.

Keywords: AlGaN, GaN, HEMT, MODFET, Temperature, Thermal Modelling, Thermal Resistance

ÖZ

Doğru ve Verimli AlGaN/GaN HEMT Isıl Modellenmesi İçin Geliştirilmiş Analitik Model

Azarifar Mohammad
Yüksek Lisans, Makina Mühendisliği bolümü
Tez Yöneticisi: Asst. Prof. Dr. F. Nazlı Dönmezer Akgün

Ocak 2017, 89 sayfa

AlGaN/GaN high electron mobility transistors (HEMTs) are popular solid-state electronic devices used for high power and frequency applications. Concerns exist about their reliability and performance due to harsh self-heating effects, which makes it necessary to correctly characterize their thermal performance. In the past many researchers used thermal modelling approaches for thermal characterization since variety of limiting factors still exist in the experimental measurements. In this study diversities and important parameters in various thermal models are investigated to provide a roadmap for the future thermal models. In addition, an analytical solution technique with high efficiency and accuracy is introduced for the correction of 2D models and for fast parametric thermal studies of HEMT devices. Using this analytical technique comprehensive thermal performance comparison of GaN-on-SiC and GaN-on-diamond for various device geometries and operating conditions is also performed.

Keywords: AlGaN, GaN, HEMT, MODFET, Temperature, Thermal Modelling, Thermal Resistance

To My Precious Parents and My Lovely Sister

AKNOWLEDGEMENTS

The research process of this thesis would have taken far longer time to be completed if I did not have the encouragement from many others. I am grateful to acknowledge those who have supported me over writing of this thesis.

First, I wish to express my deepest gratitude to my parents for allowing me to realize my own potential. All the support they have provided me over the years was the greatest gift anyone has ever given me. I would like to thank my family: my parents and my sister for supporting me spiritually throughout writing this thesis and my life in general.

Next, I would like to express my endless gratitude to my advisor Dr. F. Nazlı Dönmezer Akgün for the continuous support of my Master study and related research, for her patience, motivation, and immense knowledge. Her guidance was a bright light showing me the way in any moment of my research and writing of this thesis. I could not have imagined having a better and kinder advisor and mentor.

This research was supported by the METU-BAP (Grant no: BAP-08-11-2015-028) and the TUBITAK (Grant no: 115E756), without either of which this work would not have been possible.

TABLE OF CONTENTS

LIST OF TABLES

TABLES

LIST OF FIGURES

FIGURES

LIST OF ABBREVIATIONS

ABBREVIATIONS

1D: One Dimensional

2D: Two Dimensional

2DEG: Two Dimensional Electron Gas

3D: Three Dimensional

AlGaN: Aluminium Gallium Nitride

FEM: Finite Element Method

FET: Field Effect Transistor

GaAs: Gallium Arsenide

GaN: Gallium Nitride

HEMT: High Electron Mobility Transistor

IR: Infrared

LED: Light Emitting Diodes

MTTF: Mean Time to Failure

PCD: Poly Crystal Diamond

SCD: Single Crystal Diamond

Si: Silicon

SiC: Silicon Carbide

CHAPTER 1

INTRODUCTION

1.1 AlGaN/GaN HEMTs

High quality GaN films are introduced by Nakamura et al [1, 2] in 1991 for the development of the blue light emitting diodes (LEDs) and exhibited promising opportunities in advancing transistor fabrication. Soon after, AlGaN/GaN transistors were introduced and after two decades became available for extensive commercial and defensive devices [3]. Unique high current and voltage capabilities of GaN makes it highly valued for microwave and power switching applications. Consequently, GaN is the first technology of choice in high-power applications [4], generally in electronic warfare, satellites, radars, cable TV, and cellular communications. Popular Silicon (Si) and Gallium Arsenide (GaAs) based devices cannot compete with the highly efficient performance of the GaN devices.

Excellent performance of Gallium Nitride (GaN) based high electron mobility transistors (HEMTs) at high powers and frequencies have inspired extensive research among researchers and commercial developers of solid-state electronics [5, 6]. Solid-state electronics is the expression for the electronic devices in which charge carriers (electrons and holes) are constricted within the solid phase materials [7] (often a semiconductor), which emphases it from the older technologies such as vacuum devices, and current electro-mechanical technologies like hard drives [8]. Other common names for HEMTs are two-dimensional electron gas field effect transistor (TEGFET), heterostructure FET (HFET), selectively doped heterostructure transistor (SDHT), and modulation-doped FET (MODFET).

GaN metal insulator-semiconductor FETs (MISFETs), whose main difference from a HEMT is in the formation of the electron channel, is another important technology in the field of high voltage application transistors. However GaN HEMTs are more popular devices because of their significant noise reduction and improved performance [9].

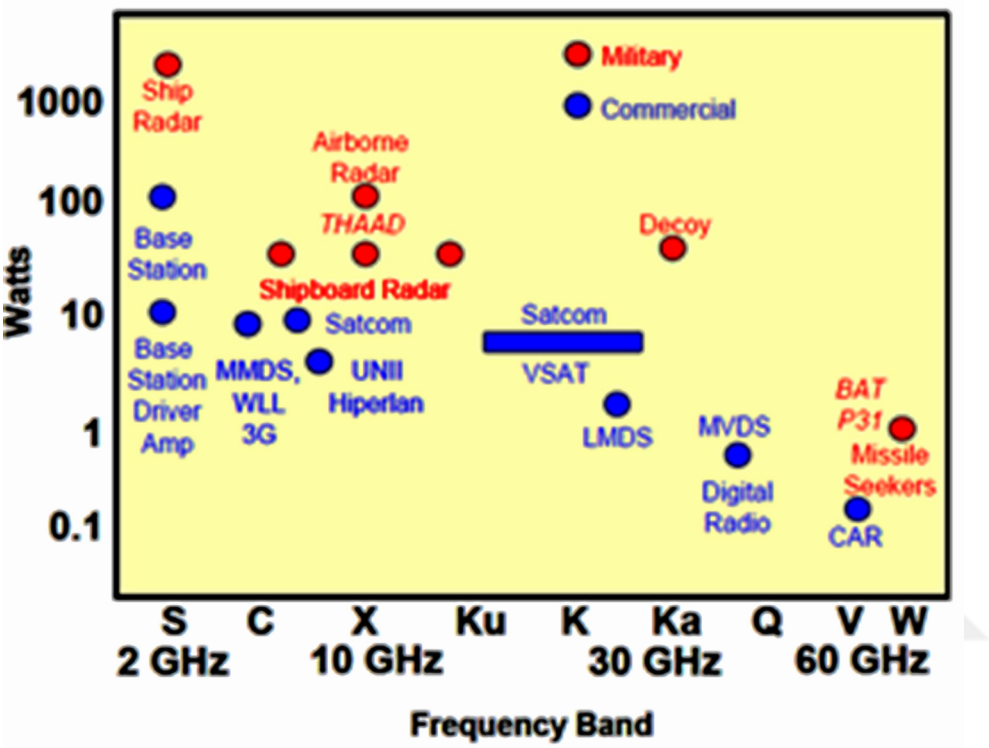

Figure 1.1 Application of GaN HEMTs [10]

Development of double-field-plate microwave GaN HEMT with 41.4 W/mm continuous-wave power density [11], and achieving world's highest breakdown voltage of 10400 V for power-switching purposes [12] demonstrate the great potentials for development of these devices. Strategies Unlimited had predicted U.S. $0.5 b market for GaN electronic devices by the end of 2010 [10], on the other hand Transparency Market Research declared this value was U.S. $0.4 b in 2014 and is expected to grow to U.S. $2.2 b in 2019 at 24.6% compound annual growth rate (CAGR). Largest aspect of GaN market belongs to radio frequency (RF) and microwave applications, targeting military applications like radar and high-performance space electronics, beside commercial applications as shown in Figure

1.1. Example are: base-station transmitters (used in wireless communications), C band Satcom (for long-distance radio telecommunications), Ku-K– band very small aperture terminal (a two-way satellite ground station with data rates range from 4 Kbit/s up to 16 Mbit/s) and broad-band satellites, local multipoint distribution systems, and digital radio [10].

1.1.1 HEMT Structure

Unique electron channel in HEMTs are created with the aid of special vertical stacking of semiconductor layers. Figure 1.2 shows the cross section of a typical, GaN HEMT structure composed of several semiconductor layers. Metal organic chemical vapor deposition (MOCVD) grown barrier ($Al_xGa_{1-x}N$) layer, acts as current isolator between the gate and the electron channel. Aluminum mole fraction, x, is optimized between 0.1 and 0.3 for desired carrier concentration and transport properties [13]. High aluminum concentration of AlGaN layer helps it to acts as a better barrier. Devices with better barriers can withstand higher charge capacities, but with cost of higher mechanical strain in the device.

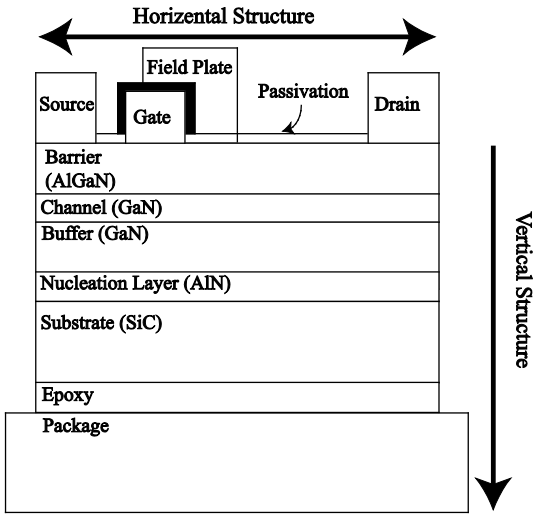

Figure 1.2 Schematic view of GaN HEMT.

High quality GaN layer located under the barrier has high mobility and saturation velocity and acts as the electron channel. Channel and buffer GaN layers, shown in

Figure 1.2, are grown on AlN (nucleation layer) with high temperature and pressure MOCVD technique. Thickness of the GaN layer is varied between 0.5 - 2 µm, depending on the required quality and the device application. Nucleation layer withstands high mechanical strains and is the source of one of the most important thermal resistances in GaN HEMTs, thermal boundary resistance (TBR). The quality of GaN crystal is low in the nucleation regions right above the AlN (barrier GaN) and improves by further crystal growth, providing a layer (channel GaN) with less defects ready for the electron transport. Substrate is the thickest layer of vertical semiconductor structure, which offers mechanical support, heat passage to the package, and electromagnetic captivation. Substrate is attached to the device package with the aid of epoxy. Sapphire and SiC are the substrates of choice in many GaN HEMTs, but for cost reduction Si substrates are also used in the industry [14]. In high performance GaN HEMTs, where the cost is not the first priority, diamond substrates are used [15].

Source, drain, and gate metal contacts (shown in Figure 1.2) are typically made from highly conductive materials such as Aluminum, Nickel, Titanium, and mostly from Gold (or mixture of the mentioned) [16]. Contacts in GaN HEMTs can be categorized into two groups: gate (Schottky), and source and drain (Ohmic). Source and drain contacts are formed with high temperature annealing of the metal to the device surface; this way contacts penetrate through the barrier layer resulting in low electrical resistance. Gate (Schottky) deposition, on the other hand, is performed at a lower temperature, thus the penetration of the gate structure into the barrier layer is avoided. Minimum Ohmic contact resistance and gate current leakage should be considered in building high quality metal contacts [17].

Other important horizontal structure in GaN HEMTs is the field plate. Introduction of field plates provided significant enhancement in the performance of GaN HEMTs [18]. As device operates, non-uniform electrical field with peak at the drain edge of the gate develops. To reduce this peak, field plates are used to prevent current collapse and impact ionizations. Sometimes, source field plates can be used to shield the gate from drain in order to reduce the feedback time between the drain and the

gate. Furthermore, gate, source, and drain are passivated with Nitride passivation, mostly using Silicon Nitride (SiN).

1.1.2 HEMT Physics

Formation of the electron channel and the properties of the AlGaN/GaN devices are directly related to the material properties of GaN. Electronic band gap, the energy difference between conduction and valence band, is one of these material properties. In general electronic band gap determines the mass of the freely moving electrons and the ability of the material to withstand applied electric field (high break down field). GaN has a very ionic wurtzite crystal structure with a high band gap of E_g = 3.4 eV, which makes it a stronger material compared to GaAs and Si , with band gaps of 1.424 eV and 1.12 eV, respectively [19-21]. Due to its large band gap, GaN is able to operate at higher voltages and higher power densities, as shown in Figure 1.3.

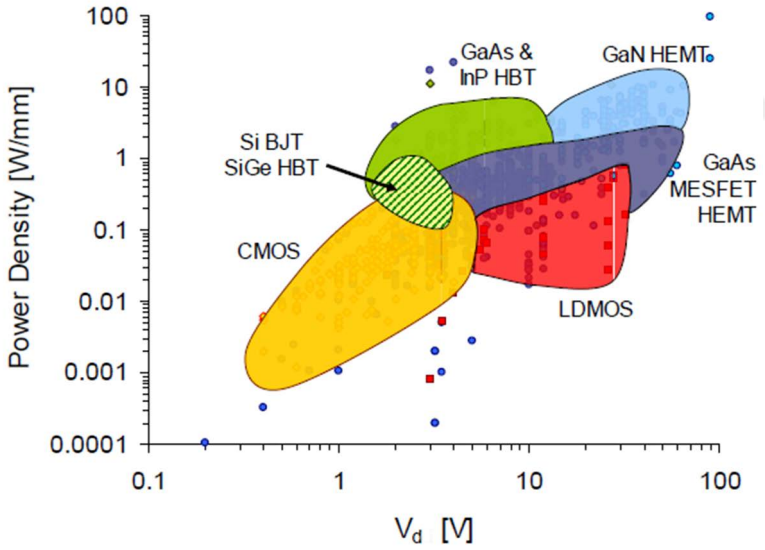

Figure 1.3 Power density vs. supply voltage (V_d) of common transistors [22] .

In zero gate voltage (when the channel is open) electrons flow freely between source and drain contacts in a very thin region called two-dimensional electron gas (2DEG). Formation of 2DEG can be understood by investigating the energy band diagram for the open channel illustrated in Figure 1.4 (of a negatively doped and undoped

AlGaN/GaN heterostructure). As shown in Figure 1.4, Fermi levels of GaN and AlGaN layers are matched in thermal equilibrium and larger band gap of AlGaN introduces a bend in the conduction bands of GaN and AlGaN. Because of this bending, a quantum well is formed in the GaN side of the interface in which the conduction band falls under the Fermi level. This causes electron agglomeration in top of the GaN layer. In doped AlGaN heterostructure electrons from AlGaN layers also fall into the quantum well and get trapped there to provide more electrons in the device [21]. Since 2DEG is located in the undoped GaN layer, the electron mobility is very high due to less scattering by dopants.

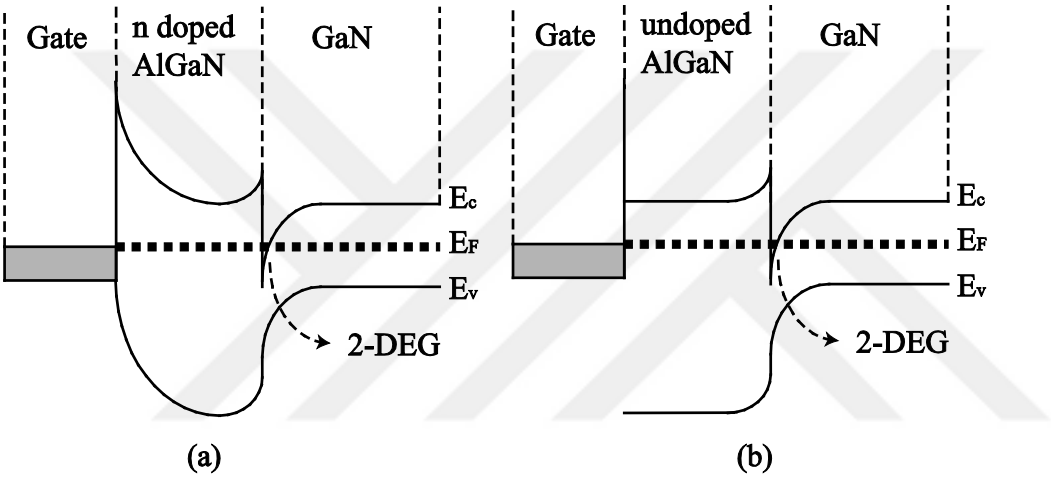

Figure 1.4 2DEG in zero gate voltage in (a) doped and (b) undoped AlGaN consideration.

Figure 1.5(b) presents the simple schematic electrical circuit in GaN HEMTs. Generally, as shown in the Figure 1.5(b), source is considered as ground and the drain (V_{ds}) as well as the gate voltages (V_{gs}) are evaluated based on this ground voltage. Density of carriers in 2DEG is controlled by biasing the gate. As shown in Figure 1.5(a), which is the schematic view of famous $I_{ds} - V_{ds}$ curve, reverse biasing the gate ($V_{gs} < 0$) decrease the depth of quantum well, and consequently the current decreases in the 2DEG. When the reverse bias reaches a sufficiently high value (called pinch or cut-off voltage, $V_{gs} = V_{Pinch}$), current stops between the drain and source. It should be mentioned that electrons move from source to the drain, but the positive current is from drain to the source. As the device operates, due to the Joule heating, heat generation occurs in the device with the value of $P = I_{ds} \cdot V_{ds}$. Power density

characterization is more common in GaN HEMT studies which can be evaluated by dividing the amount of power by the value of gate width, or gate periphery. Commercial GaN HEMTs are able to sustain power densities no more than 2 to 4 W/mm [23].

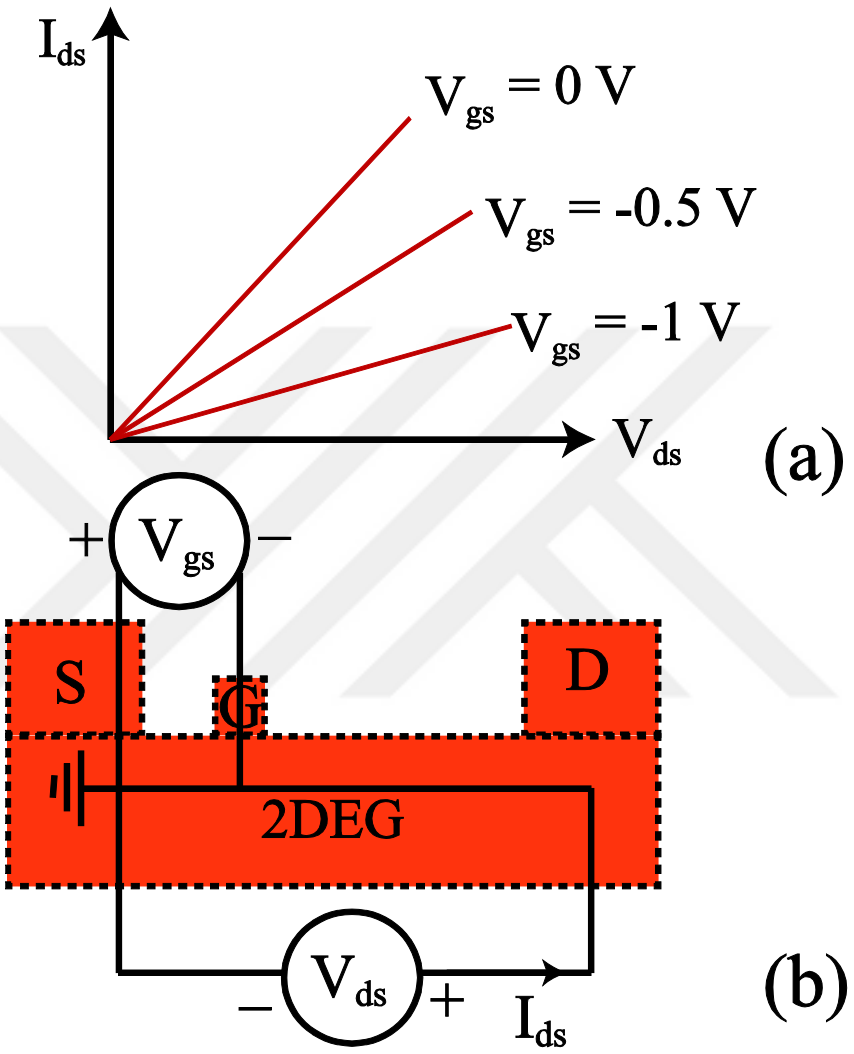

Figure 1.5. (a) Schematic I_{ds}-V_{ds} curve in different gate bias (V_{gs}). (b) Simplified schematic of circuit in HEMTs.

GaN HEMT possess relatively lower power added efficiencies in comparison with Indium phosphide (InP) and GaAs technologies [24]. This is due to higher resistances in GaN HEMTs, however ability to sustain higher voltages brings overall efficiency of GaN HEMTs to the top among RF transistors [10]. Unique channel control

mechanism in GaN HEMTs introduce less noise to the system. In addition, GaN HEMTs have lower capacitance, which can help achieving higher bandwidths. In conclusion, it can be stated that high power, high efficiency, high bandwidth, and low noise are the key electrical features of GaN HEMTs that put them in the spotlight among similar technologies.

In addition to its high breakdown field, GaN transistors benefit from high saturation velocity of the GaN crystals. Saturation velocity is the highest velocity a charge carrier can attain in the presence of high enough electrical field. To move these carriers an electrical field is essential. In the presence of an electrical field carriers gain velocity, which is the most important parameter that affects the rate of charge flow in the GaN crystals. This velocity can be evaluated by the knowledge of the field strength (that depends on the device operation condition) and the **mobility of the electrons** in the crystal (which is related to the properties of the crystal and its temperature). Electron mobility generally decreases by increasing doping density in the crystal [25]. As shown in the Figure 1.6, GaN has higher saturated electron velocity in comparison to other common semiconductors of microwave devices [26].

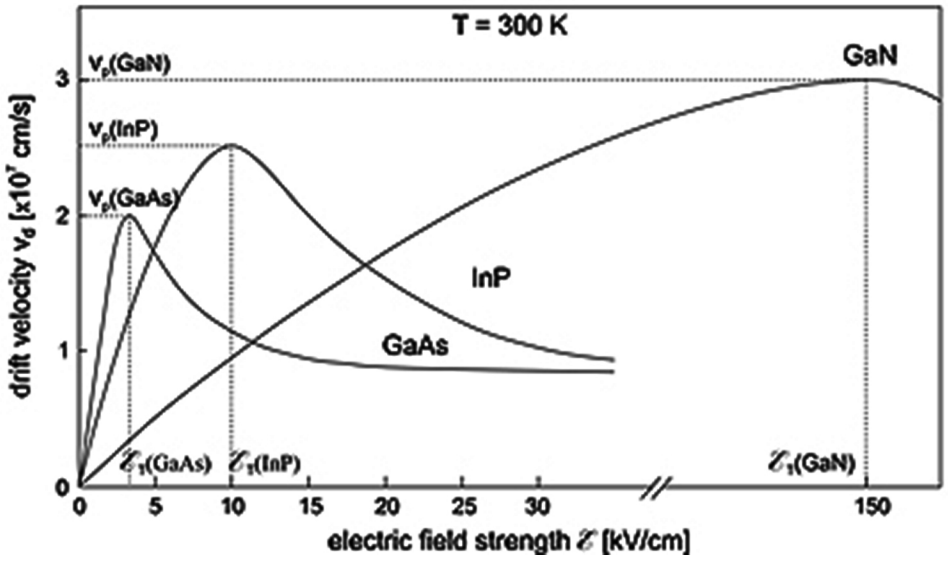

Figure 1.6 Carrier velocity dependency to the field intensity of common semiconductors used in microwave industry [26, 27].

1.1.3 Current Technology

Gate is the most important horizontal structure, which controls the device function. The smaller the gate length, the faster the device. Presented as l_g in Figure 1.7(a), gate length of 0.1 to 0.5 μm is typically used in GaN HEMT fabrication. Figure 1.7(b)

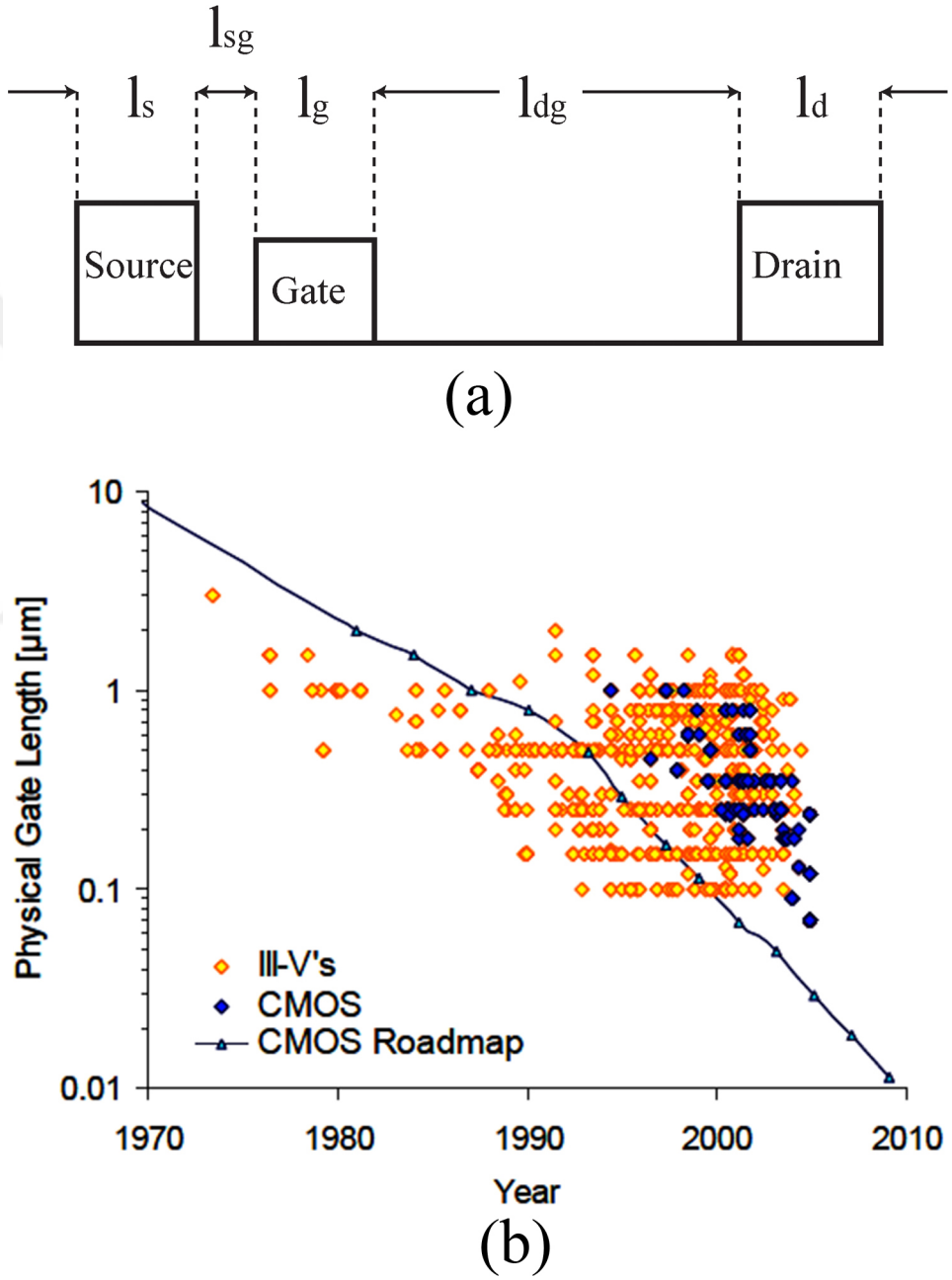

Figure 1.7 (a) Geometrical characterization of horizontal structure. (b) Gate length change in FET and CMOS transistors [22].

shows the gate size reduction in transistors in recent years.

The drain to gate spacing shown as l_{dg} in Figure 1.7(a) is of particular importance to the power output of device. Device with longer l_{dg} can deliver higher voltages, yet their power dissipation and self-heating increase because of resistance increase. Longer l_{dg} is preferred for high voltage and shorter l_{dg} is preferred for high speed and RF efficient applications. Source to gate spacing l_{sg} is typically shorter than l_{dg}. Overall 3 to 8 μm total drain-source spacing (l_{dg} + l_{sg} + l_g) is common in device fabrication.

Increasing need for high power GaN HEMTs makes it necessary to fabricated high thermal conductive devices to dissipate heat more effectively from heat generation zones. This issue resulted in fabrication of GaN HEMTs using substrates with high thermal conductivities like diamond. GaN-on-diamond is a relatively new technology with numerous concerns about its fabrication process. Silicon Carbide is another high thermal conductive substrate that have desirable properties for GaN HEMT production. It is good electrical insulator and possesses small lattice mismatch to GaN, and offers higher thermal conductivity, compared to Si or sapphire substrates [28].

First problem with diamond substrates is their difficult fabrication compared to SiC technology. Due to different crystallographic states of GaN and diamond, challenges exist in integration of GaN-on-diamond substrate. GaN and poly crystal diamond (PCD) can be integrated either by wafer bonding [29], or diamond growth on GaN buffer layer [30]. Additionally, GaN epilayers can grow on significantly high thermal conductive single crystal diamonds (SCD) [31], however GaN-on-PCD integration is preferred due to scalability [32, 33]. However, PCD is a material with slight higher thermal conductivity than SiC, and in the mean time with significant higher price.

Next issue in GaN HEMT fabrication is the TBR. In all mentioned integration processes, acoustic mismatch between materials, defects in near nucleation regions, and nucleation/bonding layer itself build a thermal barrier between GaN and

substrate, known as TBR_{eff} (in direct growth of GaN-on-SCD strain relievers are also responsible for boundary resistance [34]). Since GaN-on-SiC is more developed technology, commercial devices with low TBR_{eff} are available. However, higher TBR_{eff} in GaN-on-diamond devices can question their superiority over GaN-on-SiC.

Both academic and commercial developers are aiming to develop more reliable GaN HEMTs with higher power and frequency performance. Beside the project which this thesis is based on (METU-BAP with grant no of BAP-08-11-2015-028 and the TUBITAK with grant no of 115E756), Defense Advanced Research Agency (DARPA) of United states [35], New Energy and Industrial Technology Development Organization of Japan [36] , European joint Research and Technology project Key Organization [37], and European Space Agency[38] have funded great project about development of GaN microwave electronics.

1.2 Thermal Issues

As HEMTs performance converges to the desired application levels, the importance of their reliability and life-time increases [39]. As electronic devices work, irreversible degradations occur in the device structure. Some of these degradation mechanisms are temperature dependent and temperature rise speeds up their occurrence. This increases the failure rate and decreases the reliability of electronic devices [40, 41]. HEMT function is based on exciting carriers by external electrical field, created by biasing transistor contacts. The excited carriers transfer their energy to the semiconductor lattice, which increases the device temperature. This phenomenon is known as Joule heating effect. Figure 1.8 shows the infrared temperature measurement of the device from top view. As is can be seen in the Figure 1.8, the heat generation is concentrated along each gate (finger) of the device. Depending on the desired electrical output, GaN HEMTs can be fabricated in two or multi-finger design, as shown in Figure 1.8(a) and (b).

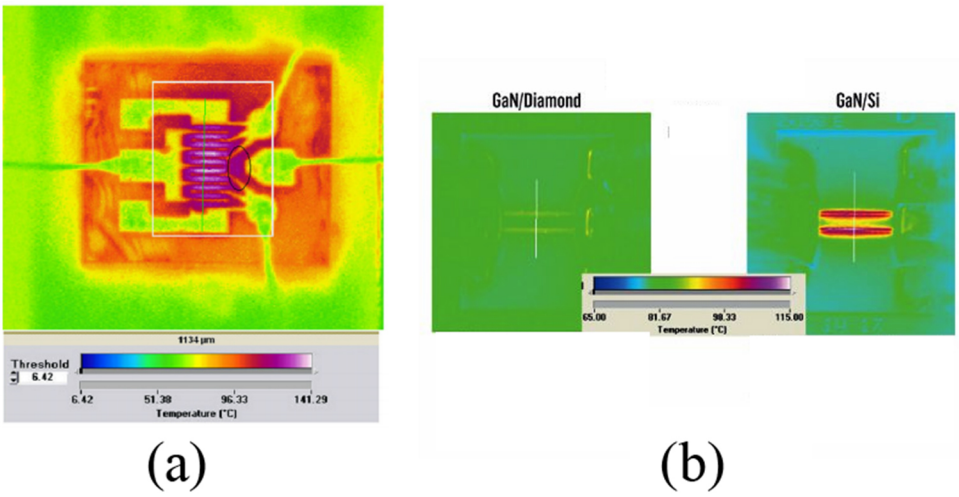

Figure 1.8 IR temperature map of (a) multi-finger [42] and (b) two-finger AlGaN/GaN HEMT [43].

Highest temperatures in devices are observed at localized self-heating zones called hotspots [44]. Hotspots occur in the drain edge of the gate in the 2DEG. HEMTs exhibit excellent reliability in low-frequency applications in normal hotspot temperatures (150-250 °C) as reported in [45, 46]. Outstanding values of mean time to failure (MTTF) of 10^7 hours in the hotspot temperature of 150 °C [47] and 10^6 hours in 200 °C [46] are obtained in accelerated DC life test in low frequency application. As it was mentioned before, global GaN market is mostly driven by the military demands. As shown in the Figure 1.1, GaN HEMTs used in the military applications need higher frequency and more power. Consequently, as stated by Mark J. Rosker, DARPA's representative, reliability of these devices is questioned since they function in hotspot temperatures above 300 °C.

Figure 1.9 shows the study of MTTF of TriQuint (name of the manufacturer [48]) HEMTs in different junction temperatures, conducted by DARPA, which studied the reliability of HEMTs for the high-frequency application in both DC and RF life test [49]. As shown in Figure 1.9 semi-exponential dependency of MTTF to the channel temperature of the device implies that even a small reduction in channel temperature can result in significant increase in the life time of the device.

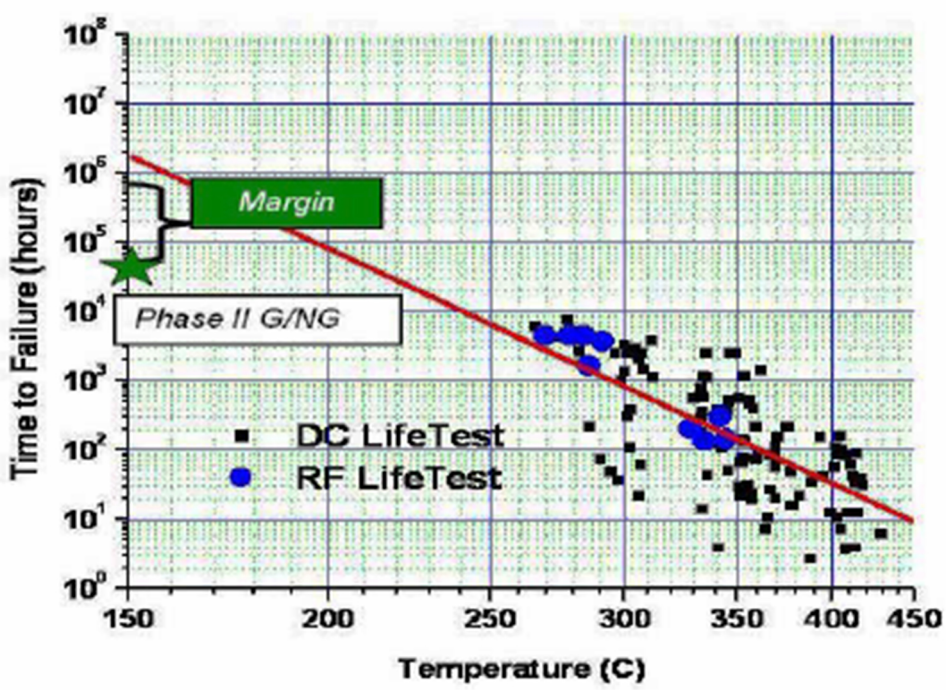

Figure 1.9 MTTF projection of TriQuint HEMTs [49]

Based on the arguments explored above, it can be stated that future market of GaN HEMTs depends on fabricating high power and, in the same time, reliable operating devices. Temperature control is among the major concerns, determining the reliability of the GaN HEMTs. Accordingly, accurate thermal characterization is needed [50, 51]. This highlights the importance of accurate thermal modeling of GaN HEMTs, which is required to characterize the thermal behavior of the devices and to investigate the possible thermal control techniques.

1.3 Thermal Characterization

Thermal characterization attempts can be classified into two groups: Experimental and theoretical. Experimental characterization of HEMT temperatures can be performed with techniques such as the infrared cameras [52], liquid crystal thermography [53], micro-Raman thermography [54], photoluminescence [55], transient thermo-reflectance [56], and pulsed current vs. voltage measurement methods [57]. Most of these techniques have high costs and limited spatial and/or temperature resolutions, hindering the precise quantification of the hotspot

temperature [58]. At its best, Riedel et al. [59] reported spatial, temporal, and thermal resolution of Raman thermography to be 0.5 μm ,10 ns, and ±5 K, respectively. Also there are reports of enhanced thermoreflectance measurement with 10 mK thermal resolution [60], and 10 ns temporal resolution in submicron imaging [61, 62]. Although, experimental techniques are improving, there is still a need for alternative methods due to their high cost and limited characterization accuracy of extremely small hotspot with reported critical size of 50 nm [63] to 500 nm [64]. Limitations and expenses of experimental techniques underlines the need for correct, detailed, and also efficient thermal modeling of GaN HEMTs [65]. Theoretical modeling of GaN HEMTs includes analytical [66], semi-analytical [67], and numerical [68] approaches.

Theoretical thermal models of GaN HEMTs are mainly based on steady state Fourier's heat diffusion equation:

$$\frac{\partial}{\partial x}\left[k_x \frac{\partial T}{\partial x}\right]+\frac{\partial}{\partial y}\left[k_y \frac{\partial T}{\partial y}\right]+\frac{\partial}{\partial z}\left[k_z \frac{\partial T}{\partial z}\right]+\dot{q}=0 \qquad (1.1)$$

In which $k_{i=(x,y,z)}$ is the thermal conductivity of device in different directions, T is the temperature and $\dot{q}$ is the heat source value that represents Joule heating in the device. Although equation 1.1 is the famous steady state heat diffusion equation, however as we are going to discuss later, challenges, controversies and uncertainties exist in the theoretical thermal models of GaN HEMTs.

For the solution of equation 1.1 to predict the device temperature analytical and numerical approaches were developed. Analytical thermal models of GaN HEMTs are based on the calculation of spreading and one-dimensional thermal resistances of the device. Since spreading thermal resistance occurs in the first 100 μm from the 2-DEG [69], analytical thermal models mostly include GaN and the substrate layers and in some cases, TBR in between these layers. Analytical approaches neglects the presence of other structures in the device geometry by assuming simple shapes for

the device. In addition, analytical thermal models make use of constant thermal conductivities and simple boundary conditions. Modeling detailed structures and/or boundary conditions by analytical approaches introduce additional complexity to the solutions. Thus, too complicated analytical solutions hinder their practicality [70].

A. M. Darwish *et al.* [71] developed closed form approximate expressions of thermal resistances of multi-finger GaN HEMT and obtained results for SiC, Si, and sapphire substrates in different geometrical considerations. The model presented acceptable agreement with experimental observations of M. Kuball *et al.* [54]. In addition, the analytical results were in good agreement with numerical results obtained from ANSYS. Despite simplicity of the solution, one of the main problems in this research was neglecting the TBR between GaN layer and the substrate. Presence of this thermal barrier alters the spreading thermal resistance of the device significantly. Without considering this important parameter, the solution presented in this paper can face great inaccuracy issues. In addition, using closed from expressions instead of Fourier series summation, can be the source of further inaccuracies in the extreme or unusual geometrical considerations.

Y. Muzychka *et al.* [72] presented more general analytical solution which evaluates thermal spreading resistance in compound orthotropic systems with interfacial resistance in between, using the separation of variables. This research is specifically conducted for heat transfer in electronics devices and is the extensions of previous existing solutions of Y. Muzychka and others in previously published works [73, 74]. This research provides Fourier series summation solution for two solid layers with TBR in between, which is the general problem in GaN HEMTs. As mentioned before, since spreading thermal resistance ends after 100 µm from the top, the solution of this research is the best match for GaN HEMT analysis. Cooperation of Y. Muzychka and K. R. Bagnall [75] resulted in more general solution for thermal spreading resistance in compound orthotropic systems with interfacial thermal resistance in between. This solution combines the Fourier summation solution presented in [72] with the influence coefficient method introduced by Y. Muzychka [76] in order to extend it for characterization of multi-finger GaN HEMTs. After this

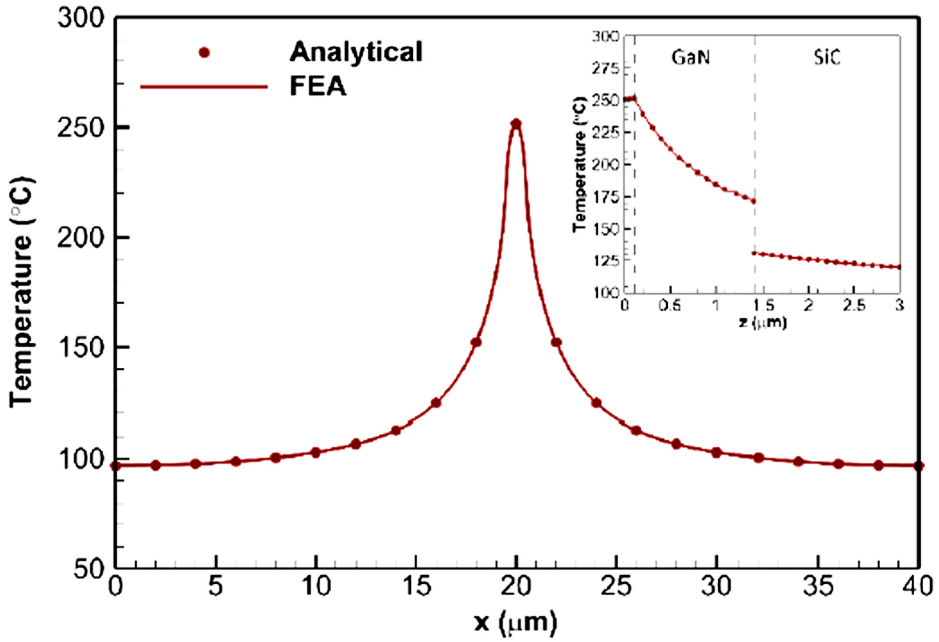

Figure 1.10 Temperature profile at the hotspot analytical and numerical 3D GaN HEMT model computed by the analytical solution and FEA model [70]

research, Y. Muzychka and K. R. Bagnall extended their solution even further, for multilayered structures (more than two layers) [77] and based on this research, specified solutions were obtained for GaN HEMTs in their next paper [70]. Sample verification results of this research is shown in Figure 1.10. The closed-form analytical solution presented in these researches can be important for other researches topics of other thermal sciences, but is unnecessarily complex for thermal characterization of GaN HEMTs. Diminishing spreading effects in less than 100 μm from 2DEG, narrows the need of analytical solution for GaN and substrate layer with TBR in between only. Thus, accurate solution provided in [72] is sufficient for analytical thermal characterization of a 2-finger GaN HEMT, and can be extended for multi-finger GaN HEMTs using the influence coefficient method presented in [76].

While analytical approaches are preferred for device optimization studies, numerical thermal modeling is used mainly for more accurate thermal characterization of the

HEMTs. Accommodation of multiscale geometries with temperature dependent material properties, and more importantly ability to import realistic heat generation distribution are some of the advantages of numerical simulations.

E. Douglas *et al.* [78] modeled a simple GaN-on-substrate structure with neglecting other geometrical structures shown in Figure 1.2 using finite element method. The effects of temperature dependent substrate materials, size of the die, and finger numbers were examined. In addition, 2D and 3D simulations were compared. Deviation in peak temperatures between 2D and 3D simulations was reported and, using 3D thermal analysis was suggested for accurate MTTF predictions.

In a similar manner, F. Bertoluzza *et al.* [79] discussed substrate material, finger characterization, the presence of passivation, and the cooling strategies in both time dependent and steady state 3D finite element thermal simulation of GaN HEMTs. With similar results to [78], importance of 3D modeling is stated. The time dependent study revealed the thermal behavior dominance of structures above GaN in short time ranges, while the substrate has little or no effect on self-heating in this case. Passivation layer found to have negligible effect in this research and importance of considering spreading thermal resistance in designing cooling strategies is highlighted.

In above numerical models (also in all of the analytical models) $\dot{q}$ in Eq.1.1 is assumed to have uniform density in the heat generation region. However, in real device operation heat is generated non-uniformly along the channel, depending on the electrical bias condition of the device [80]. In addition to the bias condition, presence of field plate can alter distribution of generated heat, which previous models are unable to characterize. As shown in Figure 1.11, in order to capture the heat generation variation effects on thermal response of the device, researchers like Heller *et al.* [58, 81] and Donmezer *et al.* [82] used electro-thermal simulators to capture the heat generation variations and later, to import it to the typical numerical thermal analysis models.

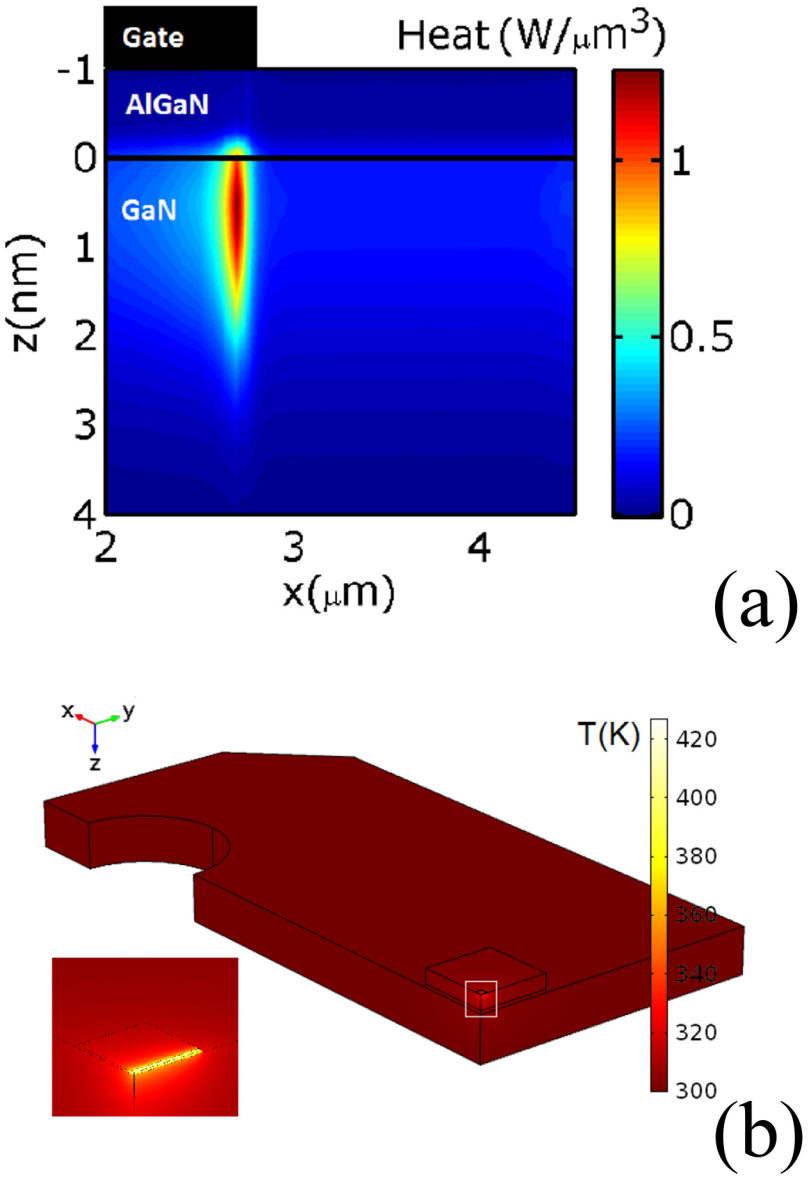

Figure 1.11 (a) Realistic Joule heating distribution of the device (b) Surface temperature profile of the device obtained using numerical simulations [44].

Heller *et al.* [81] characterized channel temperature of field plated, and non-field plated GaN HEMT using electro thermal simulation and verified the results by Raman spectroscopy. At the same power density, the importance of bias condition in temperature characterization is explained. High drain source voltage found to cause higher hotspot temperatures in the device. It was also stated that industry must

reconsider their accelerated life tests bias condition to find more applicable and reliable MTTF results.

In a similar manner Donmezer *et al.* [82] developed an electro thermal model by solving the gray phonon BTE and coupling it to the numerical heat diffusion solver (using COMSOL Multiphysics) for hotspot temperature prediction of GaN HEMTs. In this study, effect of different substrate layers were also considered. This research showed that the heat generation region occurs in nano meter size regions in the drain edge of the gate in 2DEG. Effect of considering different substrates were analysed and various heat dissipation mechanism were discussed. Similar results were also obtained by Hosch *et al.* [83] by using micro Raman and electro thermal simulators and in a similar manner, but with micro Raman technique only, by Choi *et al.* [84].

Although the four latest approaches explained, are considered more detailed and accurate methods for thermal characterization of GaN HEMTs, concerns exist about their validity [23, 79]. Limit of electro thermal solvers to 2D geometries, uncertainties in numerical convergence of solving Poisson's, current continuity, and heat conduction equation in the same time, and nonlinearities introduced by sharp changes in electron concentration and geometries are three reasons for skepticisms.

1.4 Motivation and Outline

As stated in the second section of this chapter, thermal characterization of GaN HEMTs is necessary part of developing reliable devices for high power applications. Increasing demand for higher power transistors cannot be answered unless the reliability concerns reduced by better thermal engineering of these devices. During our literature review, we have faced wide range of controversies in previous thermal modeling approaches of GaN HEMTs and realized the need to introduce a roadmap for the future thermal models of this field. We also realized that due to computational cost of numerical techniques, researchers and electro thermal simulators utilized 2D modeling techniques, which turn out to be not accurate. These topics are covered in second chapter of this thesis.

Due to high computational cost of numerical simulations, in the third chapter, an analytical approach is presented to evaluate thermal resistance of the multiscale device. For the first time, thermal characterization of die-on-package structure is formulated in one place. In chapter four, the numerical approach presented in the third chapter is used for the enhancement of 2D numerical models. Significant over-estimation of 2D thermal models and high computational cost of electro thermal and thermal simulations makes it necessary to calibrate 2D models. Based on analytical investigation of thermal resistance of the device in 2D and 3D geometries, a novel correction method is introduced for calibration of the 2D models. Next, the correction method is tested and verified with 3D numerical models.

Substrate selection is important issue in thermal control of GaN HEMTs. Comprehensive comparison is not performed over substrate selection between SiC and diamond substrates. Thus, in chapter five, a parametric study is performed for the substrate selection using the analytical procedure of the third chapter. Previous thermal performance comparisons of GaN-on-SiC (substrate of choice) and GaN-on-diamond (new technology) devices are limited to devices with identical geometry due to modeling and experimental limitations. Lastly, the important results of this thesis and future research is highlighted in the sixth chapter.

CHAPTER 2

NUMERICAL THERMAL MODELLING OF ALGAN/GAN HEMTS

As discussed in the previous chapter, it is realized that accurate thermal characterization of GaN HEMTs is necessary to understand device reliability in different operational conditions. Limited accuracy and high cost of experimental techniques highlight the importance of theoretical models. In the past, many researchers preferred to use numerical software for the development of thermal models of GaN HEMTs. When these models are compared with each other, variety of different assumptions and techniques are observed.

First and major difference of the different thermal models is their *dimensionality*. Due to computational expense of 3D models, some researchers used computationally efficient 2D approaches [85]. Two-dimensional modeling is also common in finite element electro thermal simulation software like Synopsys and Silvaco where the computational cost of 3D models are excessively high [86, 87]. However, when the results are compared up to 75% difference in the temperature predictions of 2D and 3D models has been reported [79]. Such differences stem from both the difference in the one-dimensional thermal resistance of these models (due to cross sectional areas difference of 2D and 3D geometries) and the neglected thermal spreading resistance along the third dimension in 2D models [23, 74, 78, 79, 88].

Next major difference is the *definition of the heat source*, which represents the Joule heating in the device. While researchers like Heller *et al*. [58, 81] and Donmezer *et al*. [82] used realistic Joule heating data obtained from electro thermal simulations, others used uniform rectangular heat generation regions [79, 88] or surface heat flux [89] in their thermal models. While literature presents variety of assumption in the size and shape of the heat source modeling, comparisons have not been performed and no general rule has been stated for the accurate modeling of devices [23].

Other important difference between thermal models is related to the choice of *thermal properties of materials*. For example, while some thermal models used temperature dependent material properties, others used constant thermal properties [90]. Although, it is known that the implementation of temperature dependent thermal conductivities is required for more accurate analysis of the devices, its importance on the hotspot has not been quantified and simplifications based on the temperature dependent properties has not been discussed. Moreover, the effect of effective thermal boundary resistance (TBR) between the GaN and the substrate [91, 92] is ignored in some models [90].

Finally, when different models are analyzed it was observed that the effects of *natural convection and radiation* on the heat removal from the devices have not been analyzed in detail. Although few researchers including Douglas, *et al.* [78] mentioned implementation of natural convection boundary condition in their simulations there is not enough discussion in the literature about the relative effects of natural convection and radiative heat dissipation mechanisms from HEMTs.

In this chapter, after the introduction of the device geometry and the device modeling approach, complete discussion of the effects of the different assumptions in thermal models is performed. These major diversities of previous thermal models are listed and their relative effects on the device temperature are discussed to provide a roadmap for the future thermal models of GaN HEMTs.

2.1 Approach and Geometry of the Device

To analyze different modeling techniques and to provide a roadmap that covers previous diversities in the literature, a simple 2-finger GaN HEMT device is chosen. For this purpose, a conventional 2-finger GaN HEMT as shown in the Figure 2.1 is used in the simulations. Two and three-dimensional thermal simulations of the device are performed using COMSOL Multiphysics with the aid of heat transfer module in solids to solve the steady state heat conduction equation to examine the effect of

different boundary conditions, heat source size, TBR, and t*emperature dependent thermal properties*. Due to the symmetry of the device and its boundary conditions,

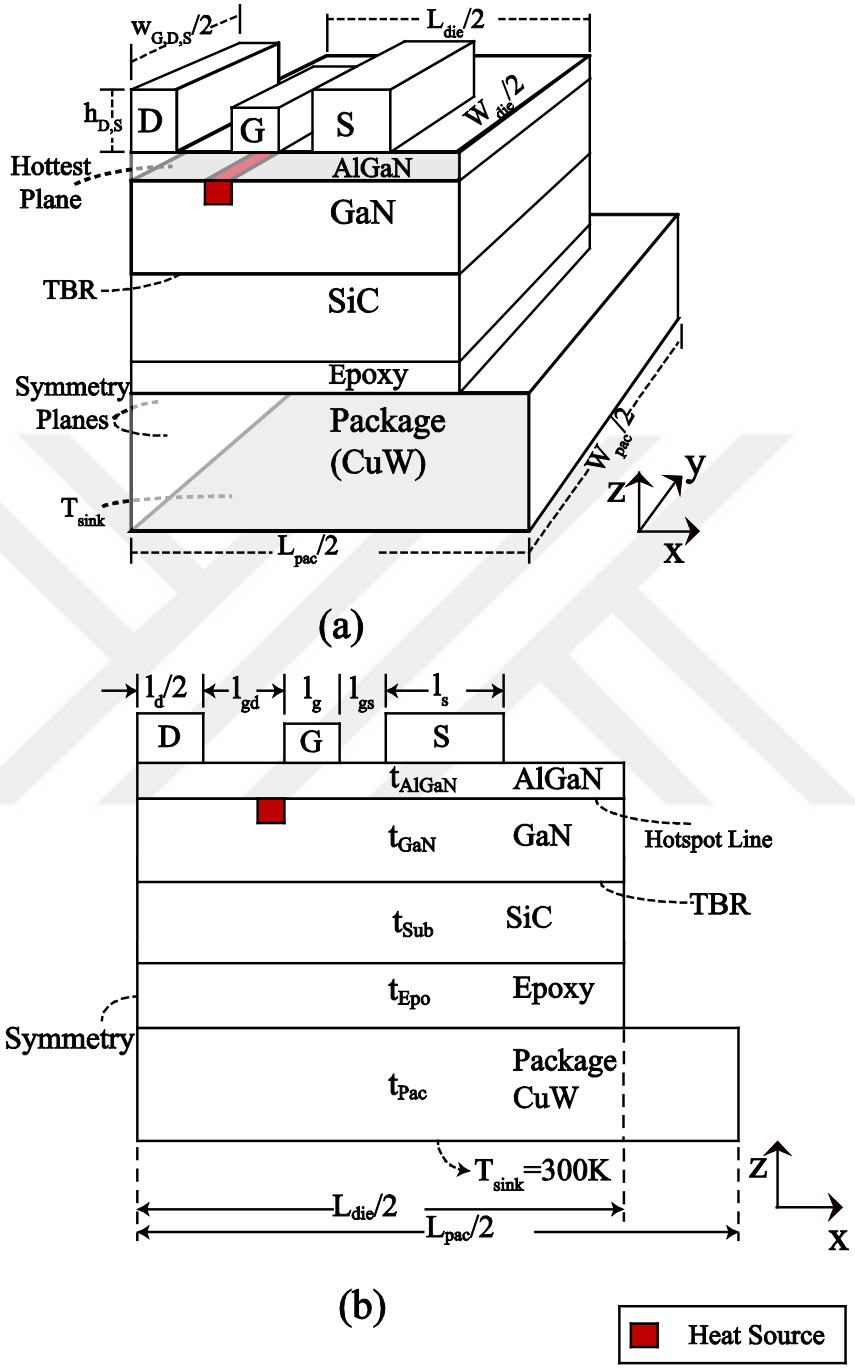

Figure 2.1 (a) The quarter of the HEMT device model used in 3D thermal simulations. (b) The cross-sectional view of the 3D model and the device model used in 2D thermal simulations.

only the quarter of the device shown in the Figure 2.1(a) is used in 3D thermal simulations. Figure 2.1(b) is the 2D representation of the 3D model that also we can see in the literature. As shown in Figure 2.1(a) 200 µm × 400 µm GaN-on-SiC die is mounted on a 6 mm × 9 mm Copper Tungsten (CuW) package using epoxy. Thickness of the GaN, SiC, epoxy and CuW are taken as t_{GaN} = 3 µm, t_{Epo} = 20 µm, t_{Sub} = 200 µm [93, 94], ,t_{Pac} = 1 mm, respectively. The lengths of the drain and source metal contacts represented as D and S in Figure 2.1(b) are both taken as $l_d = l_s$ = 25 µm while the gate length is taken as l_g = 0.4 µm. The drain-gate spacing and the source-gate spacing, shown in Figure 2.1(b) are taken as l_{gd} = 2.8 µm and l_{gs} = 0.8 µm, respectively. The die is positioned at the center of the package. Other device parameters are shown in Figure .2.1(a) such as TBR size and shape of the heat source, boundary conditions, and metal contacts.

Joule heating in the device is modeled both with surface heat flux and with volumetric heat source assumption. Detailed study of heat source characterization effect on device self-heating is presented in the section 2.2. Thermal boundary resistance is applied between GaN and the substrate layer as shown in Figure 2.1, and detailed study about its effect is provided in the section 2.2 Bottom surface/boundary of the device is assumed to be perfect heat sink with T_{Sink} = 300 K. Other surface/boundaries are assumed adiabatic, except in the Section 2.3 where the effect of radiative and convective boundary conditions are discussed. Table 2-1 presents the

Table 2-1 Temperature dependent and constant thermal conductivities at T = 300 K of materials used in thermal simulations.

Material	$k_{Material}$ (W/mK)	$k\|_{T=300\ K}$(W/mK)
$Al_{0.29}Ga_{0.71}N$	30 [95]	30
GaN	$267 - 0.425T + 3\times10^{-4}T^2$ [96]	166
SiC	$387(T/293)^{-1.49}$ [97]	373.6
Epoxy	50 [98]	50
CuW	$204 - 0.0251T - 7.62 \times 10^{-5}T^2$ [94]	189.6

temperature dependent thermal conductivity of the materials used in these simulations. Effect of thermal conductivity of the materials in accurate thermal characterization of the device is provided in the Section 2.4, and lastly 2D and 3D models are compared in Section 2.5.

Finite element meshing the device structure is of the important factors in the correct modeling of the GaN HEMTs. Due to small size of the heat generation region, very small elements are required to be structured in this region and its surrounding. To eliminate the excessive memory requirement, a careful growth of mesh is necessary from the heat source region to outer regions. The details of the tetrahedral mesh is shown in Figure 2.2. For the 3D geometry mesh independent results require more than 2.5 million elements in the simulations in 2-finger device modeling. In 2D modeling, however, ten-fold reduction in the required element number can be

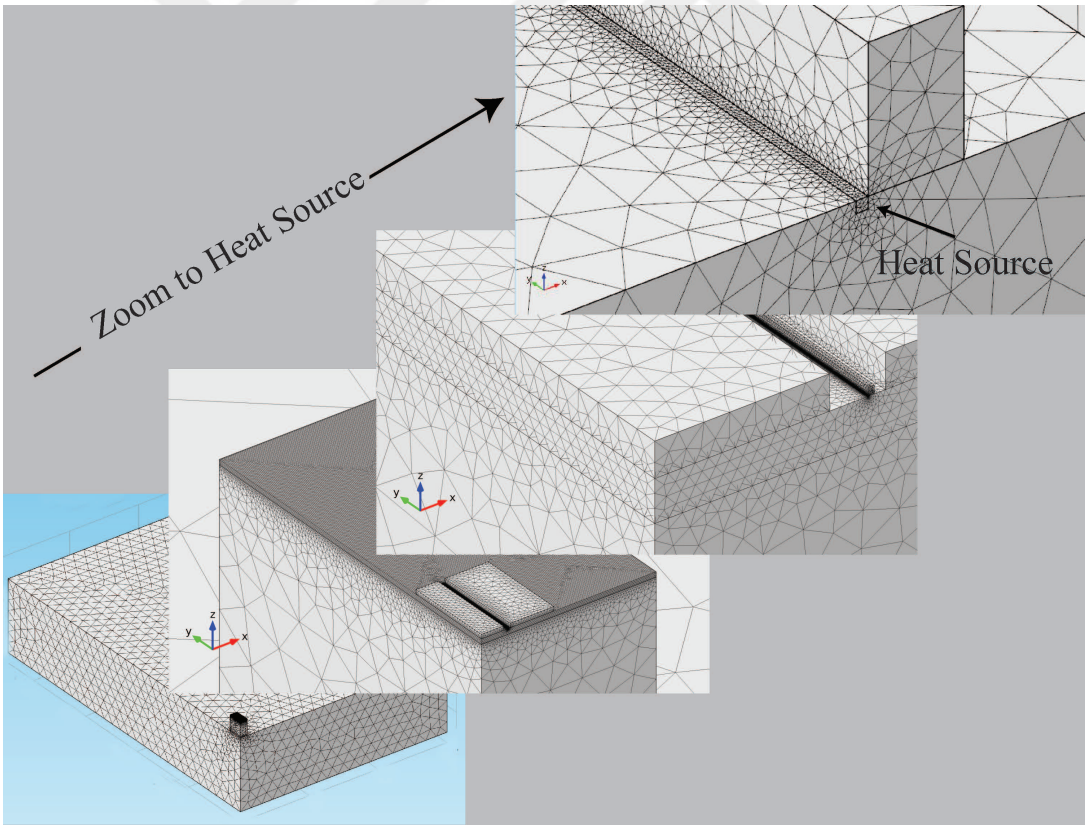

Figure 2.2 Meshing of the geometry in different zoom views toward heat source.

achieved. Our mesh independency tests revealed that meshing GaN layer (particularly near the heat generation region) is critical to capture heat spreading effects adequately.

2.2 Joule Heating and TBR

When HEMTs operate, it is often not possible to observe a uniform heat generation in the channel due to the non-uniform electrical field distribution. Thus, different biasing condition results in different heat generation distribution. To visualize the heat generation in different biasing condition, heat generation data from electro thermal solver is presented in Figure 2.3. The data is obtained from ongoing research project with cooperation of Doğacan Kara (Master student, Department of Mechanical Engineering, METU) who has provided the electro thermal data. Geometrical changes in this Section are as follows: $l_d = l_s = 37$ µm, $l_g = 0.4$ µm $l_{gd} = 2.8$ µm and $l_{gs} = 0.8$ µm, since the Sentarus simulations were done based on these values.

To compare only the effect of distribution of the heat generations in different biasing conditions, devices operated at same power densities can be modeled. By plotting the I_{ds} - V_{ds} curve and finding the cross sectional points with the constant power dissipation lines, bias conditions with similar power dissipation values can be evaluated. Heat generation distributions later can be obtained based on these biasing conditions point.

In open gate bias condition, electrical field and consequently heat generation is more uniform whereas near device pinch-off the heat generation is concentrated as shown in Figure 2.3. Thus, open gate ($V_{gs} = 0$, $V_{ds} = 3$) and near pinch-off ($V_{gs} = -3$, $V_{gs} = 9.43$) bias conditions are selected for comparison. Effective height of heat generation height is found in between 3 to 7 nm. We have found these values in agreement with previous researches [63, 81, 99, 100].

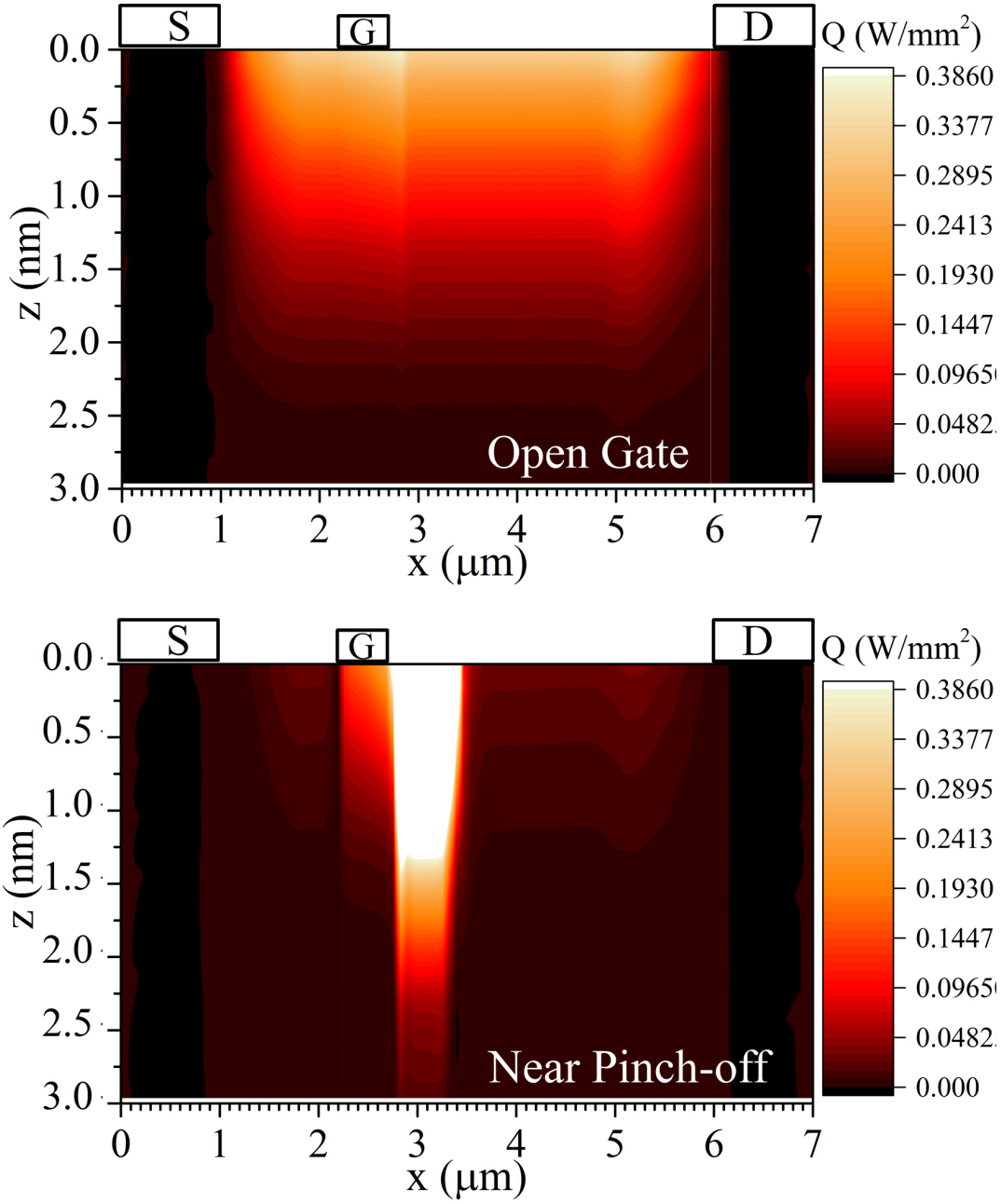

Figure 2.3 Heat generation distribution in open gate (V_{gs} = 0) and near pinch-off (V_{gs} = -3) bias conditions

Heating distribution can change along gate width or y-axis (refer to Figure 2.1), but it was reported that the variation of the heat distribution along the gate width has negligible effect on the thermal behavior of the devices [58]. As we can see in Figure 2.3, nano scale heat generation distribution is changing abruptly in z-direction. This distribution cannot be integrated to the numerical thermal models due to meshing

issues. Thus, heat generation is weight integrated in the z-direction. Figure 2.4 is the integrated heat generation of Figure 2.3 along the x-axis, obtained using MatLab script.

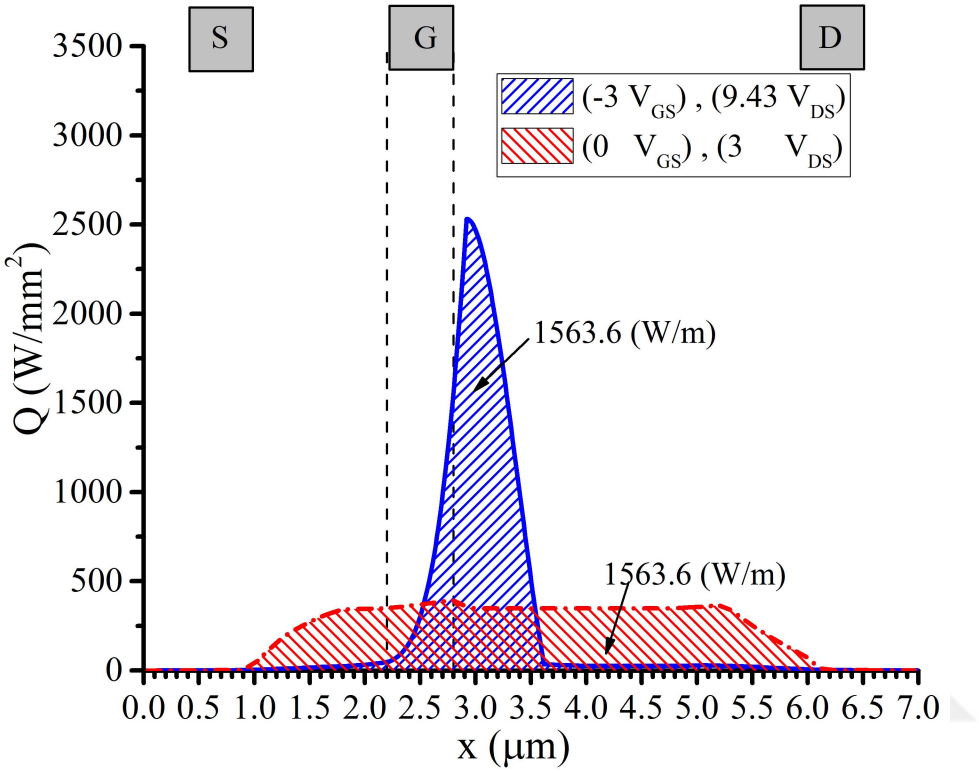

Figure 2.4 Integrated heat generation along x-axis in different bias conditions. Total value of heat generation in each case is provided on the figure.

As we can see in the Figure 2.4, total amount of heat generation in both bias conditions are equal. In absence of electro thermal data, or in analytical modeling, heat generation should be modeled uniformly in constant areas of the device. In order to compare these models with electro thermal models, uniform heat generation with critical size of 50 nm area at the drain edge of the gate [44, 63] is selected as the heat generation size in pinch-off bias condition. This is the lowest reported critical size in the literature that encouraged us to adapt this critical size as the accepted heat generation region size in our studies. For the open gate, modeling constant heat generation is assumed between drain and gate. The geometrical description of each model is (also illustrated in Fig.2.5):

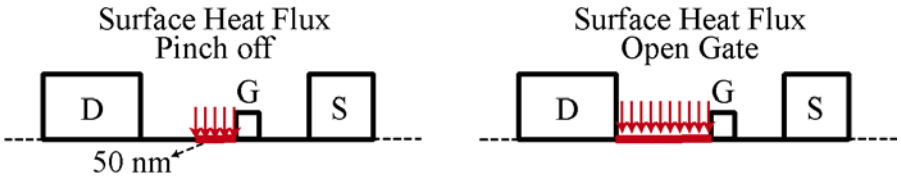

Figure 2.5 uniform surface heat flux assumption to model Joule heating.

1. Heat generation from electro thermal simulations:
    a. Heat generation in open gate bias condition from Figure 2.4.
    b. Heat generation in near pinch-off bias condition from Figure 2.4.
2. Uniform heat generation without using electro thermal simulations:
    a. Nanoscale surface heat flux of 50 nm in the drain edge of the gate adapted from [70], shown in Figure 2.5.
    b. Channel-long heat flux positioned between the source and the adapted from [101], shown in Figure 2.5.

Figure 2.6 shows the temperature profile comparison along x-axis at the hotspot line (shown in Figure 2.1) between electro thermal and thermal (with uniform heat generation) modeling in open gate and near pinch-off bias. As it can be seen in the Figure 2.6, thermal models with uniform heat generation assumption predict higher hotspot temperatures in comparison to electro thermal models. In near pinch-off, the hotspot temperature rise (ΔT) is predicted as 57.5 °C and 42 °C in thermal and electro thermal approaches, respectively. In open gate consideration, thermal models are predicting approximately same temperature rise with only 3 °C difference. Since the 50 nm area is the lowest critical heat generation length, the predicted results of pure thermal models are higher than the electro thermal simulations. We have found that by changing the heat generation region size in pure thermal model, temperature profiles match the electro thermal models. This suggests that by finding the critical size of heat generation in the desired bias condition of the device (which is often near pinch-off), one can model the 3D thermal simulations or analytical optimization without any need for importing electro thermal models. In narrower channels, the

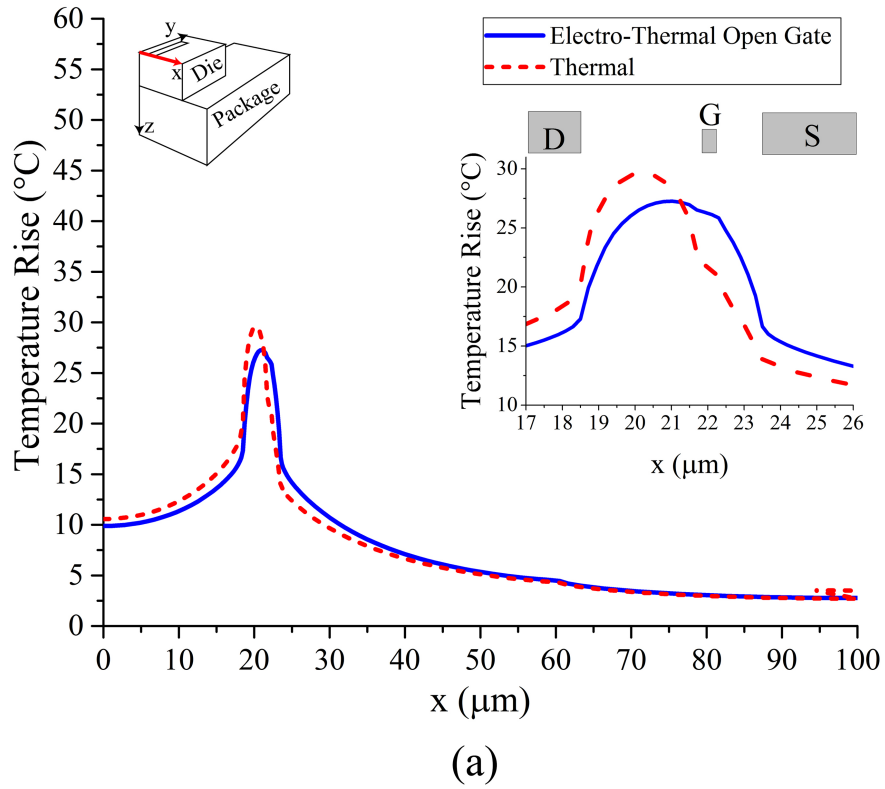

(a)

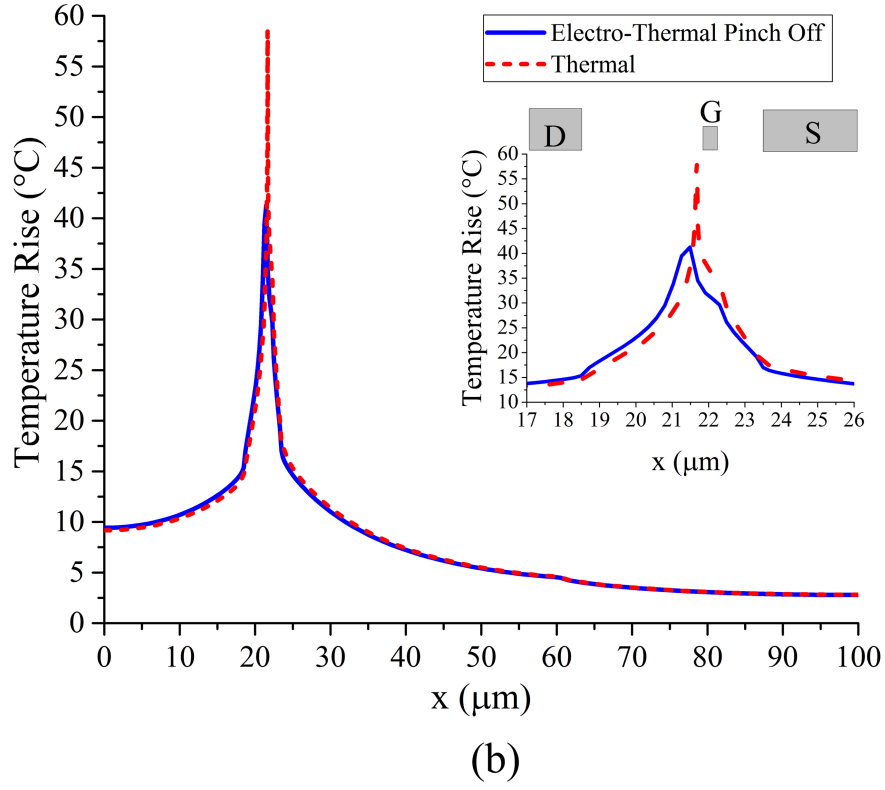

(b)

Figure 2.6 Temperature profile comparison (along x-axis at hotspot line) of electro thermal modeling and pure thermal model in (a) open gate and (b) near pinch-off bias.

heat generation can be more concentrated and its size reach to size of 50 nm, based on the bias condition. The thermal models should consider the most intense heating condition that the device is going to operate, in order to provide accurate assumption for the Joule heating in these bias conditions [81], and due to this reason we use 50 nm critical size in our models. It should be mentioned that difference in temperature distribution in above models is not because of value of the heat generation, but due to the distribution of the heat generation. In open gate model, widespread heat generation causes lower temperature rise in the device, while more localized self-heating near pinch-off condition causes more than 30°C difference in hotspot temperature rise.

Heat generation in GaN HEMTs occur inside the GaN layer volumetrically, however most of the thermal models implement the device heating as heat flux instead of volumetric heat generation. Although there is not enough data about the correct height of heat generation in the literature, we have decided to compare volumetric heat generation regions with surface heat flux assumption based on the generation dimensions introduced in [63]. Thus, two models with different heat generation regions, one with square cross section with of 50 nm, and one with surface heat flux with size of 50 nm are compared as shown in the Figure 2.7.

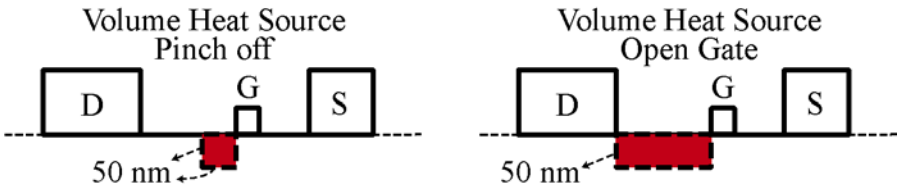

Figure 2.7 Uniform volumetric heat source assumption to model Joule heating.

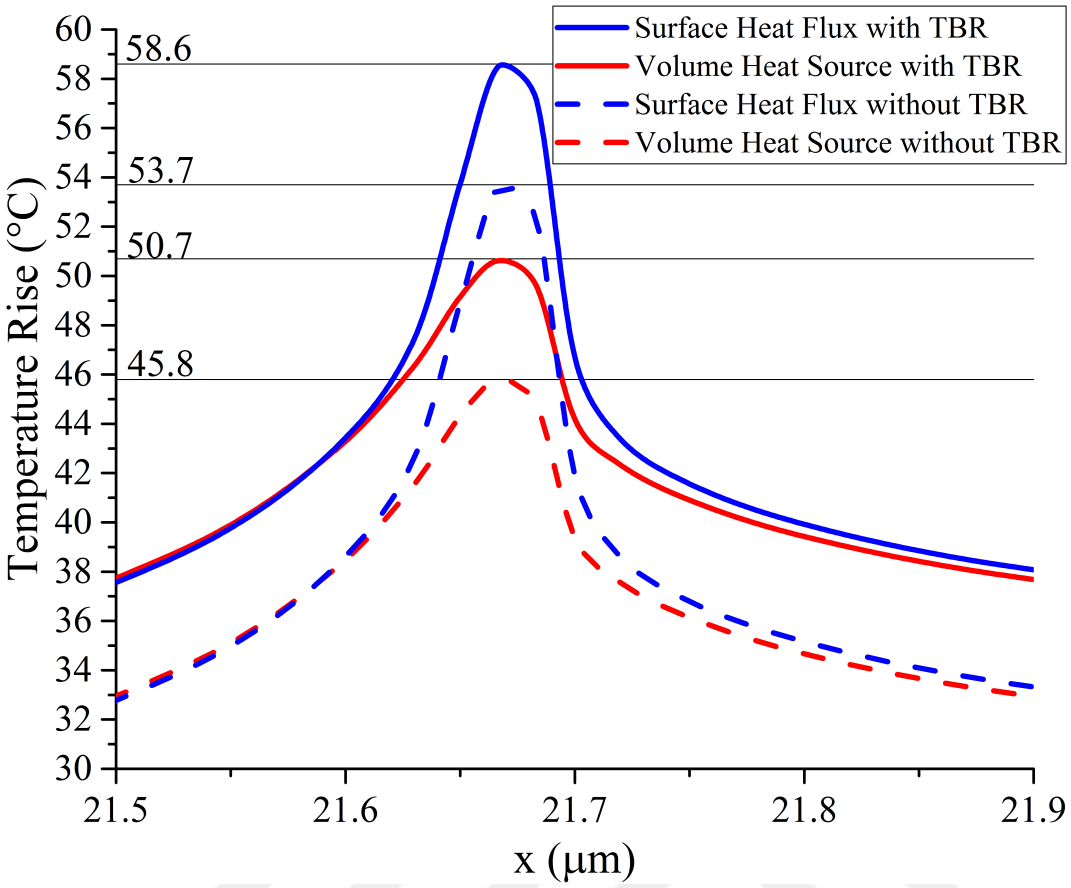

Figure 2.8 Temperature profiles along the hotspot line of the HEMT modeled with surface heat flux with volumetric heat source assumptions. Effect of including TBR is also shown.

Temperature profiles along the hotspot line (shown in Figure 2.1(b)) are presented in Figure 2.8. As seen in the Figure 2.8, surface heat flux and volumetric heat source models follow the same temperature patterns everywhere except the hotspot region, where 15% increase in the hotspot temperature can be seen. This difference is due to increased heat spreading area (top and two sides of the heat source) of the volumetric heat source model. This very important result question the validity of the surface heat flux models in near pinch-of conditions, which is the desired critical condition of the device to study the MTTF of the device. Researchers must consider this temperature over estimation when they use surface heat flux modeling since 15% difference is significant in MTTF studies.

In each of the above heat source models, effect of TBR between the substrate and the GaN layers (as represented in Figure 2.1) is analyzed. Value of the TBR strongly depends on the fabrication details [91]. For instance, reported values of the TBR of AlGaN/GaN HEMTs with SiC substrate varies between $0.1 \cdot 10^{-8}$ m^2K/W [102] to $7 \cdot 10^{-8}$ m^2K/W [54]. It is also reported that the value of the TBR increases by the temperature rise in the devices [103]. In this study TBR is assumed to be constant and equal to $3.3 \cdot 10^{-8}$ m^2K/W [103] to represent an average value.

As shown in Figure 2.8 changing heat source shape alters only the spreading thermal resistance of the device, while TBR changes total thermal resistance. Hotspot temperatures rise decreases by 9% when TBR is taken out from the thermal models. Even though the implemented value of TBR is relatively small, once it is located close to the heat source and on the path of the major heat removal, it can cause significant differences in the thermal behavior of the device. Although, the presence of TBR and other thin thermally resistive layers in other areas may not have significant effect in thermal behavior of the device, additional care must be taken when they are close to heat sources. Thus, it can be stated that while including TBR in HEMT thermal models with correct value and position is necessary to achieve accurate thermal results. Other thin layers such as AlGaN, which is not on the heat transfer path, can be omitted without significant change in results of the thermal analysis. Neglecting thins layers like AlGaN can be critical in robust meshing process and can reduce computational cost of simulations significantly.

2.3 Convection and Radiation

Typically, in thermal models of HEMTs, an adiabatic boundary condition is applied to top and the side surfaces of the device. However, often these devices are exposed to natural convection and surface radiation. To analyze the importance of these heat dissipation mechanisms, natural convective and radiative heat dissipation boundary conditions are applied to all boundaries/surfaces (except the bottom of the package and the symmetry boundaries/surfaces as show in Figure 2.1(a)). COMSOL's predefined natural convection heat transfer coefficient for air in T = 300 K, and

overestimated surface radiative emissivity of ε = 0.03 [104] are used in the thermal simulations. Natural convection coefficients for horizontal plate from upside and vertical plates were verified with [105]. By using the integration techniques, total values of convective and radiative heat dissipations from the device are evaluated. Then their ratio to the total power generation from the device are calculated. This way, the relative importance of these heat transfer modes are found to understand the accuracy of the adiabatic boundary condition assumption in which these mechanisms are ignored.

Figure 2.9 shows the percentage of the convective and radiative heat loss from the device to the total heat dissipation at different power densities. Even though the relative importance of the radiative and convective heat dissipation is higher at low power densities, heat dissipation with convection and radiation is still negligible compared to total heat dissipation from the device. In addition, it has been noted that the majority of both the natural convection and radiation heat dissipation is from the package due to its relatively large surface area. This indicates majority of the heat removal is via conduction to the perfect heat sink of T_{sink} = 300 K. Thus, the available evidence suggests that one can neglect radiation and convection in the HEMT devices and apply insulated boundary conditions instead without significant accuracy loss.

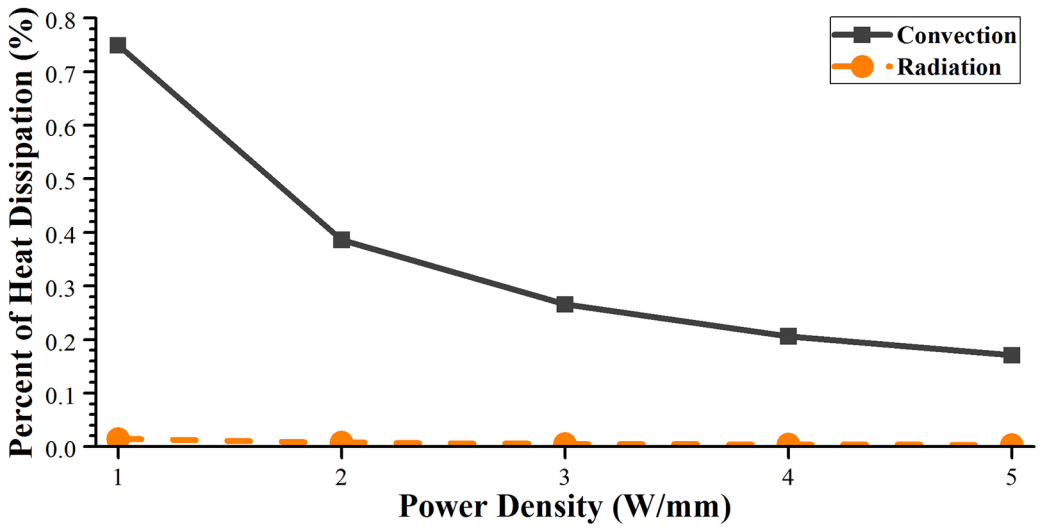

Figure 2.9 Percentage of the convective and radiative heat transfer to the total heat transfer from the device at different power densities.

2.4 Thermal Conductivity

Typically, the value of thermal conductivity of materials in HEMTs depend on the fabrication technique and temperature of the material. Although, the conductivity of materials in HEMTs cannot be stated exactly [106], common fitted equations can be found in the literature to correlate thermal conductivities to the temperature. To analyze the effects of temperature dependent material properties on the thermal performance of the device, 3D thermal simulations of devices operated at different power densities with constant and temperature dependent material properties as presented in Table 2-1.

Generally, thermal conductivities of the materials drop by the temperature rise. In HEMTs, since GaN and substrate layers reach to higher temperatures than the rest of the device, thermal conductivities of these layers drop significantly, and this issue increases the thermal resistance of the devices at high power densities. This causes hotspot temperatures to increase and becomes more important at high power densities. Hotspot temperature obtained with constant thermal conductivity models can be as low as 23 K than the hotspot temperatures predicted by temperature dependent thermal conductivity models. To illustrate the effect of temperature dependent thermal conductivities, the thermal resistance variations of the device operated at different power densities are plotted in Figure 2.10. Thermal resistance of heat conduction from heat source to the heat sink can be evaluated by equation 2.1:

$$R = (\overline{T}_{Source} - \overline{T}_{\mathrm{Sin}\,k}) / Q \tag{2.1}$$

In which R is the thermal resistance of the heat source, $\overline{T}_{Source}$ is the average temperature of the heat source, $\overline{T}_{\mathrm{Sin}\,k}$ is the average temperature of the bottom surface and Q is the total heat dissipation from the source.

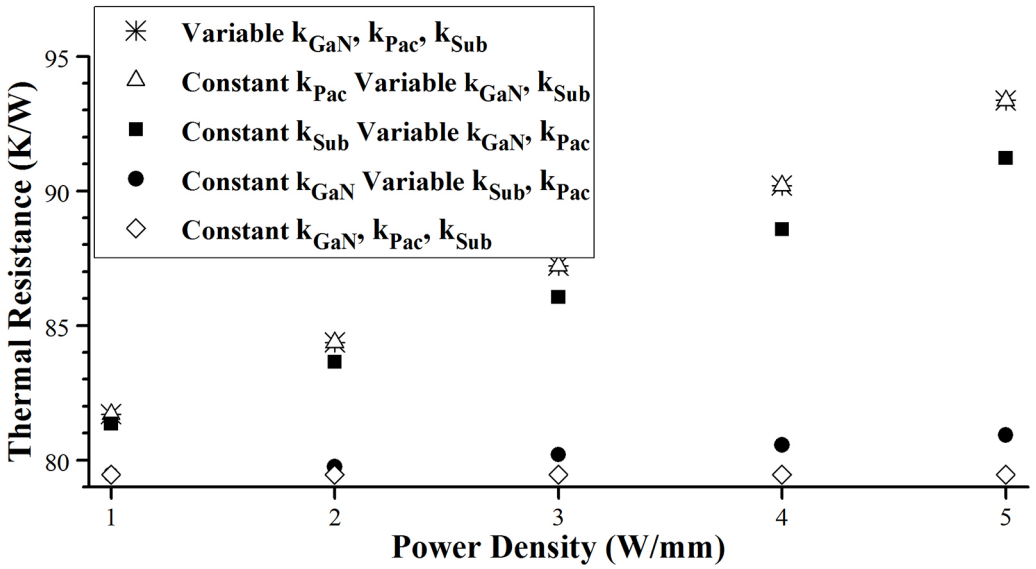

Figure 2.10 Total thermal resistances of the devices at power densities of 1-5 W/mm, when temperature dependent and constant thermal conductivities are used.

As it can be seen, in model with all layers of variable thermal conductivity significant variation in thermal resistance is observed by power density change. This is in contrast with the model with constant thermal conductivities, in which no change in thermal resistance is obtained. To analyze the importance of the thermal conductivity of each material it is decided to study their effects seperatly. This is done by keeping that layer's thermal conductivty constant. GaN and susbstrate layers presented the most importance in determination of thermal resistance in the device, however temperature depencecy of the package showed negligble effect in thermal models. This fact shows that most of the spreading thermal resistance in the device occurs in GaN and substrate layers. Additionally, it can be concluded that the thermal conductivity variations of GaN and substrate play important roles in the thermal behavior of the device and should be implemented accurately in thermal simulations.

2.5 2D Simplification

Prior to comparison of 2D with 3D models, procedure of thermal modeling in 2D models of numerical software should be explained. In advanced software like COMSOL, two-dimensional thermal models can be done by introducing the width

for the model, and calculation of one-dimensional thermal resistance is based on this width. However, other software (e.g. Sentarus TCAD) do not give the user the ability to modify this value and match the one-dimensional thermal resistance of the 2D model with the 3D model by altering the depth.

In addition to the one-dimensional thermal resistance, the neglected third dimension is the source of difference in thermal spreading of 2D and 3D GaN HEMTs models. Figure 2.11 show the temperature profile and heat transfer streamlines in top view of 3D and 2D models for the device operation at power density of 5 W/mm. As shown in the Figure 2.11, in the 3D modeling streamlines change in the y-direction and causes higher spreading thermal resistances in comparison to the equvalant 2D model. In addition to the spreading thermal resistance, there is significant difference in one-dimensional thermal resistance of 2D and 3D models.

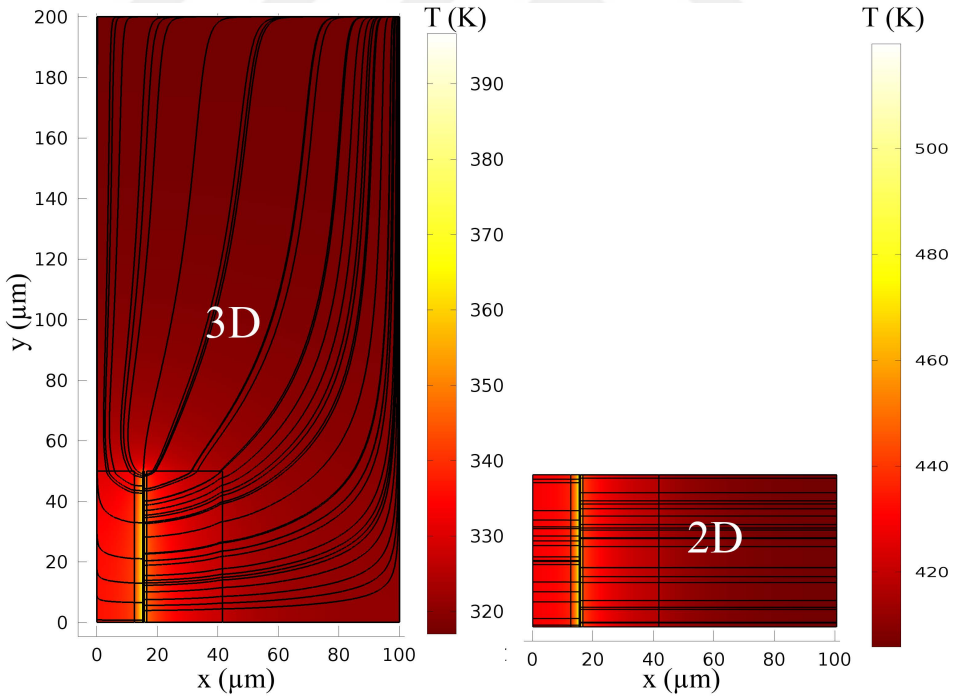

Figure 2.11 Temperature profile and heat transfer streamlines in top view of 3D and equivalent 2D models for device operating at power density of 5 W/mm.

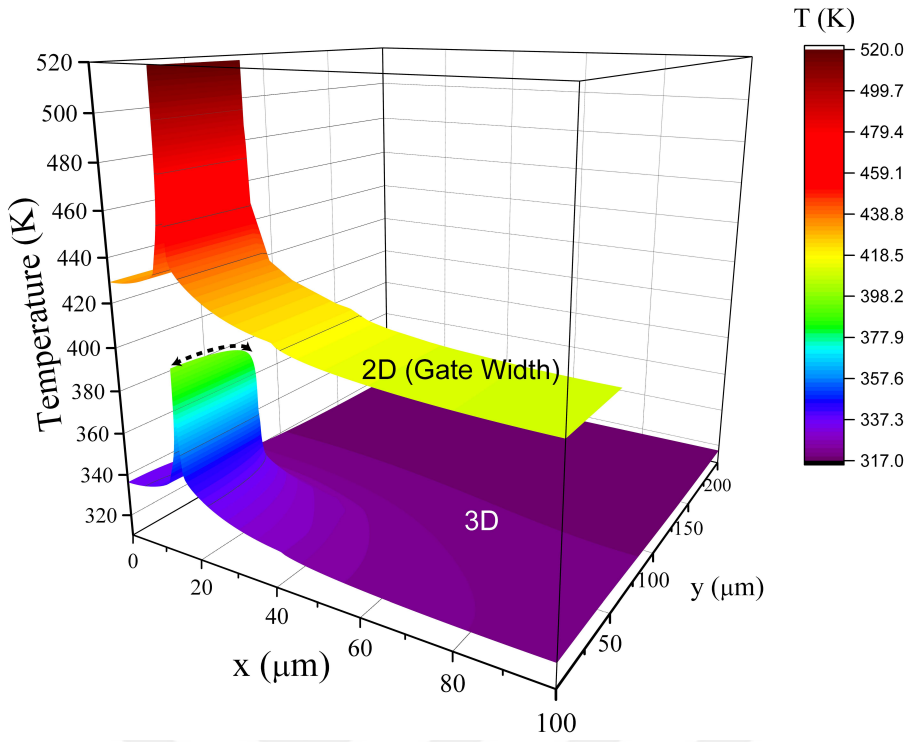

Figure 2.12 Temperature profile comparison of 3D and 2D models at power density of 5 W/mm

In order to visualize the one-dimensional thermal resistance effects in 2D and 3D model, Figure 2.12 is provided, which is the temperature distribution on the top surface of the GaN HEMT. As it can be seen in Figure 2.12, 2D model with smaller cross sectional area have higher one-dimensional thermal resistance than 2D models. Thus, overall temperature profile is moved up in comparison to the 3D model. As shown in the Figure 2.12, the highest temperatures in the 3D models occurs at the y = 0 surface. This implies that hotspot temperature evaluation can be done by correct calibration of the temperature profiles in 2D models.

Quantitative comparison of the results of 2D and 3D models is limited in the literature. For further investigation and for the better insight, analytical approach seems necessary. Thus, next chapters cover the analytical characterization of the thermal performance of GaN HEMTs.

2.6 Conclusions

This chapter examines different approaches in thermal simulation of AlGaN/GaN HEMT devices to identify the most important parameters influencing the device thermal behavior. Device modeling comparisons, leads us to the following conclusions:

- HEMTs generate heat in volumetric regions; however, there is no concise information about the size of heat generation height. This make researchers to use surface heat flux in thermal models which showed to have higher spreading thermal resistance than the heat generation from volume in pinch-off bias condition, up to 16%. This increase is due to the dissipation of heat from smaller area than the volumetric heat source models. However, in open gate consideration since the length of heat generation is significantly larger than its height, assuming surface heat flux does not alter the accuracy of the model.

- Thermal models should consider the most intense biasing case in which the device is going to operate. Increased spreading thermal resistance in closed gate conditions diminish the necessity of modeling device in open gate channel. In the absence of electro-thermal heat generation data, 50 nm critical size can be used in thermal models, since this value is the lowest reported in literature. However, for more precise modeling an electro thermal simulation is required to find the heat generation distribution size in its desired bias condition. Later based on this size, uniform heat generation assumption can be done in pure thermal models without need for importing data.

- Thin material layers and TBR located close to heat source and on the path of heat removal (i.e. substrate side) cause significant changes in thermal behavior of the device (up to 10%) by increasing spreading thermal resistance, however thin material layers in other regions (AlGaN, passivation) can be neglected without accuracy loss in usual power densities.

- Heat dissipation by radiation and natural convection from these devices are negligible at general operating power densities.

- Among all, thermal conductivity of GaN and substrate showed dominant effects on the thermal behavior of the device. Correct implementation of their temperature dependent thermal conductivities is important for reliable modeling.

- 2D simulation results found to be inaccurate when compared to 3D simulations. On the other hand, 2D models are preferred due to excessive computational cost of 3D simulations. Thus, a correction technique has to be implemented to 2D models if 2D models will be used for device modeling.

With these conclusions, a roadmap is obtained for the next thermal models of AlGaN/GaN HEMT devices.

CHAPTER 3

ANALYTICAL METHOD

Accurate numerical thermal analysis of GaN HEMTs can be expensive and time-consuming. Analytical method can be used for efficient modeling of GaN HEMTs, especially considering the small heat generation sizes. This chapter is aimed to gather all the necessary equations from different resources for the simplest analytical characterization of die-on-package structure. Package is one of the necessary parts of GaN HEMTs that have been neglected in the previous analytical characterization attempts of GaN HEMTs, and for the first time die-on-package structure is modeled analytically. Based on the analytical modeling of this chapter we can comprehensively investigate the difference of 2D and 3D models (Chapter 4) and do a full parametric study on these devices (Chapter 5).

To characterize heat conduction from the heat source to a heat sink in a solid body, one should be able to characterize spreading and one-dimensional conduction. One-dimensional conduction is a rather simple concept, which is the uniform heat diffusion all over the channel. Spreading or multidimensional conduction, on the other hand, needs complex analytical formulations that depends on the size of the heat source and composition of the channel. Additionally, analytical characterization of die-on-package structure needs separate formulation of one-dimensional and spreading diffusion in the die and in the package.

To characterize spreading effects on the die, analysis of the GaN-on-substrate structure is sufficient. We have realized that almost the entire heat spreading in the die is because of thermal resistance of the GaN-on-Substrate structure. This issue is also reported in [77] where the spreading effects found to be diminished after the first 100 µm from the top of the HEMTs. This 100 µm covers the GaN, substrate and TBR between them. However, one-dimensional thermal resistance of all layers, including

the package and epoxy must be considered in the evaluations. Analytical modeling of thermal conduction in the package is simpler than the die since it only includes single layer. It should be mentioned that the presented analytical characterizations are based on the evaluation of thermal resistance, which makes the thermal characterization of device independent from the amount of heat generation. The necessary geometrical parameters for the analytical characterization of GaN HEMTs and method is given next.

3.1 Geometry Parameters

Figure 3.1 shows the important geometrical parameters (a, b, c, d, e, f, x_c, y_c, t_{GaN}, t_{Sub}, T_{Epo}, and T_{Pac}), and fabrication parameters (TBR_{eff}, k_{GaN}, k_{Sub}, K_{Epo}, and K_{Pac}) in a 2-finger HEMT device model, necessary for analytical characterization. Studied values of geometrical parameters shown in Figure 3.1(b) and Figure 3.1(a) are in correspondence with the previous model represented in Figure 2.1 for validation purposes. Here, a = 100 µm and b = 200 µm describe the size of the die, f = 2 mm and e = 2 mm describe the size of the package, and x_c = 15.225 µm and y_c = 25 µm mark position of the heat source, and c = 50 nm and d = 50 µm identify the size of the heat source. In 2D modeling the package and die have the same length as the 50 µm long heat source (i.e. d = b = f = 50 µm).

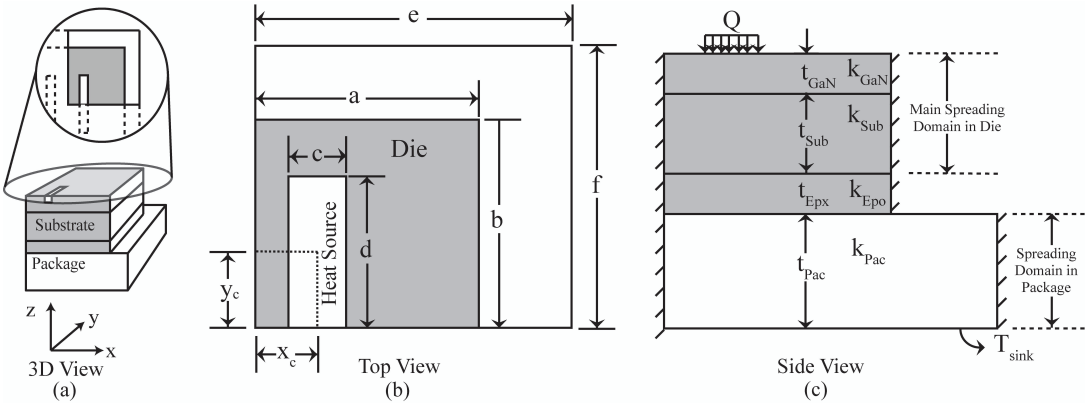

Figure 3.1 (a) Device, (b) top, and (c) side views of the simplified device geometry used to evaluate the thermal resistances.

Figure 3.2(b) shows the top view of the multi-finger device geometry. In multi-finger devices, fingers are aligned in the x-direction. Index numbers of each finger is shown in the Figure 3.2(b). Index 1 fingers are centered in the die and are the hottest fingers in the device and index numbers increase as fingers are positioned away from the center of the die. With this numbering method, only the value of x_c is changing for each finger and we can define a new positioning parameter for each finger by introducing $x_{c,i,}$ which is the distance of index *i* finger from the origin of x-axis. Using influence coefficient method introduced in [107] we can characterize the thermal resistance of index 1 fingers in the device. Thermal resistance of index 1 fingers are important since they are the hottest fingers. Thus, only the analytical characterization of index 1 fingers are presented here.

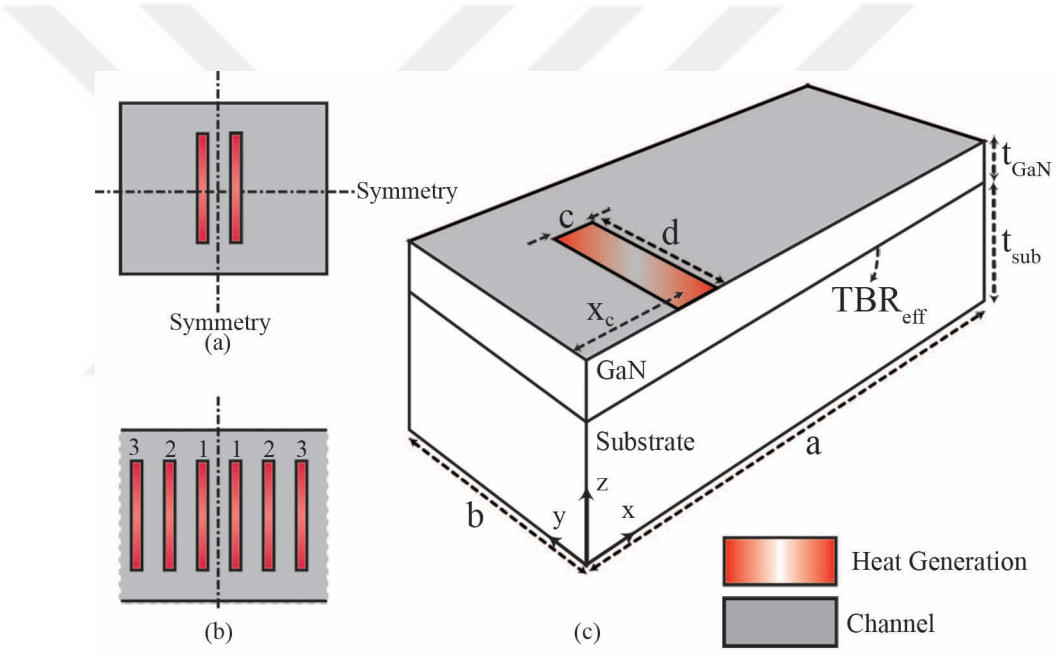

Figure 3.2 Illustration of (a) two-finger and (b) multi-finger device modeling. (c) 3D Schematic of the heterostructure.

3.2 Formulation

In a conduction channel with a small heat source as presented in Figure 3.1 surrounded by adiabatic boundaries, total thermal resistance (R_T) is composed of two different thermal resistances as shown in equation 3.1: one-dimensional resistance

(R_{1D}) and a spreading resistance (R_s). Spreading resistance vanishes as the source area approaches the substrate area.

$$R_S + R_{1D} = R_T \tag{3.1}$$

Total thermal resistance of index 1 fingers in multi-finger device ($R_{tot,1}$) can be found by equation 3.2:

$$\sum_{i=1}^{i=n} R_{s,i} + \sum_{i=1}^{i=n} R_{1D,i} = \sum_{i=1}^{i=n} R_{s,i} + nR_{1D} = R_{tot,1} \tag{3.2}$$

in which n is the number of fingers and $R_{tot,1}$ is the total thermal resistance of index 1 fingers. $R_{s,i}$ and $R_{1D,i}$ are the spreading and one-dimensional thermal resistance effect of each finger on the index 1 fingers, respectively. $R_{1D,i}$ has unique value and does not change for each finger ($R_{1D} = R_{1D,i}$) as presented in equation 3.3 as:

$$R_{1D} = \sum \frac{t_j}{k_j A_{Die}} + \frac{TBR}{A_{Die}} + \frac{t_{Pac}}{k_{Pac} A_{Pac}} \tag{3.3}$$

in which t_j and k_j are thickness and thermal conductivity of layers in the die and t_{Pac} and k_{Pac} are the thickness and thermal conductivity of layers in the package respectively. $A_{die} = a \times b$ and $A_{Pac} = e \times f$ are the cross sectional areas of die and package, respectively. a, b, e, and f are the die and package sizes shown in Figure 3.1(c). Lastly, TBR is the value of TBR_{eff}.

In multiscale analysis of HEMTs, where the die is mounted on the package spreading thermal resistance (R_s) is composed of two different spreading phenomena in the device as given in equation 3.4: First, spreading from heat source to the die ($R_{s,\,Die}$) which ends at the middle of the substrate and approximately uniform heat flux reaches to the package. Second, spreading from the die to the package ($R_{s,Pac}$).

$$R_s = R_{s,Die} + R_{s,Pac} \tag{3.4}$$

As mentioned before, spreading resistance of the die, $R_{s,Die}$, is important in the first 100 μm from the top [77], epoxy layer can be ignored and the main spreading regions in the die can be considered as GaN and the substrate layers. Equations provided in [75] to evaluate thermal spreading resistance in compound orthotropic systems with interfacial resistance can be used to evaluate thermal spreading resistance in the die:

$$\begin{aligned} R_{s,Die} = & 2\sum_{m=1}^{\infty} A_m \frac{\cos(\lambda_m x_c)\sin(0.5\lambda_m c)}{\lambda_m c} \\ & + 2\sum_{n=1}^{\infty} A_n \frac{\cos(\delta_n y_c)\sin(0.5\delta_n d)}{\delta_n d} \\ & + 4\sum_{m=1}^{\infty}\sum_{n=1}^{\infty} A_{mn} \frac{\cos(\lambda_m x_c)\sin(0.5\lambda_m c)\cos(\delta_n y_c)\sin(0.5\delta_n d)}{\lambda_m c \delta_n d} \end{aligned} \tag{3.5}$$

Here x_c, y_c, c, and d are the geometrical parameters shown in the Figure 3.1 and A_m, A_n, and A_{mn} can be calculated as [75]:

$$A_m = \frac{4\cos(\lambda_m x_c)\sin(0.5\lambda_m c)}{abck_{eff,GaN}\lambda_m^2 \phi(\lambda_m)} \tag{3.6}$$

$$A_n = \frac{4\cos(\delta_n y_c)\sin(0.5\delta_n c)}{abdk_{eff,GaN}\delta_n^2 \phi(\delta_n)} \tag{3.7}$$

$$A_{mn} = \frac{16\cos(\lambda_m x_c)\sin(0.5\lambda_m c)\cos(\delta_n y_c)\sin(0.5\lambda_m d)}{abcdk_{eff,GaN}\lambda_m \delta_n \beta_{mn} \phi(\beta_{mn})} \tag{3.8}$$

where $\delta_n = n\pi/b$, $\lambda_m = m\pi/a$, and $\beta_{mn} = (\delta_n^2 + \lambda_m^2)^{0.5}$ are the eigenvalues. When anisotropic thermal conductivity is used in thermal models effective thermal conductivity should be used in evaluations as [75]:

$$k_{eff} = \sqrt{k_z} \cdot \sqrt{k_y} \cdot \sqrt{k_x} \tag{3.9}$$

in which k_{eff}, k_x, k_y, and k_z are the effective thermal conductivity, thermal conductivities in x-direction, y-direction, and z-direction, respectively. Finally, $\phi(\xi)$ is the spreading function specific to perfect heat sink models given as [72]:

$$\phi(\xi) = \frac{1 + TBR \cdot \xi k_{eff,GaN} \cdot \tanh(\xi t_{GaN}) + \frac{k_{GaN}}{k_{Sub}} \tanh(\xi t_{GaN}) \tanh(\xi t_{Sub})}{TBR \cdot \xi k_{eff,GaN} + \frac{k_{GaN}}{k_{Sub}} \tanh(\xi t_{Sub}) + \tanh(\xi t_{GaN})} \tag{3.10}$$

By using the above equations, spreading thermal resistance of 2-finger devices can be characterized. However, in multi-finger devices as presented by equation 3.2 thermal spreading burden of each finger on index 1 finger should be characterized. This can be done by using the influence coefficient method introduced first in [107]. Thus, we can characterize the thermal resistance burden of each index i finger on the first finger by finding $R_{s,die,i}$:

$$\begin{aligned} R_{s,die,i} = {} & 2\sum_{m=1}^{\infty} A_{m,i} \frac{\cos(\lambda_m x_{c,1}) \sin(cd/4)}{\lambda_m c} \\ & + 2\sum_{n=1}^{\infty} A_n \frac{\cos(\delta_n d/2) \sin(\delta_n d/2)}{\delta_n d} \\ & + 4\sum_{m=1}^{\infty}\sum_{n=1}^{\infty} A_{mn,i} \frac{\cos(\lambda_m x_{c,1}) \sin(\lambda_m c/2) \cos(\delta_n d/2) \sin(\delta_n d/2)}{\lambda_m c \delta_n d} \end{aligned} \tag{3.11}$$

In which and $A_{m,i}$, A_n, and $A_{mn,i}$ are calculated as:

$$A_{m,i} = \frac{4\cos(\lambda_m x_{c,i}) \sin(\lambda_m c/2)}{abck_{GaN} \lambda_m^2 \phi(\lambda_m)} \tag{3.12}$$

$$A_{mn,i} = \frac{16\cos(\lambda_m x_{c,i}) \sin(\lambda_m c/2) \cos(\delta_n d/2) \sin(\lambda_m d/2)}{abcdk_{GaN} \lambda_m \delta_n \beta_{mn} \phi(\beta_{mn})} \tag{3.13}$$

In which the $x_{c,i,}$ is the distance of index *i* finger from the origin of x-axis as shown in Figure 3.2.

Next, spreading thermal resistance of the package should be characterized. we can evaluate this value using equations introduced in [74]:

$$\begin{aligned} R_{s,Pac} = & \frac{1}{2a^2\, fek_{eff,Pac}} \sum_{m=1}^{\infty} \frac{\sin^2(a\delta_m)}{\delta_m{}^3} \cdot \phi(\delta_m) \\ & + \frac{1}{2b^2\, fek_{eff,Pac}} \sum_{m=1}^{\infty} \frac{\sin^2(b\lambda_n)}{\lambda_n{}^3} \cdot \phi(\lambda_n) \\ & + \frac{1}{a^2 b^2\, fek_{eff,Pac}} \sum_{m=1}^{\infty}\sum_{n=1}^{\infty} \frac{\sin^2(a\delta_m)\sin^2(b\lambda_n)}{\delta_m{}^2 \lambda_n{}^2 \beta_{mn}} \cdot \phi(\beta_{mn}) \end{aligned} \tag{3.14}$$

where $k_{eff,Pac}$ is the effective thermal conductivity of the package, which can be evaluated using equation 3.9. Since the heat sink is kept in constant temperature, spreading function can be evaluated using [75]:

$$\phi(\xi) = \coth(\xi t_{eff,Pac}) \tag{3.15}$$

A MatLab code is developed to evaluate the of thermal resistances with 17 inputs and 4 outputs: spreading and one-dimensional thermal resistance of the die and the package. In multi-finger die, thermal resistance effect of each finger on the index 1 fingers is also calculated and summed to get the total thermal resistance.

3.3 Conclusions

Relatively high number of terms are needed in the Fourier series summation for correct evaluation of the spreading thermal resistance. In the studied cases, more than 10^4 terms are used for correct converged values. This value is 10^8 in double Fourier series summation, which required careful coding for fast and efficient evaluations.

Over all, the analytical calculations are significantly faster than 3D numerical models, but not as fast as 2D numerical models.

Table 3-1 presents the thermal resistance comparison of introduced device in section 3.1 between analytical and numerical method. One-dimensional thermal resistances values match perfectly in numerical and analytical evaluations; however, slight differences can be seen in spreading thermal resistance values. These differences can stem from number of the summations in analytical method or numerical inaccuracies. Overall, analytical method proposes acceptable accuracy in thermal resistance calculation of GaN HEMTs.

Table 3-1 Comparison of analytical and numerical thermal resistance.

Method	$R_{s,Die}$	$R_{s,Pac}$	$R_{1D,Die}$	$R_{1D,Pac}$	R_T
Numerical	83.6	6.8	12.35	1.32	104.1
Analytical	82.2	6.9	12.35	1.32	103.8

Analytical thermal modeling is useful tool for examining the problems of numerical models. Difference of 2D and 3D thermal models can be characterized carefully using analytical approach introduced in this chapter. Furthermore, we can calibrate 2D models to the 3D models using analytical method. Thus, based on the above analytical approach a calibration technique can be introduced for correct 2D numerical models (Chapter 4).

Additionally, full parametric thermal characterization of the device can be done based on the presented analytical method. Parametric studies in numerical models of GaN HEMTs needs re-meshing in each case of geometry change, which can take days of calculations and significant physical memory equipment as stated in [108]. Each parameter can be changed continuously or discreetly for the optimization or comparison purposes using analytical method. Chapter 5 presents a full parametric study in GaN HEMTs about a substrate selection, based on the analytical evaluations of this chapter.

CHAPTER 4

ANALYTICAL METHOD AS A CALIBRATION TOOL

In chapter two, it was shown that Joule heating in GaN HEMTs occurs in very small regions. Furthermore, it was shown that accurate thermal modeling of these regions requires excessive fine meshing. High mesh density near the heat generation regions and proper growth of the mesh to other parts of the device demands several millions of elements for 3D modeling. Although 2D modeling is an alternative way to reduce such computational costs. However, it was shown that, neglecting the third dimensions results in unreliable outcomes. The main reason for this unreliability is the difference in spreading and one-dimensional thermal resistances of the 2D models when compared to 3D models. The spreading thermal resistance in 3D models occurs along three directions, while in 2D models it occurs only along two directions. Additionally, there is difference in one-dimensional thermal resistance of these models that stems from difference in cross sectional area of 2D and 3D models.

Thus, accuracy enhancement is required if one choses to exploit the efficiency of numerical 2D models. To the best of our knowledge, d'Alessandro *et al*. [88] is the only researcher who has covered this topic. In order to modify 2D model he proposed a calibration technique that changes the layer thicknesses of the 2D model. Although this technique is inspiring, it cannot be used for the cases where the amount of layer thickness reduction surpasses the available thickness of the layers. Thus, an alternative method has to be developed to model devices accurately using 2D models.

In this chapter, the analytical formulation presented in the third chapter is used first for the comparison of 2D and 3D thermal models, and later for more robust and general calibration method of numerical 2D models. Lastly, this technique is applied to calibrate numerical 2D models and examined with 3D models for the accuracy test.

4.1 Calibration for 2D Models

In order to compare the difference between 3D and 2D models spreading (R_s), total thermal resistance (R_T) of the device are summarized in Table 4-1.

Table 4-1 Comparison of spreading and total thermal resistance [K/W] of 2D and 3D models.

Method	3D			2D		
	$R_{s,Die}$	$R_{s,Pac}$	R_T	$R_{s,Die}$	$R_{s,Pac}$	R_T
Analytical	82.2	6.9	103.8	79.4	33.1	188.3

According to the results, spreading thermal resistance of die in 2D models are slightly less than 3D models, which indicates that most of the spreading occurs in the x-direction. This issue helped d'Alessandro *et al*. [88] to actually calibrate 2D model without altering its spreading thermal resistance. However, as the heat source length increases (c in Figure 3.1), the spreading thermal resistance in the y-direction becomes comparable to the spreading in the x-direction. As a result of this 2D and 3D models can have different spreading thermal resistances. This issue is also observed in the package where spreading thermal resistance are significantly different in 2D and 3D models. Thus, the correction method of d'Alessandro can give wrong results when extremely narrow (c << d) heat generation is not considered.

Spreading thermal resistance in the package is approximately 10 times less than the spreading thermal resistance in the die, because heat spreads from much smaller area in the die. However, thermal resistance of the package is considerable and necessary for the correct evaluation of the hotspot temperature.

4.2 Correction Method

As mentioned in the third chapter (Figure 3.1), b and f are the only parameters that change the value of one-dimensional thermal resistance of the 2D and 3D models. Unlike one-dimensional thermal resistance, spreading thermal resistances of 2D and 3D models cannot be predicted simply, since these are functions of several parameters. Examining thermal resistance of the die and packages (presented in Table

4-1) indicates that the spreading thermal resistances of the die are nearly same since the thermal resistance in the y-direction is low in the 3D model. However spreading thermal resistance difference between 2D and 3D models is larger in the package.

To calibrate the total thermal resistance of the die and match the temperature profiles obtained by 2D to 3D model, total thermal resistance of the die should be matched without altering the spreading thermal resistance. The only possible way for this purpose is cutting from the geometry of the device to reduce thermal resistance of 2D model as d'Alessandro *et al*. [88] did. However, we mentioned before that spreading thermal resistance ends at 100 µm from top, thus for the case with a substrate thickness smaller than 100 µm, thinning the substrate is equivalent to changing the spreading thermal resistance. Thus, this method cannot be used in small dies, or as mentioned previously, when there is a package. Additionally, when the difference of b and d increases further, one can run out of height reduction. Thus, the only possible way to calibration of the 2D models is altering the thermal conductivity of the layers. However, as given in equation 3.9, changing the isotropic values of thermal conductivities result in change in both one-dimensional and spreading thermal resistance values. Thus, the two-step correction method presented herein aims to change the one-dimensional thermal resistance first, and modify the spreading thermal resistances later. The flowchart of correction technique is presented in Figure 4.1.

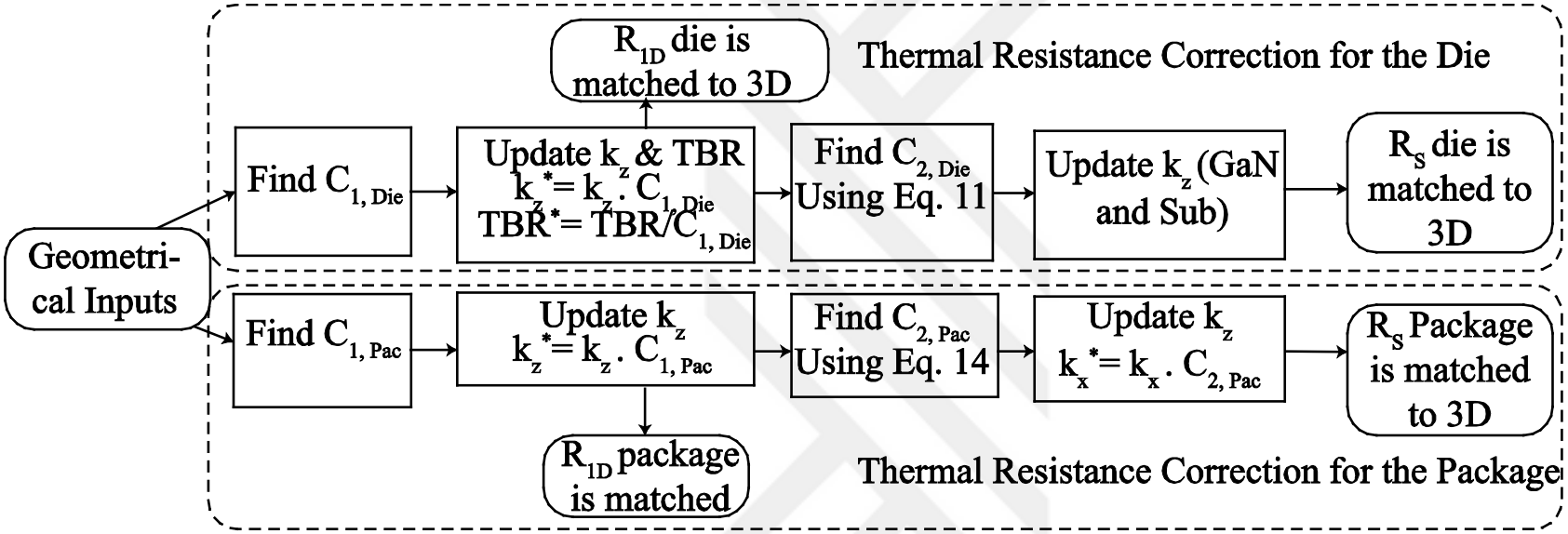

Figure 4.1 Flowchart of correction method for calibration of thermal resistance of 2D thermal model to the 3D model.

The correction method concludes two steps, at the first step the correction method aims at matching the one-dimensional thermal resistance of the device by multiplying the thermal conductivity of all the material in the z-direction by the first correction factor C_1. Since there are two major resistance blocks, die and package, for each of these blocks specific correction should be introduced. Thus, first correction factors for the die ($C_{1,Die}$) and for the package ($C_{1,Pac}$) can be found by finding the ratio of their one-dimensional thermal resistance given in Equation 3.3. Thus, we can have:

$$C_{1,Die} = b / d \tag{4.1}$$

$$C_{1,Pac} = f / d \tag{4.2}$$

It should be noted that since TBR acts as resistive and not conductive layer, its value should be divided by the first correction factor of the die. After applying these corrections to the 2D model, the new spreading thermal resistance of the 2D models should be evaluated to move on to the second step.

In the second step, it is aimed to match the spreading thermal resistances of 3D model and the 2D model with modified thermal conductivity in z-direction. Since it is known that thermal spreading resistance of the die, $R_{s,Die}$, is important in the first 100 μm from the top [77], epoxy layer can be ignored and the main spreading regions in the die can be considered as GaN and the substrate layers. By finding the ratio of spreading thermal resistances in 2D and 3D models and its dependence on the lateral thermal conductivities a new correction factor can be found. By having the values of the spreading thermal resistance a new correction factor for the lateral thermal conductivity of the die, $C_{2,Die}$ can be evaluated as:

$$C_{2,Die} = \frac{R^2_{s,Die-2D}}{R^2_{s,Die-3D}} \tag{4.3}$$

where $R_{s,Die\text{-}2D}$ is spreading thermal resistance of the die in the 2D model and $R_{s,Die\text{-}3D}$ is spreading thermal resistance of the die in 3D model. The reason for squared ratios on equation 4.3 is that, the effect of this correction factor is rooted in the process of changing spreading thermal resistance. This fact can be seen in equation 3.9, where lateral thermal conductivity is under radical sign. Our calculations shows that due to relatively low thickness of the GaN layer, this correction factor should also be applied to the substrate layer (which is one of the dominant resistive layer in the die) to change the spreading resistance of the die to achieve desired results.

A similar procedure is used to introduce the correction factor for the package in the 2D model where we have:

$$C_{2,Pac} = \frac{R_{s,Pac-2D}^2}{R_{s,Pac-3D}^2} \tag{4.4}$$

This correction method can be extended for variable thermal conductivity models with Kirchoff's transformation [109]. In addition, superposition techniques [72] can be used in case of multiple-finger design. The flowchart of correction technique is presented in Figure 4.2.

The process of calibration can be explained by presenting the schematic temperature profile along the x-axis as shown Figure 4.2. As we can see at first as presented in Figure 4.2(a), there is a significant difference between 2D and 3D models. After matching the one-dimensional thermal resistance of the device, spreading thermal resistance of the 2D models drop as shown in Figure 4.2(b). Later, as shown in Figure 4.2(c) by increasing the spreading thermal resistance of the 2D model in the next step we can achieve a satisfying calibration of 2D to 3D model.

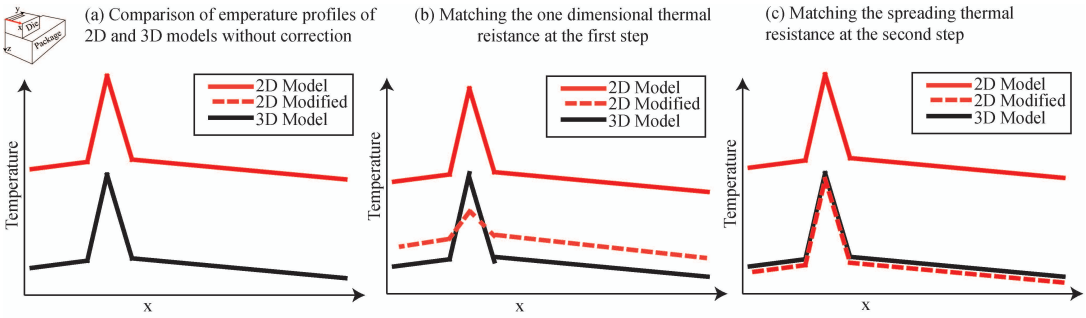

Figure 4.2 Schematic preview of temperature profile along x-axis comparison of (a) 2D and 3D models. Temperature profile change of modified 2D model is illustrated in (b) and (c).

In order to test the calibration method, 2D model presented in the Figure 3.1 is calibrated with heat source size of 50 nm and 2 µm. Table 4-2 represents the modified thermal resistances and correction factor values. As shown in the Table 4-2 in the first step, one-dimensional thermal resistance of 2D models matched perfectly to 3D models. At the second step with the correction of lateral thermal conductivities, spreading thermal resistances of models are matched to the 3D models. After applying these correction factors to the 2D model total thermal resistances are matched satisfyingly to the 3D models with 5% error.

Table 4-2 Spreading and one-dimensional thermal resistance of studied devices obtained by 3D numerical and analytically calibrated 2D numerical approaches. [K/W]

	50 nm Heat Source			2 µm Heat Source Model		
	2D (1st Step) $C_{1,Die}$ = 4 $C_{1,Pac}$ = 20	2D (2nd Step) $C_{2,Die}$ = 0.208 $C_{2,Pac}$ = 0.700	3D -	2D (1st Step) $C_{1,Die}$ = 4 $C_{1,Pac}$ = 20	2D (2nd Step) $C_{2,Die}$ = 0.173 $C_{2,Pac}$ = 0.700	3D -
$R_{s,Die}$	38.2	79.0	83.6	17.9	39.1	44.46
$R_{s,Pac}$	5.7	6.5	6.8	5.7	6.5	6.8
$R_{1D,Die}$	12.3	12.3	12.3	12.3	12.3	12.3
$R_{1D,Pac}$	1.3	1.3	1.3	1.3	1.3	1.3
R_{Total}	57.5	99.1	104.0	37.2	59.2	64.8

Figure 4.3 compares the temperature distribution obtained using 3D and modified 2D numerical models for the device operated at a power density of 5 W/mm. As shown in both figures, modified 2D models act similar to the 3D models in the evaluation of hotspot temperatures. However, temperatures decrease much faster in modified 2D models moving away from the hotspot. Figure 4.3 proves that, despite these minor

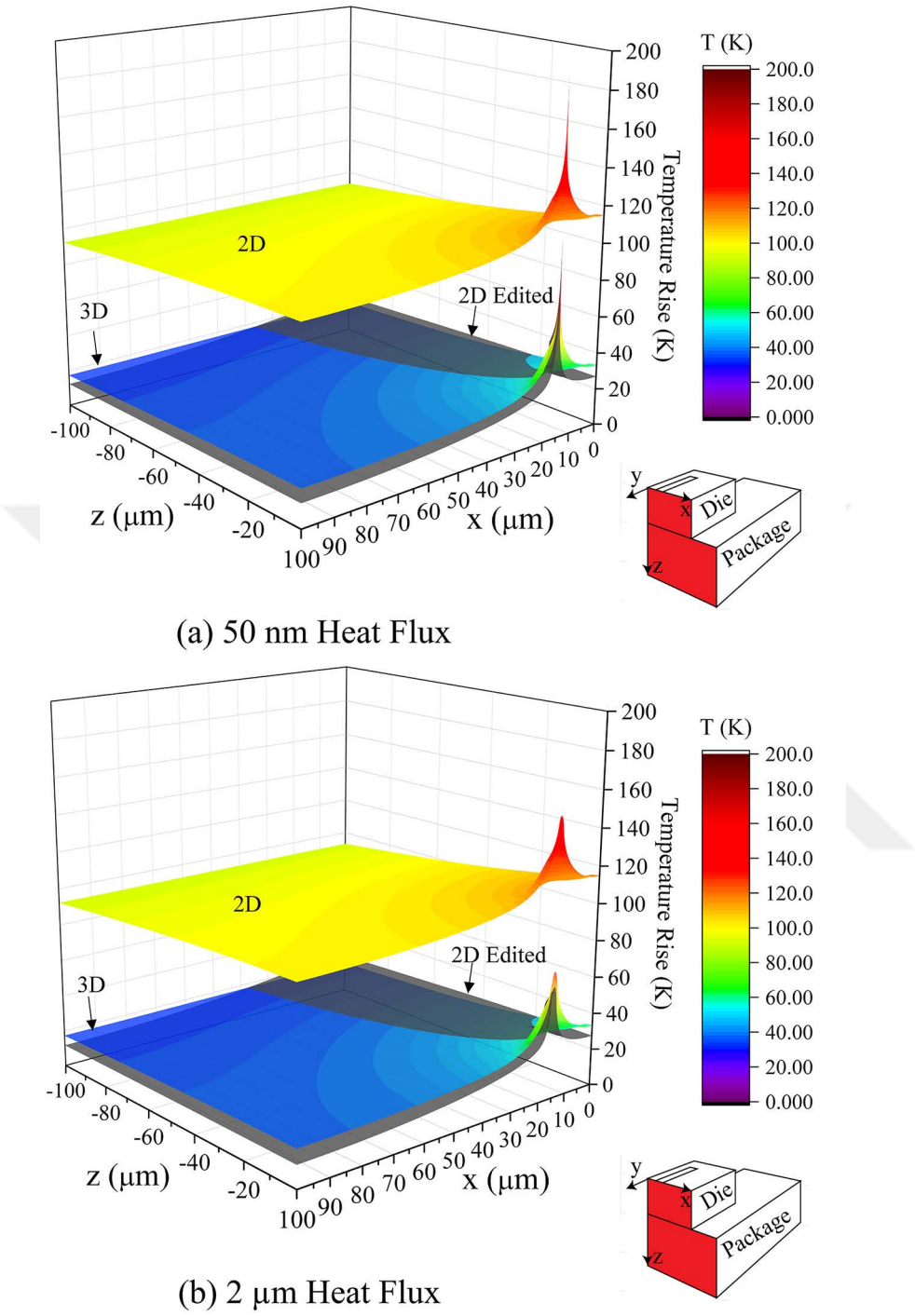

Figure 4.3 Temperature distribution along spreading layers of the device at power density of 5 W/mm on the x-z surface passing from middle of the device in (a) device with 50 nm heat source and (b) 2 μm heat source.

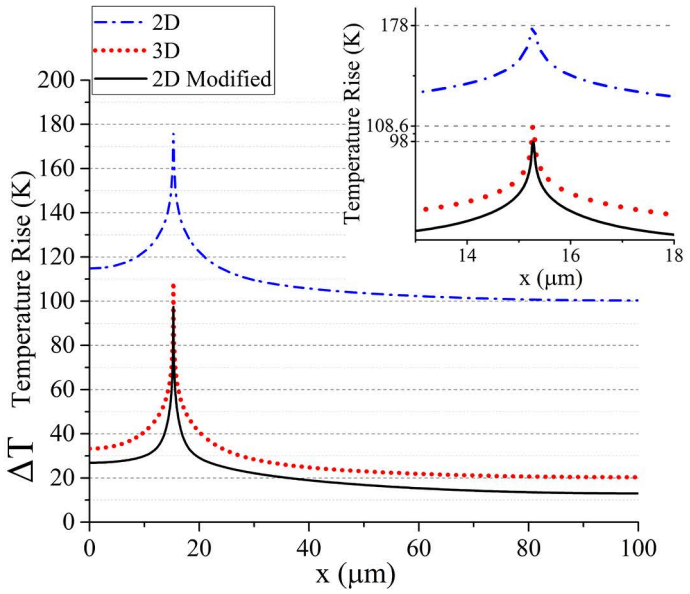

(a) 50 nm Heat Flux

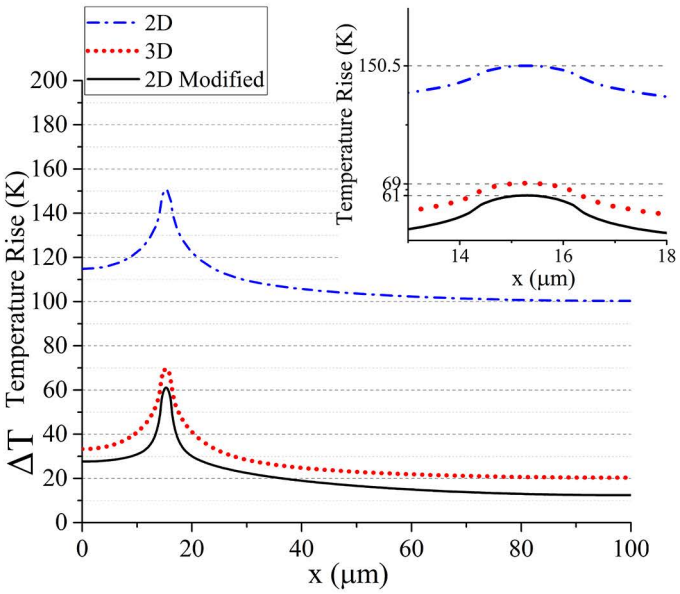

(b) 2 μm Heat Flux

Figure 4.4. Temperature profile along x-axis of the device at power density of 5 W/mm in (a) device with 50 nm heat source and (b) 2 μm heat source.

differences one can have good approximation of 3D models using simulations while maintaining the accuracy of temperature characterization of HEMT device.

For further examination of the temperature behavior of the device along the x-axis, Figure 4.4 is prepared which compares the temperature behavior of the 2D, 2D modified and 3D models in relatively large power density of 5 W/mm. Although exact match of temperature profiles was not achieved, however this improvement seems sufficient for the calibration of electro thermal modeling, or for the process of 2D numerical optimization.

4.3 Conclusions

Necessity of computational efficiency in numerical thermal models of HEMTs have limited many researchers to adaption of 2D approaches, despite numerous inaccuracy reports. In order to improve the inaccurate results of 2D thermal models, a novel computationally efficient calibration method is presented. This analytical calibration process is based on the analysis of thermal resistance of GaN HEMTs in 2D and 3D geometries. Thermal conductivity modification found to be a robust and practical calibration tool that can cover the weaknesses of previous calibration methods. Using this technique one can calibrate the 2D models and match the temperature predictions to the 3D models. Test results showed satisfying accuracy with significant reduction in computation time compared to 3D numerical models. Thus, by applying this calibration method on a 2D numerical model one can achieve both accuracy and efficiency.

The importance of this calibration method is more highlighted in numerical electro thermal simulations. Since this method alters only the thermal conductivity of the model, it does not interfere with other physics of the device. It is believed that applying this calibration on electro thermal simulations of GaN HEMTs can results in more accurate Joule heating evaluation.

CHAPTER 5

ANALYTICAL METHOD FOR SUBSTRATE SELECTION

5.1 Diamond and SiC Substrates

Using substrate with high thermal conductivity in order to reduce the thermal resistance and channel temperature rise is among the successful thermal management approaches in thermal engineering of HEMTs. It was shown that when diamond substrate are used, compared to more mature SiC technology [31], about 25% reduction in channel temperature rise was achieved. Similar comparison studies can be found in literature where thermal performance of HEMTs with SiC and diamond substrates were compared [110-113]. These comparison studied generally focus on a specific type of device and performance. It was observed that variety of geometrical parameters, operation condition, and properties of the materials also has caused differences in the reported results of thermal characterizations. Thus, there is a need for a comprehensive parametric comparison study of diamond and SiC substrate technology.

In addition to the device geometry and operation condition, intrinsic properties of HEMTs such as different values of effective thermal boundary resistance (TBR_{eff}) should be accounted. The value of this important parameter can be different depending on the variety of fabrication technique. Generally, it is believed that to take the full advantage of the thermal conductivity of the substrate, low TBR_{eff} should be achieved. Unfortunately TBR_{eff} of GaN-on-diamond structure has not been thoroughly studied, and benchmarked data is not available in literature [85]. At its lowest, TBR_{eff} of $3 \cdot 10^{-8}$ m^2K/W [114, 115] is reported for diamond substrate HEMTs. However, lower TBR_{eff} value of $1.2 \cdot 10^{-8}$ m^2K/W was also achieved by decreasing the nucleation layer thickness [116]. GaN-on-SiC, on the other hand, is a more mature technology in high power applications [117]. Prior benchmark studies report TBR_{eff}

of $2 \cdot 10^{-8}$ m^2K/W in latest commercial devices of this technology [118, 119]. Besides, with the epitaxial growth significantly lower TBR_{eff} in range of $(0.4–0.5) \cdot 10^{-8}$ m^2K/W was achieved for GaN-on-SiC structure [120]. It should be noted that significant temperature variations can be observed with small variations of TBR, and reducing it is one of the major research areas in thermal management of HEMTs.

It is also widely reported that to utilize the maximum capability of higher thermal conductivity of substrate (e.g. diamond), substrate should be located very near to the 2-DEG. However, we believe that the later statement is not always true. If thin GaN layer is utilized in the device, depending on the value of TBR_{eff}, premature thermal spreading can collide to this thermal barrier, which can result in increase of the thermal resistance. In other words, using thinner GaN layer is not always desired. It should be mentioned that to reach a desired quality of GaN film, typical thickness of 0.5-2 μm are used to be grown both on SiC and diamond substrate HEMTs.

In state of the art devices, GaN-on-SiC technology cannot compete with lower thermal resistance of GaN-on-diamond. Silicon Carbide, the standard substrate material for high power HEMTs, has thermal conductivity of ~450 W/(mK) which is reported not enough to exploit the wide band gap capacity of GaN [121]. Poly crystal diamond (PCD) with ~1.5 times, and single crystal diamond (SCD) with ~ 3 times higher thermal conductivity have shown noticeable thermal improvements in HEMTs. Then again, it should be mentioned that using high quality diamond as a substrate is an expensive fabrication technique. Thermal conductivity of PCD 620 ± 50 W/(mK) [116] can vary the from value of thermal conductivity of SCD (1500 ± 300 W/(mK)) to thermal insulation limits, depending on the quality and grain structure [122]. In addition, anisotropic behavior and reduction of thermal conductivity in nucleation sites [123] have been reported.

With above discussion one can realize that broad varieties exist in properties of used substrates. These variations bring necessity to compare GaN-on-SiC with other higher thermal conductivity substrates in more comprehensive examinations. Generally, varieties exist in horizontal and vertical geometrical parameters of the

HEMTs and also in their material, TBR_{eff}, and heat generation properties. This extensive variation in the device properties made us to compare GaN-on-SiC with GaN-on-PCD and SCD, not only in the variety of possible fabrication and function properties , but also in different dies sizes, which is missing in the literature. For this purpose due to requirement for analyze of device parameters in discrete or continuous parametric values, analytical approach of third chapter is used.

5.2 Approach and Device Geometry

The geometry of the device is obtained from the previous chapter as shown in Figure 5.1. Since most of the temperature rise and the thermal resistance of the device occur in the GaN and the substrate layer this chapter will be limited to thermal characterization of the GaN and its substrate only. Figure 5.1(c) shows the 2-finger device used for thermal performance comparison. Due to symmetry of the geometry and boundary conditions (as shown in the Figure 3.1(a)) only quarter of the device as shown in the Figure 5.1(c) is modeled. Analytical method for evaluation of spreading

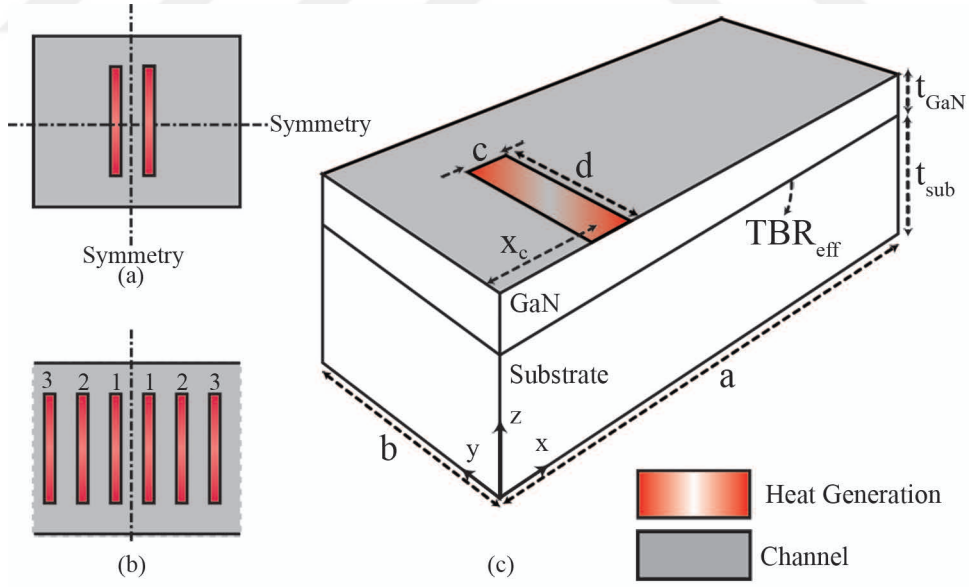

Figure 5.1 Quarter of the GaN-on-substrate studied herein. Heat generation region with size of c × d is positioned with guide of x_c on the heat transfer channel with size of a × b. t_{GaN} and t_{sub} shows the thickness of the GaN and substrate layer, respectively. Effective TBR is also set between GaN and substrate.

and one-dimensional thermal resistance of the device is presented in the third chapter.

As it can be seen from Figure 5.1 there are 9 important parameters that can change the thermal performance of GaN-on-Substrate structure. These parameters include horizontal (a, b, c, d, x_c) and vertical parameters (k_{sub}, t_{GaN}, t_{sub}, TBR_{eff}). A parametric study is performed by varying these parameters in a 2-finger GaN HEMT consideration. Later, effect of multi-finger design is studied by increasing the number of fingers from two to twenty. Study schedule of this chapter is presented in Table 5-1 and value of studied parameters are provided.

Table 5-1 Values of studied parameters and study plan

Study	Total Finger #	$k_{Substrate}$ (W/(mK))	a (µm)	b (µm)	c (nm)	d (µm)	x_c (µm)	t_{GaN} (µm)	t_{Sub} (µm)	TBR_{eff} ($m^2K/W \times 10^8$)
1	2	450, 620, 1500	100-400	100-400	50-500	25-75	30	1	100	2
2	2	450, 620, 1500	100	100	50	50	30	0.5-2	100	1- 5
3	2	450, 620, 1500	400	100	50	50	10-200	1	100	2
4	2-20	450, 620, 1500	400	100	50	50	10-60	1	100	2

5.3 Die and Heat Source Size

In the first study thermal performance of GaN-on-SiC, PCD, and SCD are compared by changing the horizontal dimensions (a, b, c, d) of 2-finger device (study 1 in Table 5-1). Die size (2a × 2b) is varied from 200 µm to 800 µm to capture its effect on the thermal resistance of the device. The heat generation region also changes in this part. Three gate widths (2 × d) of 50, 100, and 150 µm are studied. Since there is no universal rule in modeling the critical size of heat generation area, heat flux length (c) of 50, 300, and 500 nm are considered (heat generation length depends on device structure and operating condition, however we have tried to include the most intense cases beside more common conditions). Finger spacing (2 × x_c) of 60 µm is a typical value in GaN HEMT fabrication, this value is kept constant throughout this part. In addition, same

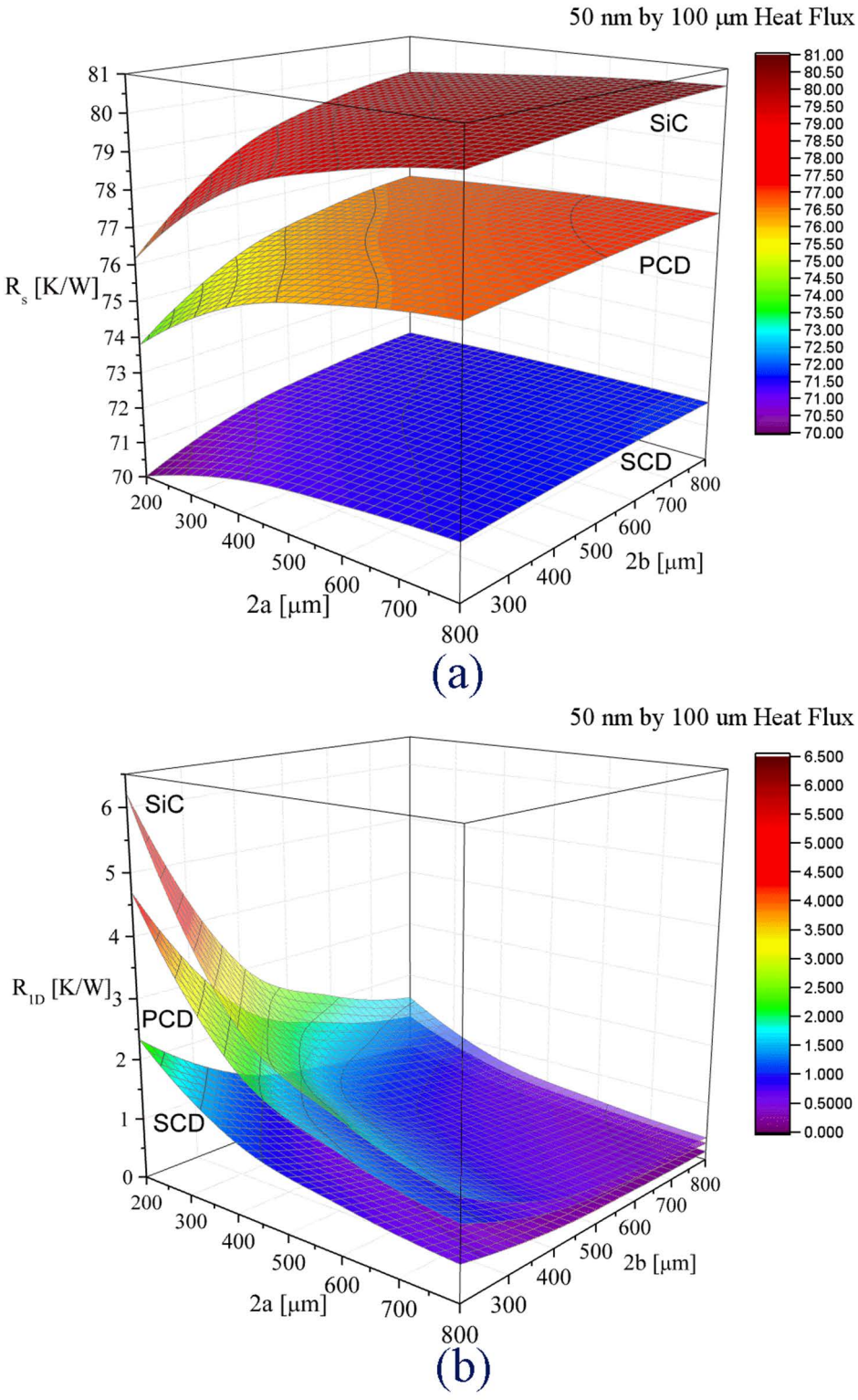

Figure 5.2 Variation of (a) spreading and (b) one-dimensional thermal resistance of GaN-on-SiC, PCD, and SCD with change in the die size in gate width of 100 µm and heat flux critical size of 50 nm. Refer to Table 1 for the other properties of the device in the first step.

thickness of GaN, substrate and equal effective TBR are used in this study. Table 5-1 shows the values of these parameters in the first step.

Figure 5.2, which presents spreading and one-dimensional thermal resistance, separately for the GaN-on-SiC, PCD, and SCD in various die sizes, indicating the dominancy of spreading thermal resistance over one-dimensional thermal resistance. The ratio of spreading to one-dimensional thermal resistance is more than 10 in the die size of 200 µm, while this ratio is more than 200 in the die size of 800 µm. In addition, spreading and one-dimensional thermal resistances act constant for dies with higher cross sectional areas, and a small variations in value of thermal resistances is seen for dies bigger than 400 µm. However, in same ratio of die size change, we observe steeper variation in the value one-dimensional thermal resistance, which stems from the hyperbolic relation between the one-dimensional thermal resistances with the area of the die. After the evaluation of spreading and one-dimensional thermal resistance, their values are added together to evaluate total thermal resistance of the device. For clarity, two sets of figures are prepared to study the variation of total thermal resistance of the devices with respect to the cross sectional area of the die; Figure 5.3, when gate width is kept constant and heat generation region is variable, and Figure 5.4, when gate width is changing in constant critical heat generation region.

Figure 5.3 shows the total thermal resistance variation in different die sizes in typical gate width of 100 µm and 3 different heat flux regions. For the dies with size of more than400 µm × 400 µm a plateau is observed, and thermal resistance showed no significant changes with respect to the area. This means that using bigger die sizes than this value impose cost premiums in production with no significant reduction in the thermal resistance of the device. As shown in the Figure 5.3, thermal resistance behavior and also the ratio of thermal resistance between GaN-on-SiC, PCD, and SCD in same gate width and different conditions (i.e. 50nm, 300nm, and 500nm) obey almost same pattern and ratios. In other words, it is sufficient to compare thermal behavior of HEMTs with different substrates in just one electrical operational

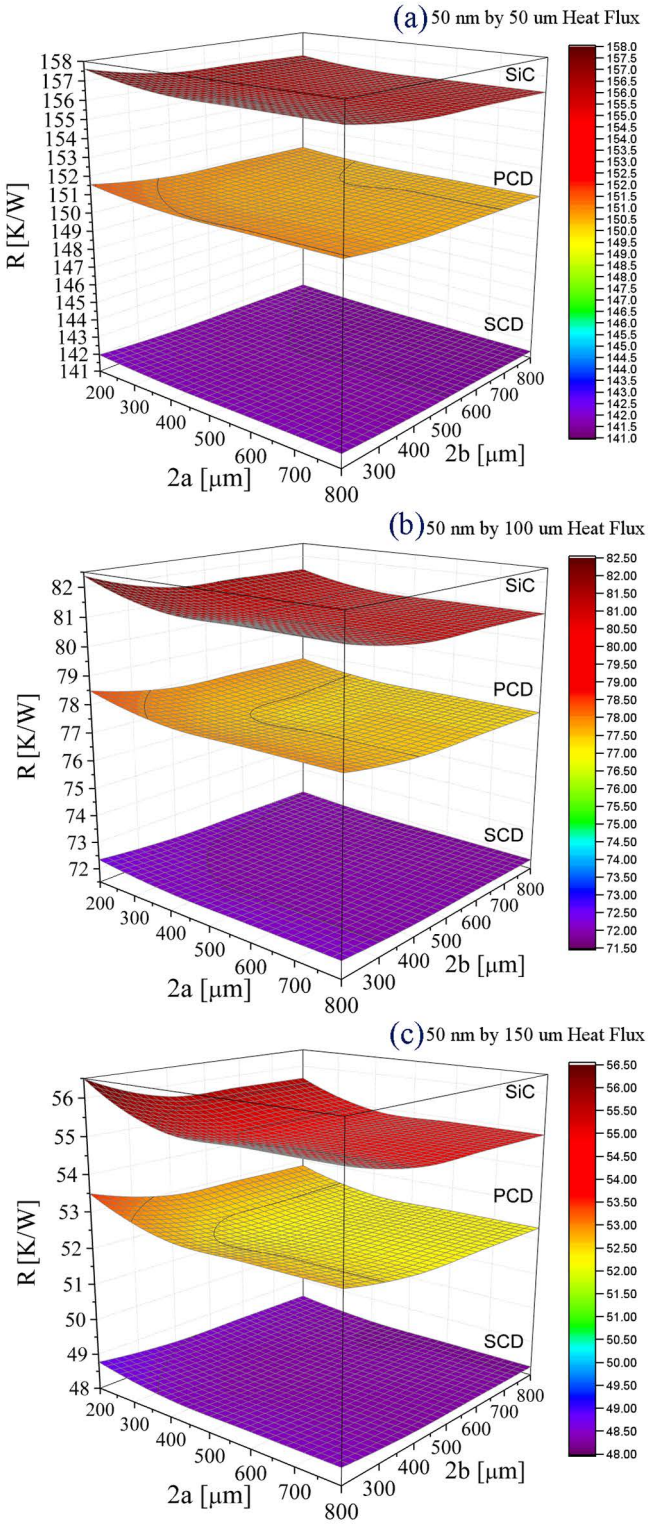

Figure 5.3 Variation of total thermal resistance of GaN-on-SiC, PCD, and SCD with change in the die size in gate width of (a)50 µm, (b) 100 µm, and (c) 150 µm and heat flux critical size of 50 nm. Refer to Table 1 for the other properties of the device in the step one.

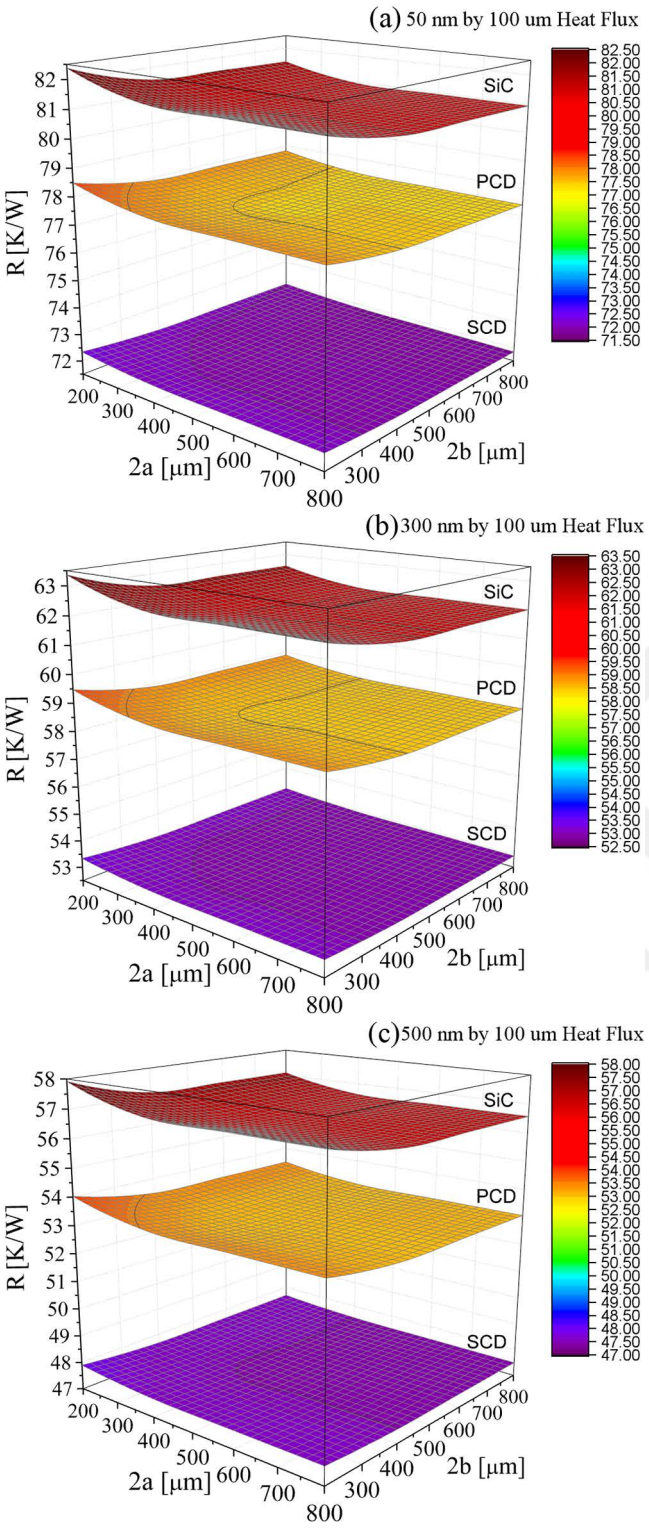

Figure 5.4 Variation of total thermal resistance of GaN-on-SiC, PCD, and SCD with change in the die size in gate width of 100 µm and heat flux critical size of (a) 50 nm, (b) 300nm, and (c) 500nm. Refer to Table 1 for the other properties of the device in the step one.

conditions, for instance, ratio of thermal resistance of GaN-on-SiC to GaN-on-diamond is almost similar in different near pinch-off conditions.

Furthermore, differences of thermal resistance in different gate widths are studied. As shown in Figure 5.4, having smaller gate width imposes higher spreading thermal resistance to the device. Same reduction ratio in gate width causes almost equal increase ratio in the thermal resistance of the device. In other words, from gate width of 150 µm to 50 µm nearly 3 times increase in value of total thermal resistance can be seen. In addition, benefit of using high thermal conductivity substrates like SCD is more highlighted in smaller gate widths, whereas in larger gate width we see moderate difference between SiC and diamond substrates. It should be mentioned that, different gate widths are used for different applications. Lower frequency operation devices (C-band, wireless) uses longer gate widths, while millimeter-wave devices implement smaller gate widths to reduce phase lag [124].

After evaluation of the total thermal resistance of the devices in various horizontal variations, average total thermal resistance reduction of 5.4% and 13.8% are observed when PCD and SCD is used instead of SiC substrate. Most of this reduction is due to the reduction in one-dimensional thermal resistance. Thus the best thermal enhancement is achieved for devices with higher one-dimensional thermal resistance and lower spreading thermal resistance. In other words, its better to use diamond substrates when die size is small (higher one-dimensional thermal resistance) and gate width is longer (lower spreading resistance). For instance when the die size of 200 µm with a 500 nm heat generation region at gate width of 150 µm is studied, thermal resistance reduction is 7.5% and 19% for PCD and SCD, respectively.

5.4 GaN Thickness and TBR

In the second study thermal performance of GaN-on-SiC, PCD, and SCD are compared by changing the vertical parameters (t_{GaN}, and TBR_{eff}) of 2-finger device (study 2 in Table 5-1). In this part, horizontal parameters are kept constant, and 50

nm critical heat generation region is selected to compare the results in the most intense heating condition. This size of heat flux region introduce higher thermal resistance, and is the lowest reported heat generation critical size. Also smaller die size in this case is chosen to magnify thermal resistance difference between devices with different substrates (smaller die size cause higher thermal resistance).

Results of second step is specified to study of thermal behavior of the devices in vertical variations; GaN thickness and TBR_{eff}. Figure 5.5 shows the variation of thermal resistance in vertical parameter variations. GaN thickness together with effect of TBR_{eff} are altered, to compare the difference of thermal behavior of SiC with diamond substrates. Figure 5.5(a) on the right illustrates thermal resistance of GaN-on-SiC while Figure 5.5(c) shows the thermal resistance of GaN-on-SCD. A reduction in values of thermal resistance from left figure to the right one can be seen, where thermal conductivity of substrate is increased (from SiC to PCD and SCD). Figure 5.5 indicates importance of GaN thickness, TBR_{eff}, and their relations in characterization of thermal resistance of the device, and we can see that benefit of using diamond can be reduced significantly when higher TBR_{eff} exists in the device.

Thermal performance of GaN-on-SiC with GaN thickness of 2 μm and TBR_{eff} of 2 m^2K/W (which is the current GaN-on-SiC commercial devices properties) is marked in Figure 4.5 with horizontal black lines. The underperform region of GaN-on-PCD and GaN-on-SCD is also highlighted in Figure 5.5(b) and (c), respectively. We define underperform as the conditions in which current GaN-on-SiC technology offers better thermal performance than GaN-on-diamond. It can be seen that underperform condition in GaN-on-PCD is having TBR_{eff} of more than 3 m^2K/W. Also GaN-on-SCD underperforms when TBR_{eff} of more than 5 m^2K/W exist in any GaN thicknesses and 4 m^2K/W in GaN thickness below. Above discussion highlights the critical importance of TBR_{eff} in fabrication of GaN-on-diamond HEMTs, particularly in GaN-on-SCD devices where strain relievers can be the major source of thermal boundary resistance.

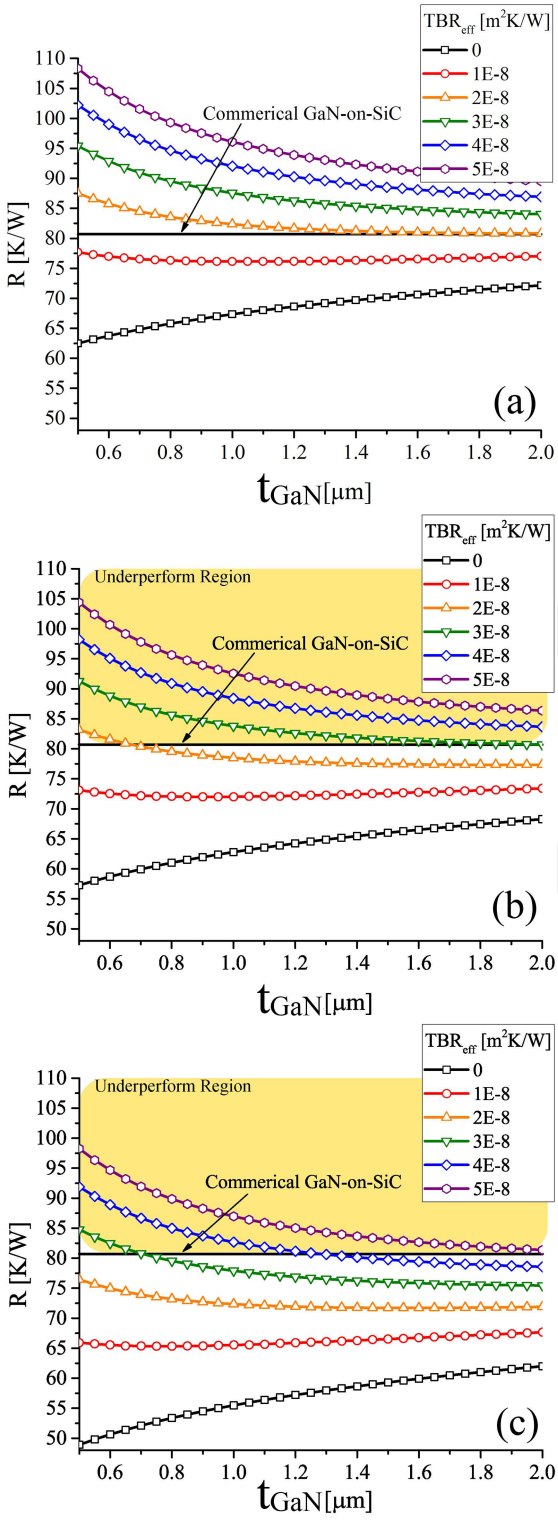

Figure 5.5 Variation of total thermal resistance of GaN HEMT device grown on a)SiC, b)PCD, and c)SCD with respect to the GaN thickness and effective thermal boundary resistance. Refer to Table 1 for the other properties of the device in second step.

Based on the at the results in the Figure 5.5, it can be concluded that using GaN thickness lower than 1 µm cause steep increase in the values of thermal resistance, particularly in higher TBR_{eff}. Previous researchers widely suggested that lower GaN thicknesses should be used to bring high thermal conductivity substrates like diamond as near as possible to the heat generation region. This suggestion is not only effective in TBR_{eff} of more than 2 m^2K/W, but also it cause significant increase in the value of thermal resistance. When heat is not spread enough in GaN layer and meets with a thermal barrier, spreading thermal resistance increases, which imposes more thermal resistance to the device. There should be more concentration on this phenomena in future studies, which we define it premature thermal spreading thermal in GaN layer. As shown in Figure 5.5 for TBR_{eff} of 1 m^2K/W we can see that the value of thermal

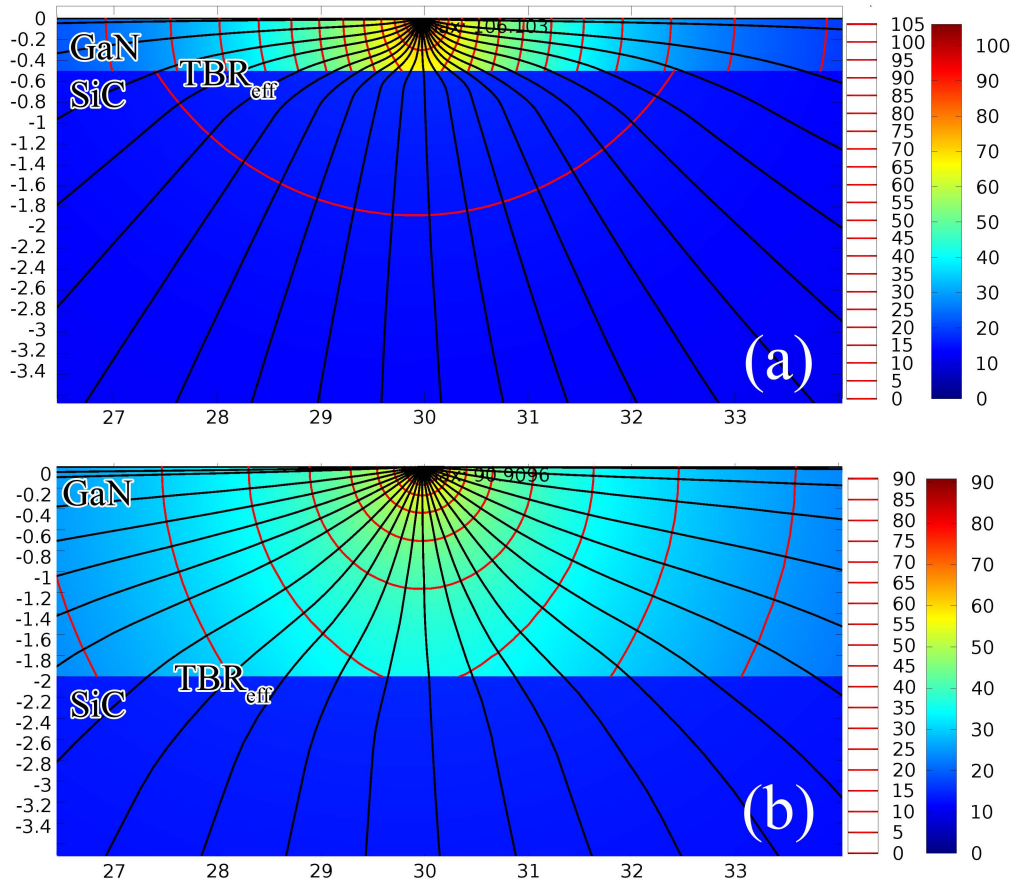

Figure 5.6 Temperature distribution near the hotspot in similar devices at power density of 5 W/mm in (a) 0.5 µm and (b) 2 µm GaN thickness consideration. Maximum temperature rise of 106.1 K and 90.9 K are predicted for the t_{GaN} = 0.5 µm and t_{GaN} = 2 µm, respectively.

resistance first decrease by increasing the thickness of GaN layer until the premature spreading ends, and then it starts to increase gradually. First reduction in the thermal resistance is due to vanishing premature spreading in the GaN layer. The later increase in the thermal resistance is due to increase in value of one-dimensional thermal resistance of GaN layer by increasing thickness. Figure 5.6 that shows the temperature distribution near the hotspot of the similar devices with 0.5 µm and 2 µm GaN layer thicknesses is provided to show the premature spreading effects more clearly in thin GaN consideration. As shown in the Figure 5.6, device with thinner GaN has 16 K higher hotspot temperature in power density of 5 W/mm.

5.5 Gate Pitch and Multi Finger Design

In this section effect of finger spacing and number of fingers in thermal resistance of the device and its effect in comparison of thermal behavior of different substrates is studied. Since number of fingers in die length of 100 µm is limited, die length of 400 µm is selected to be able to study 20-finger device and various gate pitches. The properties of the devices in this part is also presented in Table 5-1. In *third part*, finger spacing is changed from 20 µm to the maximum spacing possible. In the *last part*, 2 to 20-finger devices are studied. Thermal resistance of two hottest fingers in middle of device is characterized in this part, in order to compare it with value of thermal resistance of two-finger device in previous cases. Different gate pitches are also studied to study behavior of the device when we compare thermal behavior of GaN on different substrates in different gate numbering and various gate pitches.

As finger spacing increases, the space for heat spreading also increases, thus a lower thermal resistance can be achieved by this consideration. However, there is no significant change in the total thermal resistance of the device after particular value of finger spacing. Figure 5.7 demonstrates the effect of different finger spacing on thermal resistance of two-finger device. Finger spacing from 20 µm to 400 µm are studied and thermal resistance of device is evaluated in each case. It can be seen that for finger spacing of 20 µm to 80 µm, thermal resistance drops abruptly and after that a plateau can be seen and no significant reduction occurs. For typical finger spacing

values (20 to 60 µm) GaN-on-SiC technology is in range of thermal resistance of GaN-on-PCD technology, and thermal behavior of GaN-on-SiC can be improved by using higher gate pitches. However, thermal resistance of GaN-on-SCD is in unreachable range.

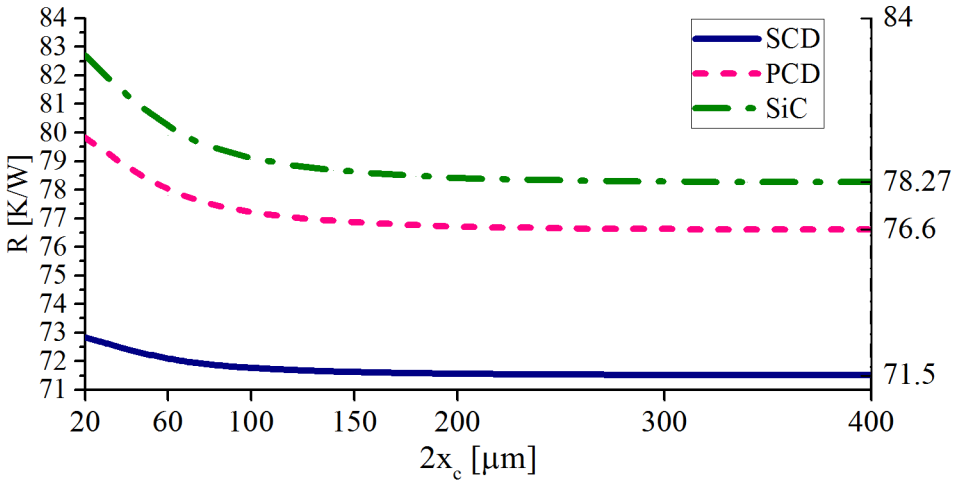

Figure 5.7 Effect of finger spacing on thermal resistance of 2-finger device. Note that there is a symmetry around half of the die length ($2x_c$=400), and the data is not presented for the higher finger spacing than this value. Refer to Table I for the other properties of the device in third step.

Based on the electrical operation condition of neighboring fingers (size and amount of generated heat) and their relative locations (gate pitch), each heat generation region has its own effect on the middle fingers of the device (indexed with number 1 in Figure 5.1(b)). Generally, near neighboring fingers have the most effect. Figure 5.8 shows the added thermal resistance to the first two-fingers (index 1) of the GaN-on-SiC, PCD, and SCD in three different gate spacing of 20, 40, and 60 µm. The effect of neighboring fingers in just one direction is presented due to symmetrical effects. As shown in the Figure 5.8, second finger had the most added thermal resistance to the device. However, comparing with GaN-on-SiC, this effect is three times smaller in the GaN-on-SCD, while in GaN-on-PCD the reduction in the effects of neighboring fingers are not significant. As illustrated in the Figure 5.8 as gate pitch increases, the effect of neighboring fingers decrease.

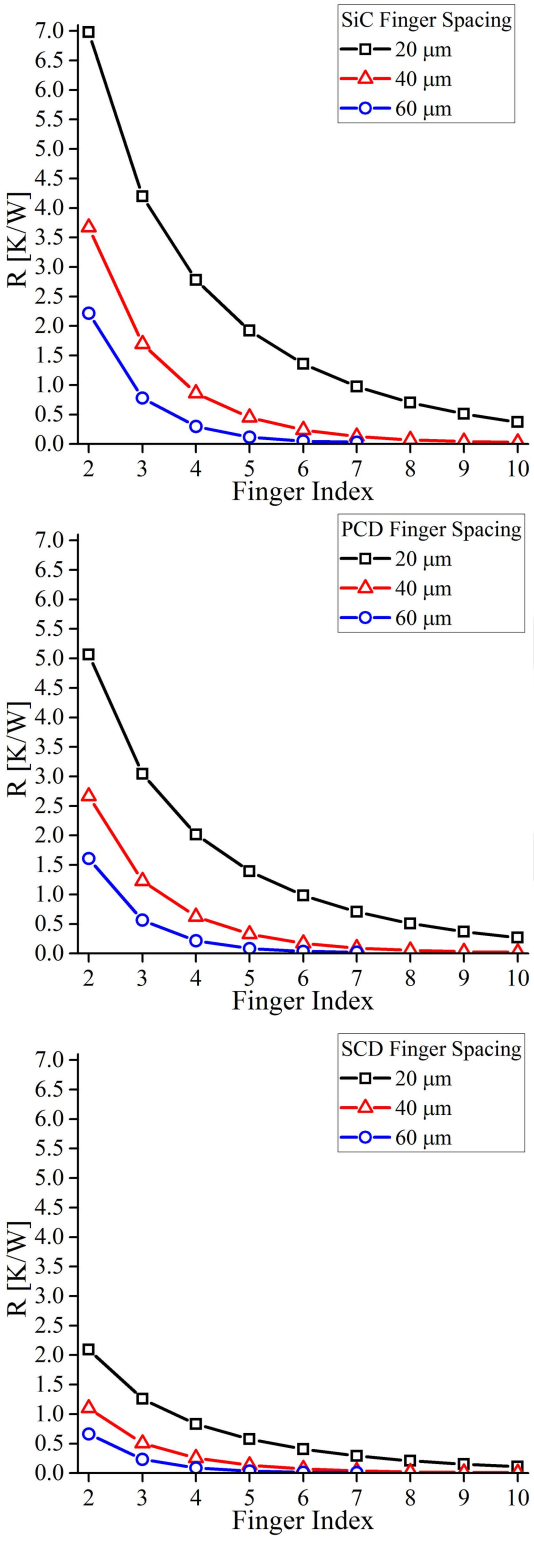

Figure 5.8 Thermal resistance burden of neighboring fingers on thermal resistance of first finger in different finger spacing.

Figure 5.8 indicated that in small gate pitches, GaN-on-SCD is the best choice for multi-finger HEMTs. In multi-finger devices, thermal resistance burden of each neighboring finger to the middle fingers (as shown in Figure 5.8) is added to the middle fingers. Consequently, in same power density, as the number of gates increase temperature rise in the middle of the devices increases. Thus, SCD can withstand more fingers with compact spacing without significant increase in the temperature rise of middle fingers.

Results of comparison between 2-finger devices in different conditions showed that there is no significant difference between GaN-on-SiC and GaN-on-diamond devices. However, when number of fingers increased and more compact devices are compared, high thermal conductivity of diamond presented its benefit. Table 5-2 shows the thermal resistance reduction percentage of GaN-on-PCD and SCD to the GaN-on-SiC device. The values of thermal resistance reductions are almost doubled in gate pitch of 20 µm for 2-finger and 20-finger devices. In other words, benefit of using diamond substrate is more highlighted in multi-finger devices. On the other hand, this difference decrease as gate pitch increases, where the neighboring heat generation region effects are reduce.

Table 5-2 Thermal resistance reduction percentage of the hottest finger in two and multi finger GaN on PCD and SCD with different finger spacing in comparison with GaN-on-SiC. [%]

Finger Spacing [µm]	Finger Number	GaN-on-PCD to GaN-on-SiC [%]	GaN-on-SCD to GaN-on-SiC [%]
20	2	5.3	13.5
	20	9.5	24.3
30	2	4.9	12.7
	20	7.6	19.6
40	2	4.7	12.2
	20	12.2	16.9
50	2	4.6	11.9
	20	5.9	15.2
60	2	4.5	11.6
	20	5.5	14.0

5.6 Conclusions

Based on the above arguments, we believe that a single improvement report cannot be stated for the use of diamond substrates. Variety of important characteristics of diamond, which just few of them are explored in this paper, should be considered in the fabrication process, in order to develop better devices than mature GaN-on-SiC technology. The key outcomes of this study can be briefly explained as:

- Between horizontal parameters, gate width exhibited the most effect on the thermal behavior of the device. However, since significant amount of heat spreading occurs in the GaN layer, diamond substrate is not able to reduce this dominant thermal resistance in the device. The reduction in the thermal resistance by implementing diamond substrates, is mostly due to the reduction of one-dimensional thermal resistance, not the spreading.
- Between vertical parameters, TBR_{eff} is the most important one. Integration process of GaN and diamond can impose unexpected thermal barrier to the device which can obstruct the benefit of thermal conductivity of diamond. In addition, having thin GaN layer is not always better depending on the value of TBR_{eff}.
- When compactness is not important, thermal behavior of the device can be improved by reconsidering gate pitch values.
- Diamond exhibited its benefit in compact multi finger devices. However, an exact improvement report cannot be sated due to its dependency on the number and spacing of the gates.

Scalability, value of the thermal conductivity, price, integration complexity, and fabrication quality are just few of the important parameters that should be considered in building GaN-on-diamond HEMTs. Since the main reason of heat generation in GaN HEMTs is the spreading thermal resistance, we believe that GaN-on-SiC HEMTs can be improved further by introducing high thermal conductivity

passivation layers on top of the device, which provide more spreading area for the heat.

CHAPTER 6

CONCLUDING REMARKS AND FUTURE RESEARCH

GaN HEMT electronics is the solution for the power hungry electronic industry. As the value of power increases in these devices, harsh self-heating reduces their reliability. Today many researchers are trying to find cost effective and high efficiency thermal characterization techniques of GaN HEMTs. Thermal modeling is a popular thermal characterization technique since it can cover the limiting factors of experimental methods. Yet there are issues such as computational efficiency of numerical methods and skepticisms about the validity of electro thermal simulations.

In this thesis, numerical and analytical thermal modeling techniques are presented and their advantages and disadvantages are discussed. A roadmap for accurate numerical modeling of devices is presented by examining controversies (including effect of thermal conductivity, Joule heating modeling methods, boundary conditions, and dimensionality) of previous thermal models. Additionally, to solve some of the problems of numerical modeling, for the first time an analytical method is studies in multiscale (die-on-package) device. This analytical model is used later as the foundation of a calibration technique that significantly reduces the computational cost of numerical models, and can be used in 2D electro thermal simulations.

Later, by use of analytical method a comprehensive parametric study is performed for comparison of SiC and new diamond substrates technologies. This study revealed an important relation between thickness of the GaN layer and thermal boundary resistance between GaN and substrate that should be considered in fabrication process of these devices.

Many other thermal issues and control techniques in GaN devices need further investigation; Accurate study of spreading thermal resistance in GaN HEMTs raise

many more questions that have not been discussed enough in the literature. Some of these issues include:

- Accurate characterization of the nanoscale thermal conductivity of the AlGaN and GaN films. Since the spreading mainly occurs in these regions, it was shown that small changes in thermal conductivity of these layers can results in important changes (more than 20% change in total thermal resistance) in thermal behavior of the device.
- Characterization of temperature dependency and anisotropicity of the materials used in device fabrication.
- Accurate optimization of GaN-on-substrate heterostructure with more emphasis on the concept of TBR between GaN and diamond. The concept of pre mature spreading presented in this thesis shows that careful optimization should be considered in fabrication of GaN-on-diamond HEMTs.
- Thermal management techniques that aim to reduce the spreading thermal resistance in the heterostructure. Although using diamond substrates presents thermal resistance reduction in GaN HEMTs, however this reduction is mainly due to change in one-dimensional thermal resistance. Future thermal management techniques should aim at the reduction of spreading thermal resistance of the device which is significantly dominant over one-dimensional thermal resistance.
- Finally the accuracy of electrothermal simulations can be improved by using the analytical calibration technique presented in this study and the electrical performance of the devices that change with the temperatures can be investigated with better accuracy.

REFERENCES

[1] S. Nakamura, T. Mukai, and M. Senoh, "High-power GaN pn junction blue-light-emitting diodes," *Japanese Journal of Applied Physics,* vol. 30, p. L1998, 1991.

[2] S. Nakamura, "GaN growth using GaN buffer layer," *Japanese Journal of Applied Physics,* vol. 30, p. L1705, 1991.

[3] J. W. Orton, *The story of semiconductors*: Oxford University Press, 2004.

[4] J. C. Zolper, "A review of junction field effect transistors for high-temperature and high-power electronics," *Solid-State Electronics,* vol. 42, pp. 2153-2156, 12// 1998.

[5] R. S. Pengelly, S. M. Wood, J. W. Milligan, S. T. Sheppard, and W. L. Pribble, "A review of GaN on SiC high electron-mobility power transistors and MMICs," *IEEE Transactions on Microwave Theory and Techniques,* vol. 60, pp. 1764-1783, 2012.

[6] A. Lidow, "GaN Transistors-The Best Emerging Technology for Power Conversion from DC through RF," in *2013 IEEE Compound Semiconductor Integrated Circuit Symposium (CSICS)*, 2013, pp. 1-4.

[7] C.-T. Sah, *Fundamentals of solid-state electronics*: World Scientific, 1991.

[8] L. J. Kamm, *Understanding electro-mechanical engineering: an introduction to mechatronics* vol. 3: John Wiley & Sons, 1996.

[9] D. Pavlidis, "HBT vs. PHEMT vs. MESFET: What's best and why," in *International Conference on Compound Semiconductor Manufacturing Technology*, 1999, pp. 1-4.

[10] U. K. Mishra, P. Parikh, and Y.-F. Wu, "AlGaN/GaN HEMTs-an overview of device operation and applications," *PROCEEDINGS-IEEE,* vol. 90, pp. 1022-1031, 2002.

[11] Y.-F. Wu, M. Moore, A. Saxler, T. Wisleder, and P. Parikh, "40-W/mm double field-plated GaN HEMTs," in *2006 64th Device Research Conference*, 2006, pp. 151-152.

[12] M. Yanagihara, Y. Uemoto, T. Ueda, T. Tanaka, and D. Ueda, "Recent advances in GaN transistors for future emerging applications," *physica status solidi (a)*, vol. 206, pp. 1221-1227, 2009.

[13] W. Lu, V. Kumar, E. L. Piner, and I. Adesida, "DC, RF, and microwave noise performance of AlGaN-GaN field effect transistors dependence of aluminum concentration," *IEEE Transactions on Electron Devices,* vol. 50, pp. 1069-1074, 2003.

[14] D. Dumka, C. Lee, H. Tserng, P. Saunier, and M. Kumar, "AlGaN/GaN HEMTs on Si substrate with 7 W/mm output power density at 10 GHz," *Electronics Letters,* vol. 40, pp. 1023-1024, 2004.

[15] P. Chao, K. Chu, and C. Creamer, "A new high power GaN-on-diamond HEMT with low-temperature bonded substrate technology," in *CS MANTECH Conference,* 2013, pp. 179-182.

[16] C. Wu, A. Kahn, A. Wickenden, D. Koleske, and R. Henry, "Aluminum, magnesium, and gold contacts to contamination free n-GaN surfaces," *Journal of Applied Physics,* vol. 89, pp. 425-429, 2001.

[17] Z. Fan, S. N. Mohammad, W. Kim, Ö. Aktas, A. E. Botchkarev, and H. Morkoç, "Very low resistance multilayer Ohmic contact to n-GaN," *Applied Physics Letters,* vol. 68, pp. 1672-1674, 1996.

[18] S. Karmalkar and U. K. Mishra, "Enhancement of breakdown voltage in AlGaN/GaN high electron mobility transistors using a field plate," *IEEE transactions on electron devices,* vol. 48, pp. 1515-1521, 2001.

[19] S. Adachi, "GaAs, AlAs, and AlxGa1− xAs: Material parameters for use in research and device applications," *Journal of Applied Physics,* vol. 58, pp. R1-R29, 1985.

[20] G. W. Neudeck and R. F. Pierret, "Modular series on solid state devices," 1988.

[21] S. M. Sze and K. K. Ng, *Physics of semiconductor devices*: John wiley & sons, 2006.

[22] J. del Alamo, "Si CMOS for RF Power Applications," in *Workshop on Advanced Technologies for Next Generation of RFIC, 2005 RFIC Symposium, June,* 2005.

[23] K. R. Bagnall, "Device-level thermal analysis of GaN-based electronics," Massachusetts Institute of Technology, 2013.

[24] L. A. Samoska, "An overview of solid-state integrated circuit amplifiers in the submillimeter-wave and THz regime," *IEEE Transactions on Terahertz Science and Technology,* vol. 1, pp. 9-24, 2011.

[25] R. S. Muller, T. I. Kamins, M. Chan, and P. K. Ko, "Device electronics for integrated circuits," 1986.

[26] J. Albrecht, R. Wang, P. Ruden, M. Farahmand, and K. Brennan, "Electron transport characteristics of GaN for high temperature device modeling," *Journal of Applied Physics,* vol. 83, pp. 4777-4781, 1998.

[27] H. Ibach and H. Lüth, "Solid-state physics: an introduction to principles of material science," *Advanced Texts in Physics, Springer-Verlag berlin Heidelberg New York,* 2003.

[28] A. Sarua, H. Ji, M. Kuball, M. J. Uren, T. Martin, K. P. Hilton, *et al.*, "Integrated micro-Raman/infrared thermography probe for monitoring of self-heating in AlGaN/GaN transistor structures," *IEEE Transactions on Electron Devices,* vol. 53, pp. 2438-2447, 2006.

[29] G. H. Jessen, J. K. Gillespie, G. D. Via, A. Crespo, D. Langley, J. Wasserbauer, *et al.*, "AlGaN/GaN HEMT on Diamond Technology Demonstration," in *2006 IEEE Compound Semiconductor Integrated Circuit Symposium*, 2006, pp. 271-274.

[30] F. Ejeckam[1], D. Babić, F. Faili[1], D. Francis[1], F. Lowe[1], Q. Diduck, *et al.*, "3,000+ Hours Continuous Operation of GaN-on-Diamond HEMTs at 350◦ C Channel Temperature," 2014.

[31] D. Dumka, T. Chou, J. Jimenez, D. Fanning, D. Francis, F. Faili, *et al.*, "Electrical and thermal performance of AlGaN/GaN HEMTs on diamond substrate for RF applications," in *2013 IEEE Compound Semiconductor Integrated Circuit Symposium (CSICS)*, 2013, pp. 1-4.

[32] F. Ejeckam, D. Babi, x, F. Faili, D. Francis, F. Lowe, *et al.*, "3,000+ Hours continuous operation of GaN-on-Diamond HEMTs at 350°c channel temperature," in *2014 Semiconductor Thermal Measurement and Management Symposium (SEMI-THERM)*, 2014, pp. 242-246.

[33] M. Gonschorek, M. Malinverni, M. A. Py, D. Martin, A. Mouti, P. Stadelmann, *et al.*, "High-mobility AlGaN/GaN two-dimensional electron gas heterostructure grown on (111) single crystal diamond substrate," *Japanese Journal of Applied Physics,* vol. 49, p. 061001, 2010.

[34] J. Cho, Z. Li, E. Bozorg-Grayeli, T. Kodama, D. Francis, F. Ejeckam, *et al.*, "Improved thermal interfaces of GaN–diamond composite substrates for HEMT applications," *IEEE Transactions on Components, Packaging and Manufacturing Technology,* vol. 3, pp. 79-85, 2013.

[35] M. J. Rosker, "The present state of the art of wide-bandgap semiconductors and their future," in *2007 IEEE Radio Frequency Integrated Circuits (RFIC) Symposium*, 2007, pp. 159-162.

[36] S. Nakajima, Y. Tateno, N. Ui, E. Mitani, K. Ebihara, K. Inoue, *et al.*, "State of the art performance for high power & high efficiency GaN HEMTs: a Japanese perspective," *Proc. WOCSDICE*, pp. 323-7, 2007.

[37] G. Gauthier and F. Reptin, "KORRIGAN: development of GaN HEMT technology in Europe," in *CS Mantech Conference*, 2006, pp. 49-51.

[38] P. Waltereit, J. Kühn, R. Quay, F. van Raay, M. Dammann, M. Cäsar, *et al.*, "High efficiency X-band AlGaN/GaN MMICs for space applications with lifetimes above 10 5 hours," in *Microwave Integrated Circuits Conference (EuMIC), 2012 7th European*, 2012, pp. 123-126.

[39] R. Quay, *Gallium nitride electronics* vol. 96: Springer Science & Business Media, 2008.

[40] A. D. Kraus and A. Bar-Cohen, "Thermal analysis and control of electronic equipment," *Washington, DC, Hemisphere Publishing Corp., 1983, 633 p.*, vol. 1, 1983.

[41] S. Singhal, J. Roberts, P. Rajagopal, T. Li, A. Hanson, R. Therrien, *et al.*, "GaN-on-Si failure mechanisms and reliability improvements," in *Reliability Physics Symposium Proceedings, 2006. 44th Annual., IEEE International*, 2006, pp. 95-98.

[42] M. Zhao, X. Liu, Y. Zheng, M. Peng, S. Ouyang, Y. Li, *et al.*, "Thermal analysis of AlGaN/GaN high-electron-mobility transistors by infrared microscopy," *Optics Communications*, vol. 291, pp. 104-109, 2013.

[43] P. Magazine, C. S. China, S. Semiconductor, and U. Solar, "Keeping cool with diamond."

[44] F. Donmezer, "Multiscale electro-thermal modeling of AlGaN/GaN heterostructure field effect transistors," 2013.

[45] S. Singhal, T. Li, A. Chaudhari, A. Hanson, R. Therrien, J. Johnson, *et al.*, "Reliability of large periphery GaN-on-Si HFETs," *Microelectronics Reliability*, vol. 46, pp. 1247-1253, 2006.

[46] K. Joshin and T. Kikkawa, "High-power and high-efficiency GaN HEMT amplifiers," in *2008 IEEE Radio and Wireless Symposium*, 2008, pp. 65-68.

[47] S. Singhal, J. Roberts, P. Rajagopal, T. Li, A. Hanson, R. Therrien, *et al.*, "GaN-on-Si failure mechanisms and reliability improvements," in *2006 IEEE International Reliability Physics Symposium Proceedings*, 2006, pp. 95-98.

[48] G. Wilcox and M. Andrews, "TriQuint Delivers High Power—Wideband GaN Technology," *Microwave Product Digest*, pp. 67-71, 2009.

[49] M. Rosker, C. Bozada, H. Dietrich, A. Hung, D. Via, S. Binari, *et al.*, "The DARPA wide band gap semiconductors for RF applications (WBGS-RF) program: Phase II results," *CS ManTech,* vol. 1, 2009.

[50] J. Zolper, "A review of junction field effect transistors for high-temperature and high-power electronics," *Solid-State Electronics,* vol. 42, pp. 2153-2156, 1998.

[51] R. S. Pengelly, S. M. Wood, J. W. Milligan, S. T. Sheppard, and W. L. Pribble, "A review of GaN on SiC high electron-mobility power transistors and MMICs," *Microwave Theory and Techniques, IEEE Transactions on,* vol. 60, pp. 1764-1783, 2012.

[52] A. Conway, P. Asbeck, J. Moon, and M. Micovic, "Accurate thermal analysis of GaN HFETs," *Solid-State Electronics,* vol. 52, pp. 637-643, 2008.

[53] H.-C. Lin, M. Khan, and T. Giao, "Dynamic liquid crystal hot spot examination of functional failures on production testers," in *20 th Symposium for Testing and Failure Analysis*, 1994, pp. 81-86.

[54] M. Kuball, S. Rajasingam, A. Sarua, M. Uren, T. Martin, B. Hughes, *et al.*, "Measurement of temperature distribution in multifinger AlGaN/GaN heterostructure field-effect transistors using micro-Raman spectroscopy," *Applied physics letters,* vol. 82, pp. 124-126, 2003.

[55] N. Shigekawa, K. Shiojima, and T. Suemitsu, "Optical study of high-biased AlGaN/GaN high-electron-mobility transistors," *Journal of applied physics,* vol. 92, pp. 531-535, 2002.

[56] M. G. Burzo, P. L. Komarov, and P. E. Raad, "Noncontact transient temperature mapping of active electronic devices using the thermoreflectance method," *Components and Packaging Technologies, IEEE Transactions on,* vol. 28, pp. 637-643, 2005.

[57] K. Jenkins and K. Rim, "Measurement of the effect of self-heating in strained-silicon MOSFETs," *Electron Device Letters, IEEE,* vol. 23, pp. 360-362, 2002.

[58] E. Heller and A. Crespo, "Electro-thermal modeling of multifinger AlGaN/GaN HEMT device operation including thermal substrate effects," *Microelectronics Reliability,* vol. 48, pp. 45-50, 2008.

[59] G. Riedel, J. Pomeroy, K. Hilton, J. Maclean, D. Wallis, M. Uren, *et al.*, "Nanosecond timescale thermal dynamics of AlGaN/GaN electronic devices," *Electron Device Letters, IEEE,* vol. 29, pp. 416-418, 2008.

[60] P. M. Mayer, D. Lüerßen, R. J. Ram, and J. A. Hudgings, "Theoretical and experimental investigation of the thermal resolution and dynamic range of

CCD-based thermoreflectance imaging," *JOSA A*, vol. 24, pp. 1156-1163, 2007.

[61] B. Vermeersch, J. Christofferson, K. Maize, A. Shakouri, and G. De Mey, "Time and frequency domain CCD-based thermoreflectance techniques for high-resolution transient thermal imaging," in *Semiconductor Thermal Measurement and Management Symposium, 2010. SEMI-THERM 2010. 26th Annual IEEE*, 2010, pp. 228-234.

[62] K. S. Chang, D. U. Kim, K. S. Park, C. B. Jeong, and G. H. Kim, "Thermoreflectance Microscope and Applications," in *CLEO: QELS_Fundamental Science*, 2016, p. JTh2A. 8.

[63] A. Venkatachalam, W. James, and S. Graham, "Electro-thermo-mechanical modeling of GaN-based HFETs and MOSHFETs," *Semiconductor Science and Technology*, vol. 26, p. 085027, 2011.

[64] S. Rajasingam, J. Pomeroy, M. Kuball, M. Uren, T. Martin, D. Herbert, *et al.*, "Micro-Raman temperature measurements for electric field assessment in active AlGaN-GaN HFETs," *IEEE Electron Device Letters*, vol. 25, pp. 456-458, 2004.

[65] S. Frégonèse, H. C. d'Honincthun, J. Goguet, C. Maneux, T. Zimmer, J.-P. Bourgoin, *et al.*, "Computationally efficient physics-based compact CNTFET model for circuit design," *Electron Devices, IEEE Transactions on*, vol. 55, pp. 1317-1327, 2008.

[66] A. M. Darwish, A. J. Bayba, and H. A. Hung, "Thermal resistance calculation of AlGaN-GaN devices," *Microwave Theory and Techniques, IEEE Transactions on*, vol. 52, pp. 2611-2620, 2004.

[67] D. I. Babić, "Thermal Analysis of AlGaN/GaN HEMTs Using Angular Fourier-Series Expansion," *Journal of Heat Transfer*, vol. 135, p. 111001, 2013.

[68] M. Garven and J. P. Calame, "Simulation and optimization of gate temperatures in GaN-on-SiC monolithic microwave integrated circuits," *Components and Packaging Technologies, IEEE Transactions on*, vol. 32, pp. 63-72, 2009.

[69] A. Bar-Cohen, J. D. Albrecht, and J. J. Maurer, "Near-junction thermal management for wide bandgap devices," in *2011 IEEE Compound Semiconductor Integrated Circuit Symposium (CSICS)*, 2011, pp. 1-5.

[70] K. R. Bagnall, O. I. Saadat, T. Palacios, and E. N. Wang, "Analytical thermal model for HEMTs with complex epitaxial structures," in *Thermal and Thermomechanical Phenomena in Electronic Systems (ITherm), 2014 IEEE Intersociety Conference on*, 2014, pp. 947-958.

[71] A. M. Darwish, A. J. Bayba, and H. A. Hung, "Thermal resistance calculation of AlGaN-GaN devices," *IEEE transactions on microwave theory and techniques*, vol. 52, pp. 2611-2620, 2004.

[72] Y. Muzychka, "Spreading Resistance in Compound Orthotropic Flux Tubes and Channels with Interfacial Resistance," *Journal of Thermophysics and Heat Transfer*, vol. 28, pp. 313-319, 2014.

[73] Y. Muzychka, M. Yovanovich, and J. Culham, "Thermal spreading resistance in compound and orthotropic systems," *Journal of thermophysics and heat transfer*, vol. 18, pp. 45-51, 2004.

[74] M. Yovanovich, Y. Muzychka, and J. Culham, "Spreading resistance of isoflux rectangles and strips on compound flux channels," *Journal of Thermophysics and Heat Transfer*, vol. 13, pp. 495-500, 1999.

[75] Y. S. Muzychka, K. R. Bagnall, and E. N. Wang, "Thermal spreading resistance and heat source temperature in compound orthotropic systems with interfacial resistance," *Components, Packaging and Manufacturing Technology, IEEE Transactions on*, vol. 3, pp. 1826-1841, 2013.

[76] Y. S. Muzychka, "Influence coefficient method for calculating discrete heat source temperature on finite convectively cooled substrates," *Components and Packaging Technologies, IEEE Transactions on*, vol. 29, pp. 636-643, 2006.

[77] K. R. Bagnall, Y. S. Muzychka, and E. N. Wang, "Analytical solution for temperature rise in complex multilayer structures with discrete heat sources," *Components, Packaging and Manufacturing Technology, IEEE Transactions on*, vol. 4, pp. 817-830, 2014.

[78] E. Douglas, F. Ren, and S. Pearton, "Finite-element simulations of the effect of device design on channel temperature for AlGaN/GaN high electron mobility transistors," *Journal of Vacuum Science & Technology B*, vol. 29, p. 020603, 2011.

[79] F. Bertoluzza, N. Delmonte, and R. Menozzi, "Three-dimensional finite-element thermal simulation of GaN-based HEMTs," *Microelectronics Reliability*, vol. 49, pp. 468-473, 2009.

[80] T. Sadi, R. W. Kelsall, and N. J. Pilgrim, "Investigation of self-heating effects in submicrometer GaN/AlGaN HEMTs using an electrothermal Monte Carlo method," *IEEE Transactions on Electron Devices*, vol. 53, pp. 2892-2900, 2006.

[81] E. Heller, S. Choi, D. Dorsey, R. Vetury, and S. Graham, "Electrical and structural dependence of operating temperature of AlGaN/GaN HEMTs," *Microelectronics Reliability*, vol. 53, pp. 872-877, 6// 2013.

[82] F. N. Donmezer, W. James, and S. Graham, "The thermal response of gallium nitride HFET devices grown on silicon and SiC substrates," *ECS Transactions,* vol. 41, pp. 13-30, 2011.

[83] M. Hosch, J. Pomeroy, A. Sarua, M. Kuball, H. Jung, and H. Schumacher, "Field dependent self-heating effects in high-power AlGaN/GaN HEMTs," in *CS Mantech Conference*, 2009, pp. 32-55.

[84] S. Choi, E. R. Heller, D. Dorsey, R. Vetury, and S. Graham, "The impact of bias conditions on self-heating in AlGaN/GaN HEMTs," *IEEE Transactions on Electron Devices,* vol. 60, pp. 159-162, 2013.

[85] H. C. Nochetto, N. R. Jankowski, and A. Bar-Cohen, "The impact of GaN/substrate thermal boundary resistance on a HEMT device," in *ASME 2011 International Mechanical Engineering Congress and Exposition*, 2011, pp. 241-249.

[86] S. D. U. Guide and E. Version, "Synopsys Inc," *Mountain View, CA, USA,* 2013.

[87] A. U. s. Manual, "Silvaco," *Santa Clara, CA,* 2010.

[88] V. d'Alessandro and N. Rinaldi, "A critical review of thermal models for electro-thermal simulation," *Solid-State Electronics,* vol. 46, pp. 487-496, 2002.

[89] L. F. Eastman, V. Tilak, J. Smart, B. M. Green, E. M. Chumbes, R. Dimitrov, *et al.*, "Undoped AlGaN/GaN HEMTs for microwave power amplification," *IEEE Transactions on Electron Devices,* vol. 48, pp. 479-485, 2001.

[90] J. Park, M. W. Shin, and C. C. Lee, "Thermal modeling and measurement of GaN-based HFET devices," *Electron Device Letters, IEEE,* vol. 24, pp. 424-426, 2003.

[91] J. Cho, E. Bozorg-Grayeli, D. H. Altman, M. Asheghi, and K. E. Goodson, "Low thermal resistances at GaN–SiC interfaces for HEMT technology," *Electron Device Letters, IEEE,* vol. 33, pp. 378-380, 2012.

[92] K. Filippov and A. Balandin, "The effect of the thermal boundary resistance on self-heating of AlGaN/GaN HFETs," *MRS Internet Journal of Nitride Semiconductor Research,* vol. 8, p. e4, 2003.

[93] K. D. Chabak, J. K. Gillespie, V. Miller, A. Crespo, J. Roussos, M. Trejo, *et al.*, "Full-wafer characterization of AlGaN/GaN HEMTs on free-standing CVD diamond substrates," *Electron Device Letters, IEEE,* vol. 31, pp. 99-101, 2010.

[94] N. Donmezer and S. Graham, "The impact of noncontinuum thermal transport on the temperature of AlGaN/GaN HFETs," *Electron Devices, IEEE Transactions on,* vol. 61, pp. 2041-2048, 2014.

[95] W. Liu and A. A. Balandin, "Temperature dependence of thermal conductivity of AlxGa1− xN thin films measured by the differential 3ω technique," *Applied Physics Letters,* vol. 85, pp. 5230-5232, 2004.

[96] J. Zou, D. Kotchetkov, A. Balandin, D. Florescu, and F. H. Pollak, "Thermal conductivity of GaN films: Effects of impurities and dislocations," *Journal of applied physics,* vol. 92, pp. 2534-2539, 2002.

[97] E. Burgemeister, W. Von Muench, and E. Pettenpaul, "Thermal conductivity and electrical properties of 6H silicon carbide," *Journal of Applied Physics,* vol. 50, pp. 5790-5794, 1979.

[98] X. Chen, F. N. Donmezer, S. Kumar, and S. Graham, "A numerical study on comparing the active and passive cooling of AlGaN/GaN HEMTs," *Electron Devices, IEEE Transactions on,* vol. 61, pp. 4056-4061, 2014.

[99] F. N. Donmezer, M. Islam, S. Graham, and D. Yoder, "Modeling the Hotspot Temperature in AlGaN/GaN High Electron Mobility Transistors Using a Non-Gray Phonon BTE Solver," in *ASME 2012 International Mechanical Engineering Congress and Exposition*, 2012, pp. 1175-1188.

[100] E. R. Heller and A. Crespo, "Electro-thermal modeling of multifinger AlGaN/GaN HEMT device operation including thermal substrate effects," *Microelectronics Reliability,* vol. 48, pp. 45-50, 1// 2008.

[101] J. Park, M. W. Shin, and C. C. Lee, "Thermal modeling and measurement of AlGaN-GaN HFETs built on sapphire and SiC substrates," *Electron Devices, IEEE Transactions on,* vol. 51, pp. 1753-1759, 2004.

[102] V. Turin and A. Balandin, "Performance degradation of GaN field-effect transistors due to thermal boundary resistance at GaN/substrate interface," *Electronics Letters,* vol. 40, pp. 81-83, 2004.

[103] A. Sarua, H. Ji, K. Hilton, D. Wallis, M. J. Uren, T. Martin, *et al.*, "Thermal boundary resistance between GaN and substrate in AlGaN/GaN electronic devices," *Electron Devices, IEEE Transactions on,* vol. 54, pp. 3152-3158, 2007.

[104] A. Sievers, "Thermal radiation from metal surfaces," *JOSA,* vol. 68, pp. 1505-1516, 1978.

[105] T. L. Bergman, F. P. Incropera, D. P. DeWitt, and A. S. Lavine, *Fundamentals of heat and mass transfer*: John Wiley & Sons, 2011.

[106] A. Angelini, M. Furno, F. Cappelluti, F. Bonani, M. Pirola, and G. Ghione, "Thermal design of power GaN FETs in microstrip and coplanar MMICs," in *Gallium Arsenide and Other Semiconductor Application Symposium, 2005. EGAAS 2005. European*, 2005, pp. 145-148.

[107] Y. S. Muzychka, "Influence coefficient method for calculating discrete heat source temperature on finite convectively cooled substrates," *IEEE Transactions on Components and Packaging Technologies*, vol. 29, pp. 636-643, 2006.

[108] S. Russo, V. d'Alessandro, M. Costagliola, G. Sasso, and N. Rinaldi, "Analysis of the thermal behavior of AlGaN/GaN HEMTs," *Materials Science and Engineering: B*, vol. 177, pp. 1343-1351, 2012.

[109] R. Bialecki and A. J. Nowak, "Boundary value problems in heat conduction with nonlinear material and nonlinear boundary conditions," *Applied mathematical modelling*, vol. 5, pp. 417-421, 1981.

[110] D. I. Babi, x, Q. Diduck, P. Yenigalla, A. Schreiber, D. Francis, *et al.*, "GaN-on-diamond field-effect transistors: from wafers to amplifier modules," in *MIPRO, 2010 Proceedings of the 33rd International Convention*, 2010, pp. 60-66.

[111] K. Hirama, M. Kasu, and Y. Taniyasu, "RF high-power operation of AlGaN/GaN HEMTs epitaxially grown on diamond," *IEEE Electron Device Letters*, vol. 33, pp. 513-515, 2012.

[112] J. G. Felbinger, M. V. S. Chandra, Y. Sun, L. F. Eastman, J. Wasserbauer, F. Faili, *et al.*, "Comparison of GaN HEMTs on Diamond and SiC Substrates," *IEEE Electron Device Letters*, vol. 28, pp. 948-950, 2007.

[113] J. W. Pomeroy, M. Bernardoni, D. C. Dumka, D. M. Fanning, and M. Kuball, "Low thermal resistance GaN-on-diamond transistors characterized by three-dimensional Raman thermography mapping," *Applied Physics Letters*, vol. 104, p. 083513, 2014.

[114] J. Cho, L. Zijian, E. Bozorg-Grayeli, T. Kodama, D. Francis, F. Ejeckam, *et al.*, "Thermal characterization of GaN-on-diamond substrates for HEMT applications," in *Thermal and Thermomechanical Phenomena in Electronic Systems (ITherm), 2012 13th IEEE Intersociety Conference on*, 2012, pp. 435-439.

[115] J. Anaya, H. Sun, J. Pomeroy, and M. Kuball, "Thermal management of GaN-on-diamond high electron mobility transistors: Effect of the nanostructure in the diamond near nucleation region," in *2016 15th IEEE Intersociety Conference on Thermal and Thermomechanical Phenomena in Electronic Systems (ITherm)*, 2016, pp. 1558-1565.

[116] H. Sun, R. B. Simon, J. W. Pomeroy, D. Francis, F. Faili, D. J. Twitchen, *et al.*, "Reducing GaN-on-diamond interfacial thermal resistance for high power transistor applications," *Applied Physics Letters,* vol. 106, p. 111906, 2015.

[117] J. G. Felbinger, M. Chandra, Y. Sun, L. F. Eastman, J. Wasserbauer, F. Faili, *et al.*, "Comparison of GaN HEMTs on diamond and SiC substrates," *IEEE Electron Device Letters,* vol. 28, pp. 948-950, 2007.

[118] N. Killat, J. W. Pomeroy, J. L. Jimenez, and M. Kuball, "Thermal properties of AlGaN/GaN high electron mobility transistors on 4H and 6H SiC substrates," *physica status solidi (a),* vol. 211, pp. 2844-2847, 2014.

[119] A. Manoi, J. W. Pomeroy, N. Killat, and M. Kuball, "Benchmarking of thermal boundary resistance in AlGaN/GaN HEMTs on SiC substrates: Implications of the nucleation layer microstructure," *IEEE electron device letters,* vol. 31, pp. 1395-1397, 2010.

[120] J. Cho, E. Bozorg-Grayeli, D. H. Altman, M. Asheghi, and K. E. Goodson, "Low thermal resistances at GaN–SiC interfaces for HEMT technology," *IEEE Electron Device Letters,* vol. 33, pp. 378-380, 2012.

[121] D. C. Dumka, U. Chowdhury, J. L. Jimenez, T.-M. Chou, A. Ketterson, D. M. Fanning, *et al.*, "Near-Junction Thermal Management in High Power GaN HEMTs," in *Government Microcircuit Applications & Critical Technology Conference,* 2012, pp. 213-216.

[122] M. A. Angadi, T. Watanabe, A. Bodapati, X. Xiao, O. Auciello, J. A. Carlisle, *et al.*, "Thermal transport and grain boundary conductance in ultrananocrystalline diamond thin films," *Journal of Applied Physics,* vol. 99, p. 114301, 2006.

[123] J. Graebner, S. Jin, J. Herb, and C. Gardinier, "Local thermal conductivity in chemical-vapor-deposited diamond," *Journal of applied physics,* vol. 76, pp. 1552-1556, 1994.

[124] D. Francis, F. Faili, D. Babić, F. Ejeckam, A. Nurmikko, and H. Maris, "Formation and characterization of 4-inch GaN-on-diamond substrates," *Diamond and Related Materials,* vol. 19, pp. 229-233, 2010.